

GEORGIA DOT RESEARCH PROJECT 14-26

**IMPLEMENTATION OF AASHTO LRFD
SPECIFICATIONS: BEARING CAPACITY AND
SETTLEMENT CALCULATIONS FOR SHALLOW
FOUNDATIONS OF BRIDGES AND WALLS**



**OFFICE OF RESEARCH
15 Kennedy Drive
Forest Park, GA 30297-2532**

TECHNICAL REPORT STANDARD TITLE PAGE

1. Report No.: FHWA-GA-16-1426		2. Government Accession No.:		3. Recipient's Catalog No.:	
4. Title and Subtitle: Geotechnical LFRD Calculations of Settlement and Bearing Capacity of GDOT Shallow Bridge Foundations and Retaining Walls			5. Report Date: 9 August 2016		
			6. Performing Organization Code:		
7. Authors: Shehab S. Agaiby and Paul W. Mayne			8. Performing Organization Report No.: GDOT 14-26 (GTRC 2006Y13)		
9. Performing Organization Name and Address: Georgia Tech Research Corporation 505 Tenth Street, N.W. Atlanta, GA 30332-0402			10. Work Unit No.:		
			11. Contract or Grant No.: RP14-26/00135290		
12. Sponsoring Agency Name and Address: Georgia Department of Transportation Office of Materials & Research 15 Kennedy Drive Forest Park, GA 30297-2534			13. Type of Report and Period Covered: Final Report: April 2015 - June 2016		
			14. Sponsoring Agency Code:		
15. Supplementary Notes: Prepared in cooperation with the U.S. Department of Transportation, Federal Highway Administration					
16. Abstract: The AASHTO codes for Load Resistance Factored Design (LFRD) regarding shallow bridge foundations and walls have been implemented into a set of spreadsheet algorithms to facilitate the calculations of bearing capacity and footing settlements on natural soils in the State of Georgia. Specifically, the approach applies to soils exhibiting drained behavior during loading, including clean to silty and clayey sands and granular soils of the Atlantic Coastal Plain and residual silty sands to sandy silts of the Appalachian Piedmont and Blue Ridge geologies. The methodology permits the sizing of foundations based on site-specific data input for a given project, using in-situ field data obtained from either: (a) standard penetration tests (SPT), (b) cone penetration tests (CPT), and/or (c) flat plate dilatometer tests (DMT). This report provides the background information concerning the equations, calculation procedures, and reference sources that are used. Specifically, the technical review covers the calculations of bearing capacity from limit plasticity theory, settlement predictions using elastic continuum solutions, and geoparameter evaluations from SPT, CPT, and DMT, as well as examples for each of these tests.					
17. Key Words: Bridge foundations, bearing capacity, geotechnical design, footings, settlements, wall foundations			18. Distribution Statement:		
19. Security Classification (of this report): Unclassified		20. Security Classification (of this page): Unclassified		21. Number of Pages: 160	
				22. Price:	

GDOT Research Project No. RP 14-26

Geotechnical Load Factored Resistance Design (LFRD) Calculations of Settlement and
Bearing Capacity of GDOT Shallow Bridge Foundations and Retaining Walls

Final Report

IMPLEMENTATION OF AASHTO LRFD SPECIFICATIONS:
BEARING CAPACITY AND SETTLEMENT CALCULATIONS FOR SHALLOW
FOUNDATIONS OF BRIDGES AND WALLS

by

Shehab S. Agaiby
Research Assistant - Geosystems Engineering

and

Paul W. Mayne, PhD, P.E.
Professor - Civil & Environmental Engineering

Georgia Institute of Technology
Civil & Environmental Engineering
790 Atlantic Drive
Atlanta, Georgia 30332-0355

Contract with

Georgia Department of Transportation
Office of Materials & Research
15 Kennedy Drive
Forest Park, GA 30297-2534

9 August, 2016

The contents of this report reflect the views of the authors who are responsible for the facts and the accuracy of the data presented herein. The contents do not necessarily reflect the official views or policies of the Georgia Department of Transportation or the Federal Highway Administration. This report does not constitute a standard, specification, or regulation.

Table of Contents

Cover Page	
FHWA Abstract	i
Table of Contents.....	ii
List of Figures.....	iv
List of Tables.....	x
1. Introduction and Research Objectives	1
1.1 Introduction.....	1
1.2 Geology of the State of Georgia	2
1.3 Research Objectives	3
1.4 Prior Efforts and Recommended Procedures	4
2. Bearing Capacity of Shallow Foundations	11
2.1 B.C. of Shallow Foundations in Practice	18
2.1.1 Undrained Loading	18
2.1.2 Drained Loading.....	19
2.2 Load Resistance Factored Design (LRFD).....	19
3. Settlement Computation for Shallow Foundations.....	23
3.1 Foundation Displacements and Settlements	23
3.2 Foundation Displacements	27
3.3 Approximate Displacement Influence Factors	28
3.4 Poisson's Ratio.....	31
3.5 Finite Layer Thickness.....	33
3.6 Foundation Rigidity	33
3.7 Foundation Embedment.....	37
3.8 Final Form of Settlement Equation	38
4. Input Parameters Using Standard Penetration Tests (SPT).....	41
4.1 Overview of the Standard Penetration Test (SPT).....	41
4.2 Equipment	41
4.3 Procedures.....	42
4.4 Corrections to the SPT N-value.....	45
4.5 Soil Unit Weight from SPT	52
4.6 Effective Friction Angle from SPT	56

4.7 Soil Modulus of Elasticity from SPT	59
4.8 Stress History from SPT	61
5. Input Parameters Using Cone Penetration Tests (CPT)	67
5.1 Overview of the Cone Penetration Test (CPT)	67
5.2 Equipment	67
5.3 Procedures	69
5.4 Parameters Measured	71
5.5 Soil Identification and Classification from CPT	74
5.6 Soil Unit Weight from CPT	79
5.7 Effective Friction Angle from CPT	81
5.8 Modulus of Elasticity from CPT	84
5.9 Stress History from CPT	87
6. Input Parameters Using the Flat Dilatometer Tests (DMT)	91
6.1 Overview of the Flat Dilatometer Test (DMT)	91
6.2 Equipment	91
6.3 Procedures	93
6.4 Parameters Measured	94
6.5 Soil Unit Weight from DMT	96
6.6 Effective Friction Angle from DMT	96
6.7 Modulus of Elasticity from DMT	97
6.8 Stress History from DMT	100
7. References	103
APPENDICES	
Appendix A: Guidelines on how to use the Excel spreadsheets	113
Appendix B: Illustrated Example using SPT data	121
Appendix C: Illustrated Example using CPT data	129
Appendix D: Illustrated Example using DMT data	137

List of Figures

Figure 1.1 Geology of the State of Georgia.....	3
Figure 1.2 Schematic bearing resistance chart showing strength limit state and service limit state criteria as a function of effective footing width (Samtani et al., 2010)	6
Figure 1.3 Schematic alternative bearing resistance chart in format of stress vs. settlement curves for range of effective footing widths and settlements.....	7
Figure 1.4 Excerpt from AzDOT Design Manual (ADOT SF-2, 2010).....	8
Figure 1.5 Excerpt from MnDOT Design Manual (courtesy Rich Lamb).....	9
Figure 2.1 Geometry of failure zones beneath foundation as per Vesic limit plasticity solution (1975)	12
Figure 2.2 Bearing capacity factors (N_q , N_c , N_γ) for spread footing foundations	13
Figure 2.3 Inclined load without eccentricity and the projected direction, θ	16
Figure 2.4 Values of bearing factor $N_{\gamma m}$ as a function in the effective friction angle ϕ'	20
Figure 3.1 Displacement influence factors for different points (center, corner, edges) under a uniform rectangular loading.....	29
Figure 3.2 Strain influence factors from elastic theory for a circular foundation.....	32
Figure 3.3 Displacement influence factors for flexible rectangular footing of different geometries on finite elastic layer.	35
Figure 3.4 Effect of foundation rigidity on centerpoint settlement of circular foundation (after Mayne and Poulos, 1999).....	37
Figure 3.5 Embedment modifier term for shallow foundation settlements (after Mayne and Poulos, 1999).....	39
Figure 4.1 Drilling rigs for conducting SPT: (a) CME truck rig (b) GeoProbe systems	42
Figure 4.2 Split-Barrel samplers used in SPT: (a) closed and (b) open.....	43
Figure 4.3 Illustration of setup and procedure for the Standard Penetration Test (SPT)	44
Figure 4.4 Various autohammers from different manufacturers	45
Figure 4.5 SPT- N values from Vermont: (a) Uncorrected data; and (b) Corrected data to 60 % efficiency. (Data from VTRANS, 2008).....	48
Figure 4.6 SPTs at Northwestern University: (a) Uncorrected N values; (b) Energy-Corrected N_{60} values.....	49

Figure 4.7 Relationship for unit weight in terms of shear wave velocity and depth (Mayne, 2001)	54
Figure 4.8 Interrelationship between dry unit weight and wet unit weight.....	55
Figure 4.9 Relationship between shear wave velocity V_s and SPT N-value (data after Imai & Tonouchi, 1982).....	56
Figure 4.10 Peak friction angle of sands from SPT resistance (data from Hatanaka & Uchida, 1996; Mayne & Brown, 2003)	58
Figure 4.11 Effective friction angle of clays versus Plasticity Index	59
Figure 4.12 DMT modulus – SPT relationship in Piedmont Residuum (data from Mayne & Frost, 1988).....	60
Figure 4.13 DMT modulus – SPT N_{60} relationship for a variety of soil types (modified after Gordon & Mayne 1986).....	61
Figure 4.14 Effective preconsolidation stress versus N_{60} for soils (after Mayne 1992).	65
Figure 5.1 Different cone penetrometers and piezocones used in production testing and research.....	69
Figure 5.2 Illustration of Cone Penetration Test (CPT)	70
Figure 5.3 Measurement locations on cone penetrometers: a. Electric Cone Penetrometer, CPT; b. Piezocone Penetrometer with filter behind tip, $CPTu_2$; c. Piezocone Penetrometer with mid-face filter, $CPTu_1$; d. Seismic Piezocone, $SCPTu_2$	73
Figure 5.4 Illustration of unequal end areas of CPT (Jamiolkowski et al. 1985)	74
Figure 5.5 Color coded Soil Behavioral Type (SBT _n) Chart for normalized CPT (after Robertson 2009).....	77
Figure 5.6 CPT Soil Classification Zones Using Nine-Part Soil Behavioral Type (after Robertson 2009).....	78
Figure 5.7 Unit weight directly estimated from CPT sleeve resistance and effective stress (Mayne et al., 2010).....	79
Figure 5.8 Unit weight directly estimated from CPT sleeve resistance and effective stress (Mayne, 2014)	80
Figure 5.9 Direct CPT approach for evaluating ϕ' in clean sands (Mayne, 2006).....	83
Figure 5.10 Trend between drained constrained modulus and net cone tip resistance in various soils, including three case studies with backfigured moduli	86

Figure 5.11 Relationship between the DMT elastic modulus and the cone tip net resistance in Piedmont soils (modified after Mayne and Liao, 2004)	87
Figure 5.12 General Approach to σ_p' interpretation of soils by CPT net cone resistance.....	88
Figure 5.13 Preconsolidation exponent parameter m' trend with CPT material index, I_c	89
Figure 6.1 Main Components of the Flat Dilatometer Test: a. Steel DMT blade with inflatable membrane; and b. Pressure Control Unit	92
Figure 6.2 Illustration of Setup and Procedure for the Flat Dilatometer Test (DMT)	94
Figure 6.3 Total Unit Weight in terms of DMT Index Parameters (Mayne et al., 2002)	97
Figure 6.4 Effective Friction Angle of Sands in terms of DMT Horizontal Stress Index (modified after Mayne 2015).....	98
Figure 6.5 Illustration of direct evaluation of E_D from DMT readings at Cherokee County, GA ...	99
Figure 6.6 Relationship between effective preconsolidation stress and dilatometer net contact pressure ($p_0 - u_0$) for clays.....	101
Figure 6.7 Relationship between effective preconsolidation stress and dilatometer net contact pressure ($p_0 - u_0$) for all soil types.....	102
Figure B.1 Raw SPT Input Data	122
Figure B.2 Footing Input Parameters and Energy Rating	122
Figure B.3 Foundation Shape and Geometry	122
Figure B.4 Percentage of Clay Readings	123
Figure B.5 Specific Settlement Values Input	123
Figure B.6 Alternative (a): Raw SPT Input Data: Depth, Measured N (bpf), and Soil Type	123
Figure B.7 Alternative (b): Raw SPT Input Data: Row Field Blows per 6 inches	124
Figure B.8 Additional Notes Box	124
Figure B.9 Average Unit Weight, Friction Angle, and Soil Modulus of Elasticity using SPT Input Data	124
Figure B.10 Profiles of SPT Input and Output Data.....	125
Figure B.11 Factored BC-Footing Width Design Chart with different settlement contours for Constant L value	126
Figure B.12 Factored BC-Footing Width Design Chart with different settlement contours for Square Footing (Constant L/B ratio = 1).....	126
Figure B.13 Factored BC-Footing Width Design Chart with different settlement contours for Rectangular Footing (L/B = 5).....	127

Figure B.14 Factored BC-Footing Width Design Chart with different settlement contours for Strip Footing ($L/B = 10$)	127
Figure B.15 Factored BC-Settlement Design Chart with different footing width contours for footings with Constant Length	128
Figure B.16 Factored BC-Settlement Design Chart with different footing width contours for Square Footing ($L/B = 1$)	128
Figure C.1 Raw CPT Input Data.....	130
Figure C.2 Footing Input Parameters	130
Figure C.3 Foundation Shape and Geometry	130
Figure C.4 Percentage of Clay Readings	131
Figure C.5 Raw CPT Input Data.....	131
Figure C.6 Soil Type based on CPTu Input Data	132
Figure C.7 Additional Notes Box	132
Figure C.8 Average Unit Weight, Friction Angle, and Soil Modulus of Elasticity from CPT Input Data	132
Figure C.9 CPT Profiles of Input and Output Data.....	133
Figure C.10 Factored BC-Footing Width Design Chart with different settlement contours for Constant L value	134
Figure C.11 Factored BC-Footing Width Design Chart with different settlement contours for Square Footing (Constant L/B ratio = 1).....	134
Figure C.12 Factored BC-Footing Width Design Chart with different settlement contours for Rectangular Footing ($L/B = 5$).....	135
Figure C.13 Factored BC-Footing Width Design Chart with different settlement contours for Strip Footing ($L/B = 10$)	135
Figure C.14 Factored BC-Settlement Design Chart with different footing width contours for footings with Constant Length	136
Figure C.15 Factored BC-Settlement Design Chart with different footing width contours for Square Footing ($L/B = 1$).....	136
Figure D.1 Raw Input DMT Data.....	138
Figure D.2 Footing Input Parameters and DMT Calibration Factors	138
Figure D.3 Foundation Shape and Geometry.....	138
Figure D.4 Percentage of Clay Readings.....	139

Figure D.5 Raw DMT Input Data.....	139
Figure D.6 Soil Type based on DMT Input Data	140
Figure D.7 Additional Notes Box	140
Figure D.8 Average Unit Weight, Friction Angle, and Soil Modulus of Elasticity using DMT Input Data	140
Figure D.9 Profiles of DMT Input and Output Data.....	141
Figure D.10 Factored BC-Footing Width Design Chart with different settlement contours for Constant L value	142
Figure D.11 Factored BC-Footing Width Design Chart with different settlement contours for Square Footing (Constant L/B ratio = 1).....	142
Figure D.12 Factored BC-Footing Width Design Chart with different settlement contours for Rectangular Footing (L/B = 5).....	143
Figure D.13 Factored BC-Footing Width Design Chart with different settlement contours for Strip Footing (L/B = 10)	143
Figure D.14 Factored BC-Settlement Design Chart with different footing width contours for footings with Constant Length	144
Figure D.15 Factored BC-Settlement Design Chart with different footing width contours for Square Footing (L/B = 1).....	144

List of Tables

Table 2.1 Bearing Capacity Factors N_c (Prandtl, 1921), N_q (Reissner, 1924), and N_γ (Vesic, 1975)	13
Table 2.2 Coefficients C_{wq} and $C_{w\gamma}$ for Various Groundwater Cases (AASHTO, 2014).....	14
Table 2.3 Shape Factors s_c , s_q , and s_γ (AASHTO, 2014).....	15
Table 2.4 Load Inclination Factors i_c , i_q , and i_γ (AASHTO, 2014).....	16
Table 2.5 Depth Factor d_q (AASHTO, 2014).....	17
Table 2.6 Recommended Resistance Factors for Geotechnical Resistance of Shallow Foundations at the Strength Limit State (after AASHTO, 2014).....	21
Table 2.7 Recommended Resistance Factors for Shallow Foundations on Natural Deposited Granular Soil Conditions (after Paikowsky et al., 2010).....	22
Table 4.1 Definition of different correction factors: depth effect (C_N), energy efficiency (C_E), borehole diameter (C_B), sampling method (C_S), and rod length (C_R)	47
Table 4.2 Summary of Energy Ratios (ER) Measured from AutoHammers in USA.....	50
Table 5.1 Soil Behavioral Type and Zone Number as defined by CPTu Material Index, I_c	78
Table 6.1 Equations defining correction factor $R_M = M_{DMT}/E_D$	99

1. Introduction and Research Objectives

1.1 Introduction

Per the 2007 AASHTO bridge specifications, a systematic means for the calculation of bearing stresses and settlements of shallow foundations supporting bridge piers and retaining walls in light of load resistance factored design (LRFD) was identified (Paikowsky et al. 2010). As the process is iterative between bridge design team, which contains the structural engineering group, and the geotechnical engineering branch, who analyze the foundation systems, a series of design charts and spreadsheet solutions for selecting and optimizing the foundation sizes were deemed necessary for implementation.

For shallow foundation systems, the magnitude of foundation displacements increases with the applied loading and bearing stresses, thus consideration of the current factor of safety (FS) should be given. The success of the predicted foundation response depends upon a number of different factors, each of which can be quantified in terms of their reliability, uncertainty, and accuracy. Important factors can include: foundation size and shape, analysis method, input data, geologic setting, and other variables. On the geotechnical resistance side, the site exploration phase can obtain data using: (a) soil borings with SPT N-values; (b) cone penetrometer testing (CPT) with up to 3 or more continuous electronic readings with depth; and (c) flat plate dilatometer testing (DMT) that provides 2 pressure measurements at 20-cm vertical depth intervals.

Foundation settlements can be assessed using a variety of different methods, including theoretical (e.g. elasticity solutions; spring models), empirical/statistical approaches, and

numerical simulations (e.g., finite differences, finite elements). In our experience, the utilization of elastic continuum theory provides a sound and rational framework that permits the consideration of all foundation sizes, shapes, and various ground conditions, including homogeneous, finite/infinite, and layered media (e.g. Harr 1966; Poulos & Davis 1974; Mayne & Poulos 1999, 2001; Das 2011).

1.2 Geology of the state of Georgia

The state of Georgia is composed of four separate geologic areas, as illustrated by **Figure 1.1**: Piedmont; Blue Ridge, Coastal Plain, and Valley & Ridge/Plateau. As such, the natural soils and rocks, as well as compacted fills made from native geomaterials in these regions, can behave somewhat differently from each other. We can group the Appalachian Piedmont and Blue Ridge together due to their similarity. Here, the ground is underlain by residuum derived by the in-place weathering of metamorphic and igneous bedrock. Primary rock types include gneiss and schist, with later intrusions of granitic formations. The residual soils are often found to be silty, ranging from micaceous fine sandy silts to silty fine sands, that transition with depth to saprolites, partially-weathered rocks, and bedrock refusal.

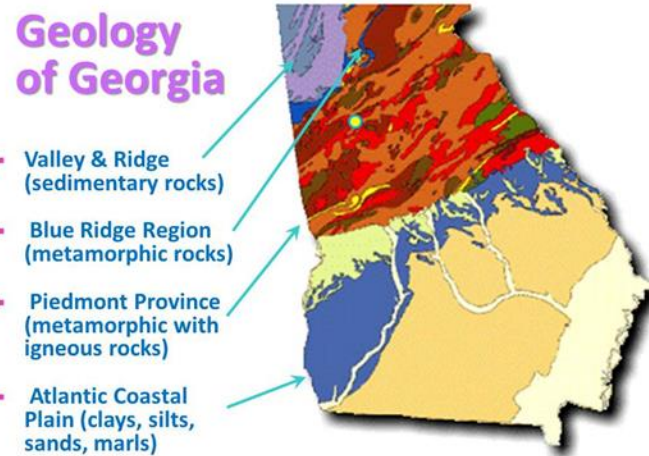


Figure 1.1 *Geology of the State of Georgia*

In contrast, the Coastal Plain consists of various marine sediments that were deposited in various times ranging from very old Cretaceous to Miocene to recent Holocene ages, including complex interbedding of clays, silts, sands, and gravels. Finally, the Valley & Ridge/Plateau include sedimentary type bedrocks (shales, limestones, sandstones) that have also produced a clayey to sandy type residuum cover, as well as karstic terrain, sinkholes, and caves (Weary, 2005).

1.3 Research Objectives

The project will provide a methodology for the sizing of spread footing foundations for GDOT bridge structures and retaining walls which address AASHTO design recommendations in computing bearing stresses and settlements by changing from Allowable Stress Design (ASD) to Load Resistance Factor Design (LRFD), as discussed by Sargand & Masada (2006), Samtani et al., (2010), Paikowski et al. (2010), and others.

The main research objective was to create training documents and excel spreadsheets to allow the use of standard penetration tests (SPT), cone penetration tests (CPT), and/or dilatometer test (DMT) data, as well as specific foundation information, as input to generate the necessary bearing capacity and settlement calculations and graphs in accordance with LRFD guidelines and supporting AASHTO, NCHRP, and FHWA documentation. The focus and applicability were directed for foundations on granular soils and/or soils exhibiting drained behavior, since less than 1% of shallow foundations for highway bridges are placed on clay soils (Paikowsky et al. 2010).

The two LRFD criteria (limit state and service state) are used to develop graphs of applied foundation stress (factored bearing capacity) versus footing effective width at various adopted settlement tolerances for a given foundation length (L) or rectangular distortion (L/B ratio) of shallow footings. Three different output formats can be generated for the bearing capacity (BC) versus settlement design chart: (a) bearing capacity vs. effective footing width for different settlement values at constant length (L) value, (b) bearing capacity vs. effective footing width for different settlement values at constant rectangular distortion ratio (L/B), and (c) bearing capacity vs. settlement chart for different footing width values at constant L/B ratio. Separate spreadsheets for different site-specific input data (SPT, CPT, and DMT) were developed.

1.4 Prior Efforts and Recommended Procedures

Elastic theory provides the primary and accepted solutions for the calculations of stresses beneath shallow foundations and the associated displacements (e.g. Harr 1966; Gibson

1967, Fraser & Wardle 1976, Poulos & Davis 1974). In fact, the well-known Schmertmann (1970) CPT procedure for footing settlements, as well as his DMT methodology (Schmertmann 1986), both utilize elastic theory as the basis for settlement calculations. Elastic solutions also provide a common basis for evaluating pile load tests and load-displacement and axial load transfer distributions (Niazi & Mayne 2012; Niazi et al. 2014). The use of the DMT modulus within an elastic continuum framework has shown to be quite successful in forecasting foundation settlements in the Piedmont residual soils (e.g. Brown & Mayne 2012; Mayne 2005). In the Piedmont, the DMT modulus has also been related to both the SPT N_{60} value (Mayne & Frost 1988; Mayne & Brown 2003) and to measured CPT resistances (Mayne & Liao 2004). The measured shear wave velocity (V_s) of the ground has also been shown to provide a fundamental stiffness that is important in foundation deformation problems (Burns et al. 2008; Mayne & Poulos 1999; 2001; Elhakim & Mayne 2008).

In coastal plain deposits, the use of elasticity theory is also warranted, albeit perhaps fewer case studies of actual foundation measurements have been published and reported in Georgia, primarily because the majority of the state population is located around Atlanta that lies within the Piedmont geology.

An alternative approach to elasticity theory that has become attractive is the development of direct in-situ methods that are derived from full-scale foundation response (i.e., load-displacement-capacity) which are then statistically related to the SPT, CPT, DMT, and/or V_s measurements (Mayne 2007; Viswanath & Mayne 2012, Uzielli & Mayne 2012; Mayne et al. 2012; Mayne & Woeller 2014).

Supporting materials from NHI, FHWA, and other state DOTs recommend that calculations including graphs be prepared by the geotechnical engineer that will display the varying bearing stresses, foundation sizes, and settlement criteria for each foundation element. There are many forms to display the BC-settlement-footing size design charts. **Figure 1.2** presents a schematic of bearing resistance contours as a function of effective footing width for different settlement values (1s, 2s, and 3s) combining both strength limit state and service limit state criteria. Alternatively, **Figure 1.3** presents a schematic of bearing resistance contours as a function of expected settlement value for different effective width values (B'_{f1} , B'_{f2} , B'_{f3} , and B'_{f4}).

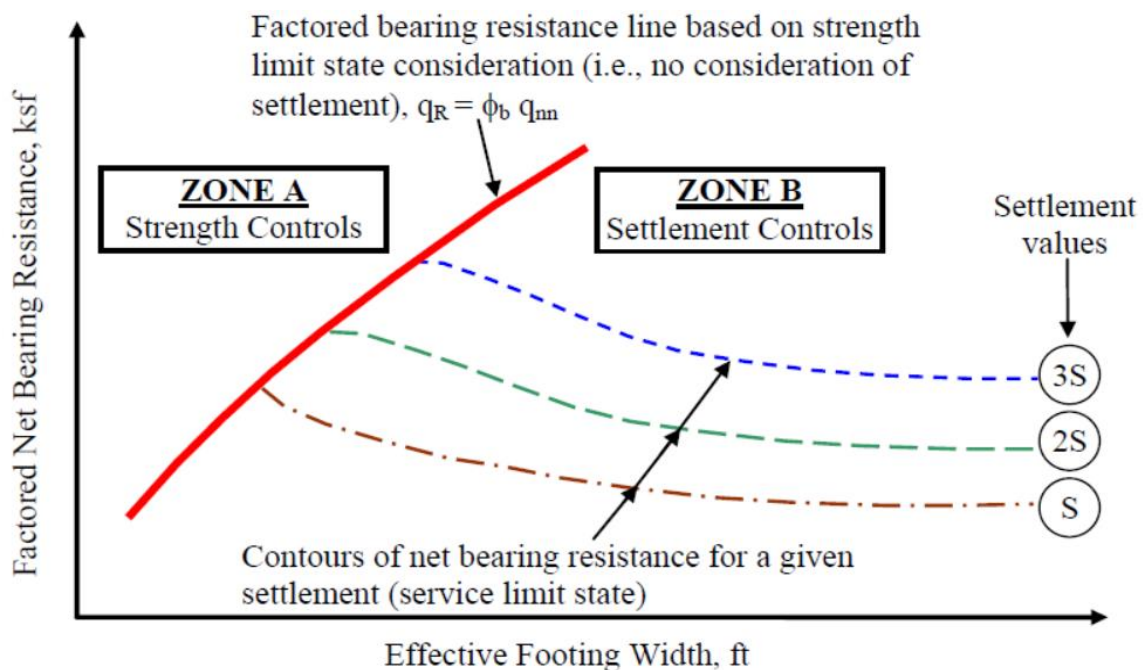


Figure 1.2 Schematic Bearing resistance chart showing strength limit state and service limit state criteria as a function of effective footing width (Samtani et al., 2010)

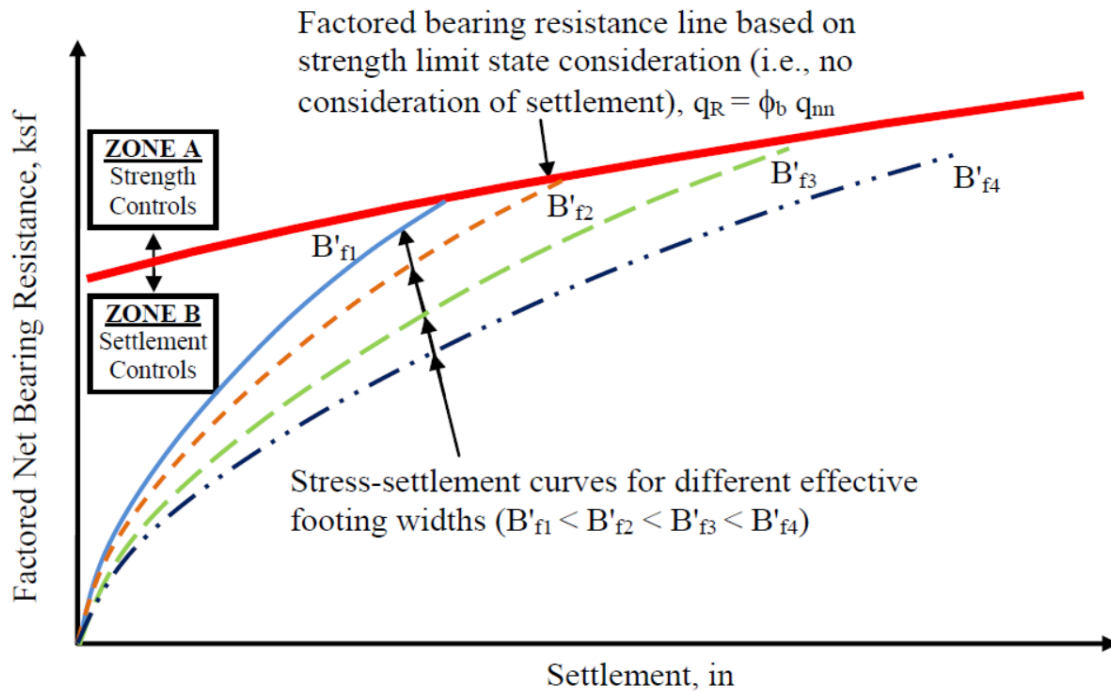


Figure 1.3 Schematic alternative bearing resistance chart in format of stress vs. settlement curves for range of effective footing widths and settlements (Samtani et al., 2010)

Prior efforts by other DOTs concerning AASHTO LRFD design of shallow foundations have been reviewed, including documents prepared by AZDOT (as shown in **Figure 1.4**), and MnDOT (as shown in **Figure 1.5**), as well as DOTs from OH, WA, CA, SC, and MO. Preliminary graphs of applied bearing stress versus effective footing sizes and foundation settlement have been prepared for granular soils (sands) to address LRFD criteria.

For the case of footings bearing on clays and fine-grained soils with time-dependent behavior, a case-by-case study is recommended since the expected performance of the foundations under drained primary consolidation settlements may also be accompanied by time-rate-of-consolidation, as well as possible undrained distortion displacements and considerations of long-term creep.

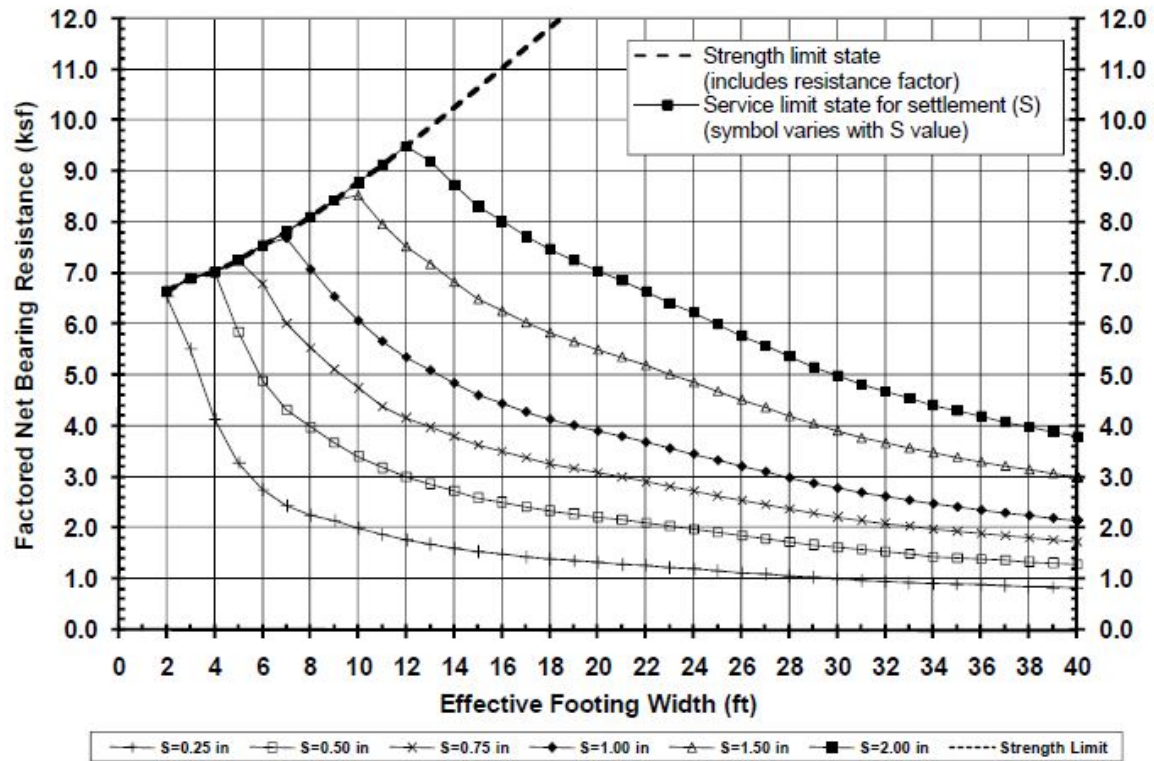


Figure 1.4 Excerpt from AzDOT Design Manual (ADOT SF-2, 2010)

Exception to the above would be for the residual soils of the Piedmont and Blue Ridge geologies since these are comprised mainly of fine sandy silts (ML and MH) to silty fine sands (SM), and occasional clayey sands (SC), sometimes used with a modified type of USCS symbols, i.e. SM-ML. These residual soils behave essentially under a drained response (or partially drained response) during foundation loading because the coefficient of consolidation (c_v) and permeability (k) are sufficiently high such that undrained behavior is not experienced under normal rates of construction. Details on the interpretation and behavior of Piedmont soils have been documented by Mayne et al. (2000), Mayne & Brown (2003), and Brown & Mayne (2012).

Effective Footing Width vs Service Load

Settlement for Elastic Shallow Foundations on Finite Homogenous Layer ,
(Mayne 2011) using Shear Wave Velocity and CPT Tip Stress

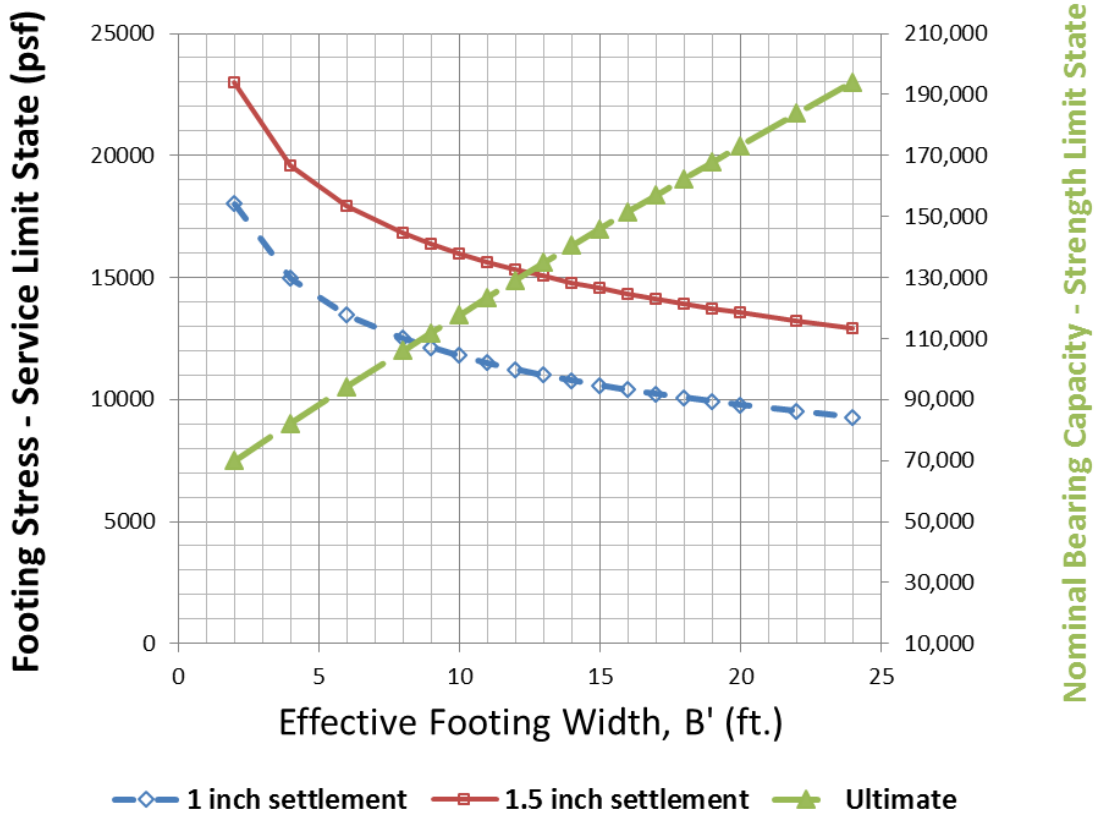


Figure 1.5 Excerpt from MnDOT Design Manual (courtesy Rich Lamb)

2. Bearing Capacity of Shallow Foundations

Foundations must be designed to preclude ultimate collapse or failure of the soil under loading. For a vertically-loaded foundation, an ultimate stress condition exists. The maximum force is referred to as the bearing capacity which is associated with full mobilization of the shear strength of the underlying soil along a prescribed failure surface. In Load Resistance Factored Design (LRFD), this is termed as "limit state".

Theoretical solutions of the "limit state" or geotechnical bearing capacity problem have been developed using upper and lower bound plasticity theorems, limit equilibrium, and cavity expansion theory, as well as numerical modeling simulations. Depending upon the specific assumptions made regarding the soil stress-strain characteristics, drainage conditions, rate of loading, boundary conditions, initial stress state, homogeneity, uniformity, or layering, a number of different solutions have been generated and published in the geotechnical literature.

In the presented section, the general shear solution used in conventional practice is based on limit plasticity theory and set of solutions as summarized by Vesić (1975) with the following assumptions: plastic equilibrium, plane strain conditions, soil above the foundation level is surcharged, and the general failure zones can be presented as active Rankine, radial shear (Prandtl), and passive Rankine zones as presented in **Figure 2.1**.

The form of the general bearing capacity equation has three main components:

$$q_n = c \cdot N_c + \frac{1}{2} \cdot B \cdot \gamma \cdot N_\gamma + \sigma_{vo}' \cdot N_q \quad [2.1]$$

ultimate bearing stress = cohesion term + unit weight term + surcharge term

where c is either the undrained shear strength (s_u) in total stress analyses (TSA) or effective cohesion intercept (c') in effective stress analyses (ESA), σ_{vo}' = effective overburden vertical stress, B = foundation width (i.e., smaller dimension for rectangular foundation, or d = diameter of equivalent circular foundation), γ = average bulk or effective unit weight of the soil (depending upon the prevailing groundwater conditions), and the N terms are bearing factors that are functions of the foundation shape and effective stress friction angle (ϕ') of the soil. Specifically, the corresponding respective bearing capacity factor terms are those for cohesion (N_c) defined by Prandtl (1921), self weight (N_γ) defined by Vesić (1975), and overburden or surcharge (N_q) defined by Reissner (1924). The equations defining the bearing capacity (N) factors are presented in **Table 2.1** and plotted in **Figure 2.2** as a function of the effective friction angle (ϕ') of the soil.

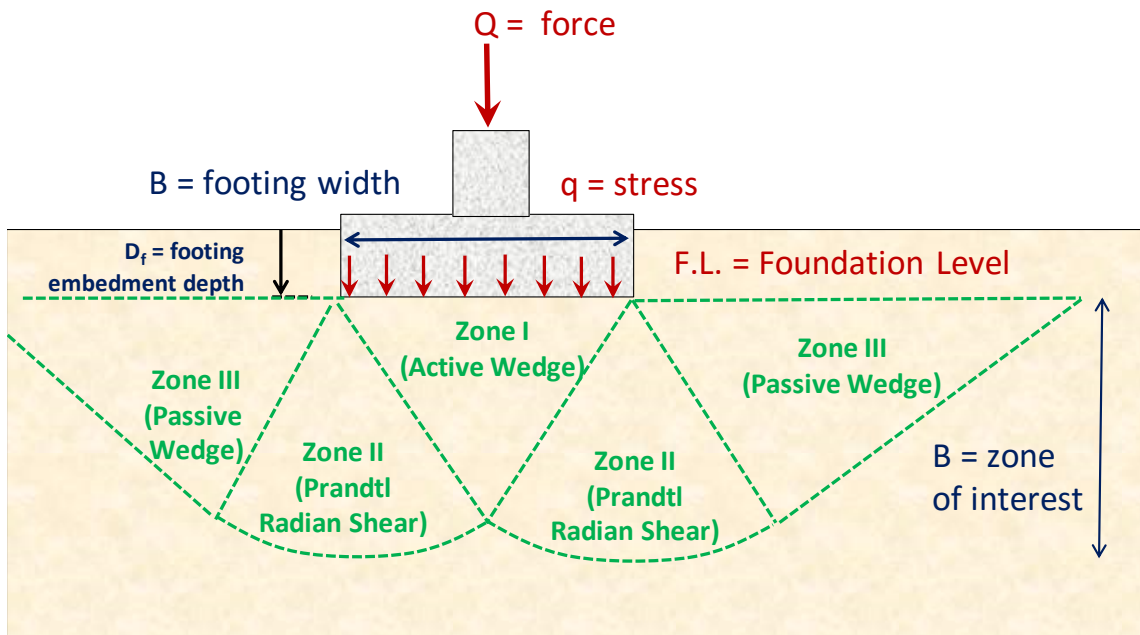


Figure 2.1 Geometry of failure zones beneath foundation as per Vesic limit plasticity solution (1975)

Table 2.1 Bearing Capacity Factors for strip footing: N_c (Prandtl, 1921), N_q (Reissner, 1924), and N_γ (Vesic, 1975)

Factor	Type Analysis	Friction Angle	Cohesion Term (N_c)	Unit Weight Term (N_γ)	Surcharge Term (N_q)
Bearing Capacity Factors N_c, N_γ, N_q	TSA	$\phi' = 0$	$2 + \pi$	n/a	1.0
	ESA	$\phi' > 0$	$(N_q - 1) \cdot \cot \phi'$	$2 \cdot (N_q + 1) \cdot \tan \phi'$	$\exp(\pi \cdot \tan \phi') \cdot \tan^2(45 + \phi'/2)$

Notes: n/a = not applicable; TSA = total stress analysis (e.g., "undrained" loading); ESA = effective stress analysis (e.g., "drained" loading).

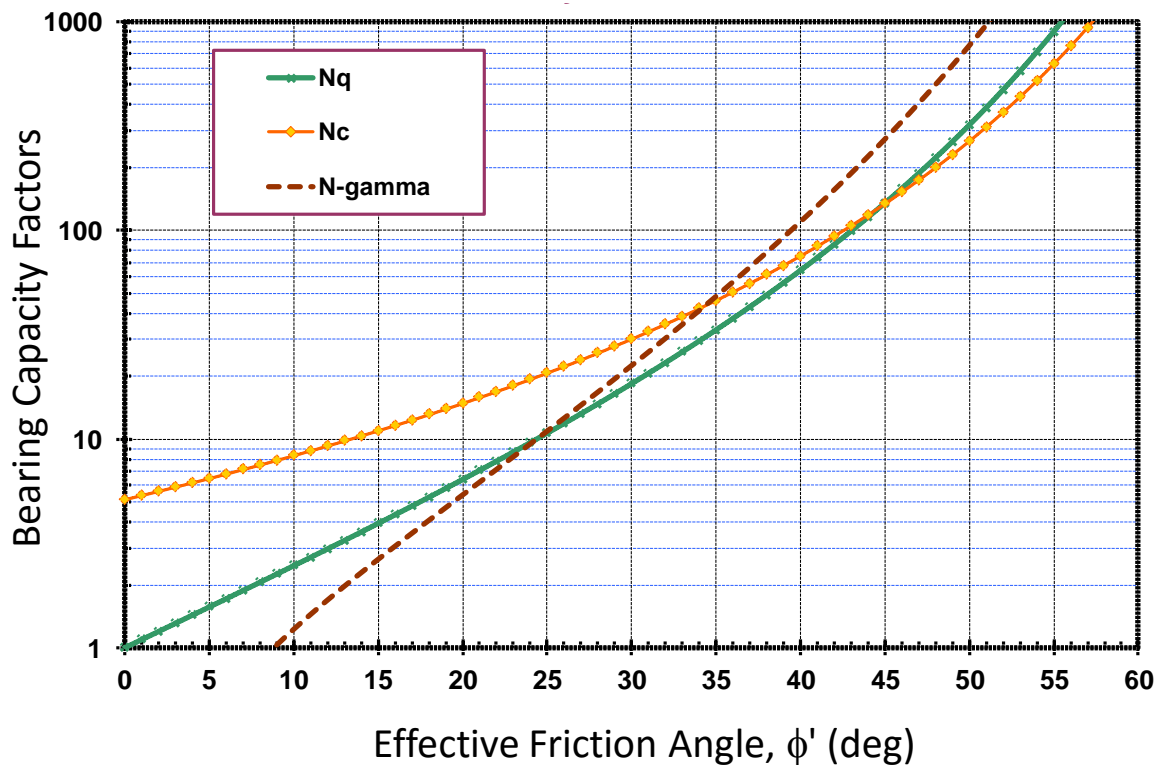


Figure 2.2 Bearing Capacity Factors (N_q, N_c, N_γ) for Spread Footing Foundations (plane strain case for strip footing)

The bearing capacity terms (N_q, N_c, N_γ) must each be modified to account for a number of additional factors, as specified in AASHTO (2008), including foundation shape

(rectangular distortion ratio L/B), embedment depth (D_f), groundwater depth (D_w), and load inclination. This results in:

$$q_n = c \cdot N_{cm} + 0.5 \cdot \gamma \cdot B \cdot N_{\gamma m} \cdot C_{w\gamma} + \gamma \cdot D_f \cdot N_{qm} \cdot C_{wq} \quad [2.2]$$

where C_{wq} and $C_{w\gamma}$ are correction factors to account for the buoyance effect of the groundwater and can be defined using **Table 2.2** following AASHTO (2014).

Moreover, one should also consider the possibilities of groundwater table fluctuations over the life of the structure. That is, if the footing is located near a river, lake, coastal region, or high groundwater, a raised water level or flooding may occur at some time in the future and that prospect should be analyzed as the worst case scenario.

Table 2.2 Coefficients C_{wq} and $C_{w\gamma}$ for Various Groundwater Cases (AASHTO, 2014)

Depth to water table, D_w	Modifier for surcharge bearing term, C_{wq}	Modifier for friction bearing term, $C_{w\gamma}$
$D_w \leq 0$	0.5	0.5
$D_w = D_f$	1.0	0.5
$D_w > 1.5 B + D_f$	1.0	1.0

Notes: B = foundation width; D_w = Groundwater Depth; D_f = Foundation Embedment Depth

The modified bearing factor terms (N_{cm} , $N_{\gamma m}$, N_{qm}) can be defined as follows:

$$N_{cm} = N_c s_c i_c \quad [2.3]$$

$$N_{\gamma m} = N_\gamma s_\gamma i_\gamma \quad [2.4]$$

$$N_{qm} = N_q s_q i_q d_q \quad [2.5]$$

Each of the modified bearing factors have dual subscripts, with the first subscript: "c, γ , and q" for bonding (cohesion), unit weight, and surcharge/overburden, respectively; and the second subscript "m" for modified that accounts for the footing shape (s) presented in **Table 2.3**, the load inclination (i) illustrated in **Figure 2.3** and presented in **Table 2.4**, and the footing embedment depth (d) presented in **Table 2.5**.

The bearing capacity equation can also be modified to account for eccentric loading, base tilt, sloping ground surface, and soil rigidity. These effects require the use of additional modifier terms designated as zeta (ζ) factors presented elsewhere (Vesić, 1975; Kulhawy et al., 1983; Paikowsky et al. 2010).

Table 2.3 Foundation Shape Factors s_c , s_q , and s_γ for Bearing Capacity (AASHTO, 2014)

Factor	Friction Angle	Cohesion Term (s_c)	Unit Weight Term (s_γ)	Surcharge Term (s_q)
Shape Factors s_c, s_γ, s_q	$\phi' = 0$	$1 + \left(\frac{B}{5L}\right)$	1.0	1.0
	$\phi' > 0$	$1 + \left(\frac{B}{L}\right)\left(\frac{N_q}{N_c}\right)$	$1 - 0.4\left(\frac{B}{L}\right)$	$1 + \left(\frac{B}{L}\tan\phi'\right)$

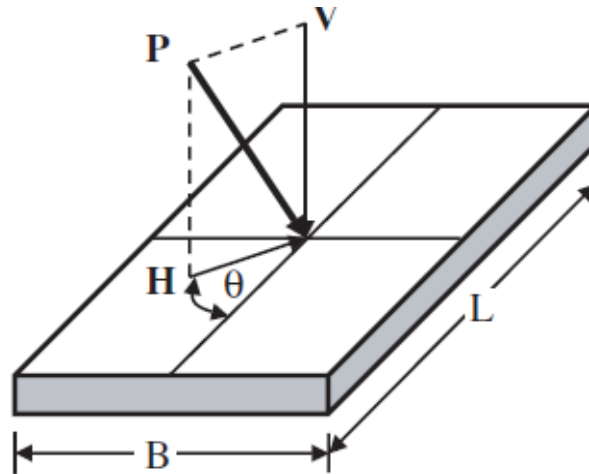


Figure 2.3 *Inclined load without eccentricity and the projected direction, θ*
 (V: vertical load, H: horizontal load, P: projected load, and θ : inclination angle)
 (from Paikowsky et al., 2010)

Table 2.4 *Load Inclination Factors i_c , i_q , and i_r for Bearing Capacity (AASHTO, 2014)*

Factor	Friction Angle	Cohesion Term (i_c)	Unit Weight Term (i_r)	Surcharge Term (i_q)
Load Inclination Factors i_c, i_r, i_q	$\phi' = 0$	$1 - \frac{n \cdot H}{c \cdot B \cdot L \cdot N_c}$	1.0	1.0
	$\phi' > 0$	$i_q - \frac{1 - i_q}{N_q - 1}$	$\left[1 - \frac{H}{V + c \cdot B \cdot L \cdot \cot \phi_f}\right]^{(n+1)}$	$\left[1 - \frac{H}{V + c \cdot B \cdot L \cdot \cot \phi_f}\right]^n$

NOTE:

$$\text{Where } n = \left[\frac{(2 + L'/B')}{(1 + L'/B')} \right] \cos^2 \theta + \left[\frac{(2 + B'/L')}{(1 + B'/L')} \right] \sin^2 \theta$$

Table 2.5 Depth Factor d_q for Bearing Capacity (AASHTO, 2014)

Friction Angle, ϕ' (Degrees)	D_f / B	d_q
32	1	1.20
	2	1.30
	4	1.35
	8	1.40
37	1	1.20
	2	1.25
	4	1.30
	8	1.35
42	1	1.15
	2	1.20
	4	1.25
	8	1.30

Note: $\phi' = \phi_f$ = effective stress friction angle of soil

The depth correction is recommended only when the soil above the foundation level is as competent as the soil below the foundation level, otherwise it should be taken as 1.0 (AASHTO, 2014). The depth correction factor can be expressed as:

$$d_q = 1 + 2 \tan\phi' \cdot (1 - \sin\phi')^2 \cdot \arctan(D_f/B) \quad (\text{Note: } \arctan \text{ in radians}) \quad [2.6]$$

The three terms of the general bearing capacity equation were derived separately, thus it is appropriate to apply them using one term at a time. The equation is used directly for either shallow or deep foundations and the calculation is performed for either totally undrained ($c = c_u = s_u$ that assumes " $\phi = 0$ " analysis) or else fully drained (ϕ' and $c' = 0$). Specifically, the term "undrained" loading refers to a condition of constant volume ($\Delta V/V = 0$) in the soil medium, while "drained" loading applies to the case of no excess porewater pressures ($\Delta u = 0$). Partially-drained and partly undrained are intermediate states.

For static loading of sands and granular soils, it is most common for a drained analysis to be conducted. The exception here would be in the case of footings on loose saturated sands in high seismicity areas where soil liquefaction potential is high and can be anticipated during a large earthquake. For foundations on clays and cohesive silts, both a short-term (undrained) analysis and a long-term (drained) analysis should be performed. Using the modified bearing factors, the general bearing capacity solution reduces to the following two cases:

UNDRAINED: assuming " $\phi = 0$ " for fast loading in silts, clays, and soils with low permeability ($\Delta V/V = 0$). In this case, $N_{qm} = 1$ and therefore:

$$q_n = c \cdot N_{cm} + 0.5 \cdot \gamma \cdot B \cdot N_{\gamma m} \cdot C_{w\gamma} \quad [2.7]$$

DRAINED: assuming $c' = 0$ for all loading conditions on sands and for the slow drained loading of silts and clays with $\Delta u = 0$. In this case, the bearing capacity is:

$$q_n = \gamma \cdot D_f \cdot N_{qm} \cdot C_{wq} + 0.5 \cdot \gamma \cdot B \cdot N_{\gamma m} \cdot C_{w\gamma} \quad [2.8]$$

2.1 B.C. of Shallow Foundations in Practice

In the case of shallow footings bearing at or near the ground surface, the overburden term (σ_{vo}') is small and can be neglected. The usual approach for *shallow foundations* is simplified to:

2.1.1 Undrained Loading: $q_n = c \cdot N_{cm} = N_{cm} \cdot s_u \quad [2.9]$

where $N_{cm} = 5.14$ for strip footing; 5.65 for rectangle ($A/B = 2$), and 6.14 for square or circular footing. The parameter $c = c_u = s_u$ = undrained shear strength of the soil (generally applied to clays and silty soils) is taken as a representative value from the footing base to

a depth of approximately B to $1.5B$ beneath the base. The value of s_u is best assessed from the relationship:

$$s_u/\sigma_{vo}' = \frac{1}{2} \sin\phi' \text{OCR}^\Lambda \quad [2.10]$$

where ϕ' = effective stress friction angle, OCR = overconsolidation ratio, and $\Lambda = 1 - C_s/C_c$ where C_s = swelling index and C_c = virgin compression index. If ϕ' is unknown, assume a value $\phi' = 28^\circ$ to 30° . The value of Λ is generally ≈ 0.8 to 0.9 .

2.1.2 Drained Loading:
$$q_n = 0.5 \cdot \gamma \cdot B \cdot N_{\gamma m} \cdot C_{w\gamma} \quad [2.11]$$

where $N_{\gamma m}$ is the modified bearing factor for friction and expressed as a function of both effective friction angle (ϕ'), foundation shape (A = plan dimension length and B = plan dimension width), as plotted in **Figure 2.4**. The value for water table correction factor ($C_{w\gamma}$) depends upon the bearing elevation, groundwater depth, and footing size. Values of bearing factor $N_{\gamma m}$ and $C_{w\gamma}$ are given by the aforementioned equations and γ = average bulk unit weight of the soil.

2.2 Load Resistance Factored Design (LRFD)

After computing the nominal bearing stress (q_n) of the shallow foundation under design, it is recommended per AASHTO (2008) bridge specifications to compute a factored bearing resistance (q_R) following the load resistance factored design (LRFD) method. In LRFD, a bearing resistance factor ϕ_b is used to compute the factored resistance where:

$$q_R = \phi_b \cdot q_n \quad [2.12]$$

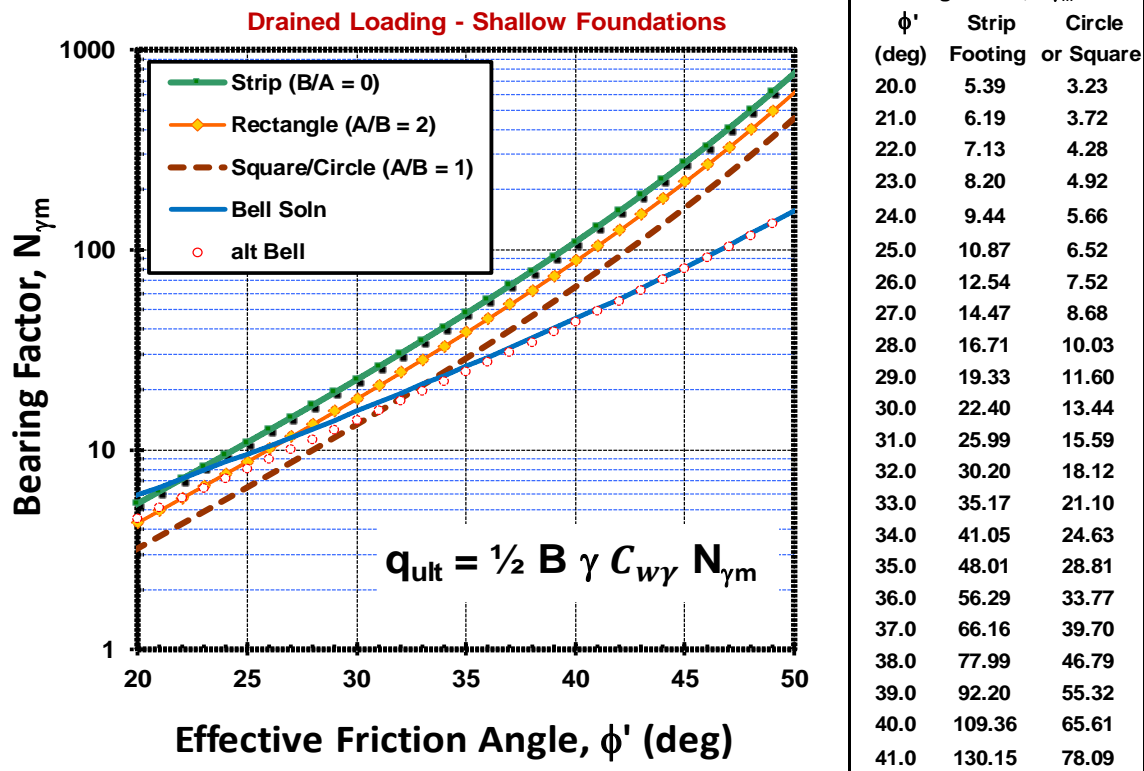


Figure 2.4 Values of bearing factor $N_{\gamma m}$ as a function of effective friction angle ϕ'

The values of the bearing resistance factor ϕ_b can be obtained from one of two sources: (a) AASHTO LRFD design manual; or (b) calibration based on statistical analyses. **Table 2.6** presents the recommended values of ϕ_b according to the latest AASHTO LRFD-7 design manual (2014) where the resistance factors are developed using reliability theory and calibration by fitting substantial representative statistic data to the Allowable Stress Design (ASD). In ASD, the calculated factors of safety (FS) range from 2.5 to 3.0 and correspond to bearing resistance factors (ϕ_b) of 0.55 to 0.45, respectively. The main issue with using such a table is the applicability of the same resistance factor value for all grades of soil type regardless of the loading conditions or the particular strength characteristics;

i.e., $\phi_b = 0.50$ for all clays irrespective of its undrained shear strength, liquidity index, plasticity characteristics, or continuity (intact versus fissured); or $\phi_b = 0.50$ for all sands using CPT regardless of its relative density, friction angle, or mineralogy (quartz-silica versus carbonate-calcareous content).

Table 2.6 Recommended Resistance Factors for Geotechnical Resistance of Shallow Foundations at the Strength Limit State (after AASHTO, 2014)

Method / Soil / Condition		Resistance Factor	
Bearing Resistance	Resistance Factor, ϕ_b	Theoretical Method (Munfakh et al., 2001), for Clays	0.50
		Theoretical Method (Munfakh et al., 2001), for Sands using CPT	0.50
		Theoretical Method (Munfakh et al., 2001), for Sands using SPT	0.45
		Semi-empirical methods (Meyerhof, 1957), for all soils	0.45
		Footings on Rock	0.45
		Plate Load Test (PLT)	0.55

To overcome the wide applicability of the values recommended by the AASHTO, a second source was used to define the bearing resistance factors as presented in **Table 2.7** following the recommendations of Paikowsky et al. (2010) that focused on granular soils with friction angles ranging from $30^\circ < \phi' < 45^\circ$ and relative densities with $D_R > 35\%$. The soils were divided into distinct classes based on effective friction angle and different loading conditions. Corresponding LRFD reduction factors were suggested based on statistical analyses (λ and COV) of *computed bias resistance*, defined as the ratio of measured/predicted resistance for a database of well documented case studies.

Table 2.7 Recommended Resistance Factors for Shallow Foundations on Natural Deposits of Granular Soil (after Paikowsky et al., 2010)

Soil Friction Angle, ϕ'	Loading Conditions			
	Vertical – Centric or Eccentric	Inclined - Centric	Inclined - Eccentric	
			Positive	Negative
30° - 34°	0.40	0.40	0.35	0.65
35° - 36°	0.45			0.70
37° - 39°	0.50		0.45	0.40
40° - 44°	0.55			
> 45°	0.65	0.50	0.45	

Using the aforementioned limit plasticity solutions and modifier terms for shape, depth, and groundwater conditions, plus the recommended resistance factors from AASHTO LRFD specifications, the bearing capacity stresses for the limit state were determined for a variety of rectangular footings of different widths (B) and rectangular distortions (L/B). The soil input parameters for bearing capacity determinations concerning footings on granular soils includes evaluations of the unit weight (γ) and effective friction angle (ϕ') that were determined from in-situ test results (e.g., SPT, CPT, DMT), as detailed in later sections of this report.

Even though the Piedmont/Blue Ridge soils may classify as fine-grained soils per USCS, in reality, their behavior is primarily a drained to partially-drained response during normal rates of construction for shallow foundations and MSE walls. The methodology discussed herein would be considered applicable for these geomaterials.

3. Settlement Computation for Shallow Foundations

3.1 Foundation Displacements and Settlements

For static loading of building foundations, there can be up to three types of displacements that may occur during the construction and occupancy phases: (1) immediate or initial undrained distortion (mainly on soft clays); (2) drained settlement due to primary consolidation (all built footings experience this phase); and (3) long-term creep due to secondary compression (primarily significant in organic clays and peats). These settlements can be written together as:

$$\rho_{total} = \frac{q \cdot d \cdot I \cdot (1 - \nu_u^2)}{E_u} + \frac{q \cdot d \cdot I \cdot (1 - \nu^2)}{E'} + \frac{C_{\alpha e}}{1 + e_o} \Delta z \cdot \log t$$

Total = **undrained distortion** + **drained settlement** + **long-term creep**
Displacements: *initial* *primary consolidation* *secondary compression*

The undrained distortion phase only occurs if the rate of loading is fast relative to the low permeability of the ground, generally involving deep thick deposits of soft saturated clays and silts. If this phase is relevant, then Poisson's ratio is $\nu_u = 0.5$ corresponding to zero volume change and concerns over undrained bearing capacity may prevail. For foundations situated on clay subsoils, it is standard practice to calculate vertical deflections during undrained loading using a three-dimensional elastic solution (Skempton and Bjerrum, 1957; D'Appolonia et al., 1971; Foott and Ladd, 1981). The undrained stiffness is expressed by an undrained modulus (E_u) that is derived from triaxial

tests or in-situ field method such as the pressuremeter test (PMT). Vertical deflections that occur under undrained loading are properly termed as “undrained distortion”.

The most common and prevalent settlement component is that due to drained primary consolidation, normally calculated from $e\text{-}\log\sigma'_v$ graphs, as obtained from one-dimensional consolidation tests on undisturbed samples. The settlement calculations rely on evaluating the effective preconsolidation stress (σ'_{vmax}), the recompression index (C_r), virgin compression index (C_c), and swelling index (C_s). If time-rate-of-consolidation will occur, the coefficient of consolidation (c_v) is also required. Full details on these calculation procedures are given elsewhere (Perloff and Baron, 1976; Lambe and Whitman, 1979; Holtz and Kovacs, 1981). In consolidation settlement, the footing loading should not exceed the preconsolidation stress in the ground. Elasticity theory is used in the aforementioned approach to calculate the vertical stress increase in the underlying sublayers of soil.

An alternate approach uses the constrained modulus (D') also evaluated from one-dimensional consolidation test data, where $D' = \Delta\sigma'_v / \Delta\varepsilon_v$ and is related to the equivalent elastic Young's modulus E' by (Lambe & Whitman 1979):

$$D' = \frac{E'(1-\nu')}{(1+\nu')(1-2\nu')} \quad [3.1]$$

For strain levels associated with foundation deflections, the majority of strains in the soil mass are small strains on the order $\varepsilon < 0.1\%$ and a value of Poisson's ratio in the range of $0.1 < \nu' < 0.2$ is appropriate. The drained moduli can be determined using laboratory tests

on undisturbed samples (e.g., oedometer tests, drained triaxial tests), or field tests (e.g., pressuremeter and/or flat dilatometer tests), provided that the tests are conducted at strain rates relevant to drained loading ($\Delta u = 0$) and appropriate stress levels and/or relevant strains comparable to the full scale situation. In sands, the material permeability is high and permits rapid drainage upon loading. In clays and silts, the rates can be very slow depending upon the permeability and degree of overconsolidation.

Settlements due to drained primary consolidation occur for every footing or foundation under working loads. That is, every foundation that has ever been built and loaded to design has experienced some movement or settlement that occurred under drained primary consolidation. Thus, this is the type of settlement deserving primary attention for the majority of bridge and wall structures. For special cases when these structures bear on soft compressible clays, a case-by-case basis of geotechnical analyses will be necessary.

Creep over time (t) continues unabated for many decades or longer. Creep settlements are therefore analogous to getting older; i.e., time marches on but cannot cease. Thus, creep is not normally a significant foundation problem, except in cases involving very soft organic soils, particularly OH clays, silts, and peats. The phenomenon of creep in soils is represented by the coefficient of secondary compression ($C_{\alpha e}$). The magnitude of $C_{\alpha e}$ has been linked to the virgin compression index (C_c). Thus, $C_{\alpha e}$ may be estimated from the empirical relationships (Mesri, 1973): sands ($C_{\alpha e} / C_c$) = 0.03; inorganic clays and silts: ($C_{\alpha e} / C_c$) = 0.04; organic clays ($C_{\alpha e} / C_c$) = 0.06 to 0.08.

As the GDOT bridge structures and walls will be considered for foundations situated on sands and granular geomaterials, as well as natural Piedmont soils (fine sandy silts and silty fine sands), the focus herein is for calculating drained settlements due to primary consolidation. For this, elasticity theory may be used to calculate the magnitudes of shallow foundation settlements in two ways: (a) propagating induced stresses with depth and using results from e - $\log \sigma'_v$ data; or (b) displacement influence factors where strains are accumulated with depth and elastic moduli (D' and/or E') are input parameters. Poulos and Davis (1974) provide a compilation of rigorous elastic solutions that are specific to the following cases: foundation shape (circular, square, rectangular), soil homogeneity (modulus either constant or varying with depth), finite layer depth, multi-layering, foundation roughness, interface roughness, Poisson effect (radial strains), foundation stiffness (footing versus mat), and drainage conditions (undrained versus drained).

Foundation settlements for sands are not commonly evaluated via one-dimensional consolidation theory because of the difficulties in sampling of undisturbed specimens for laboratory testing. Instead, drained settlements on sands are usually calculated using displacement influence factors (Gibson 1967; Harr, 1966; Poulos & Davis 1974; Harr 1977; Das 2011) and data obtained from in-situ tests (Beradi, et al., 1991; Fellenius 1996, 2009; Sargand et al. 2003; Mayne 2006).

The method of displacement influence factors is justifiably applicable to calculating both undrained distortional-type and drained consolidation-type settlements for all soil types. It can be shown that the one-dimensional e - $\log \sigma'_v$ approach is merely a subset of the

more general three-dimensional elasticity solution (Fellenius, 1996; 2009), whereby the radial strains are neglected and correspond to the simple elastic case with Poisson's ratio $\nu = 0$. In lieu of the compression indices, a constrained modulus is used to describe the stiffness of the soil matrix compressibility, where $m_v =$ coefficient of volumetric compressibility (Janbu, 1969; Schmertmann, 1986). For the recompression portion of the $e\text{-}\log\sigma_v'$ curve, corresponding to overconsolidated soils, for example, it is a simple matter to show that (Stamatopoulos and Kotzias, 1978):

$$D' = 1/m_v = \ln(10) \sigma_{v0}' (1+e_o) / C_r \quad [3.2]$$

3.2 Foundation Displacements

The general form for settlement calculation by displacement influence factors is:

$$s = \rho = \frac{q \cdot B \cdot I}{E_s} \quad [3.3]$$

where $s = \rho =$ foundation settlement, $q =$ applied stress, $B =$ foundation width, $E_s =$ equivalent average elastic soil modulus, and $I =$ displacement influence factor. Rigorous solutions to obtain the displacement influence factors are fairly involved and require the establishment of equilibrium equations, continuity equations, constitutive relationships, and kinematics, as well as complex integrals (Ueshita and Meyerhof, 1967; Gibson, 1967; Stark and Booker, 1997). The solutions depend upon several parameters, including foundation shape (A and B), Poisson's ratio (ν), modulus variation with depth, soil layering, finite layer thickness (h), foundation roughness, and interface adhesion.

A great variety and number of solutions exist in the literature for different theories, initial governing assumptions, foundation geometries, and specific situations (Poulos and Davis, 1974; Teferra and Schultz, 1988). Most of the solutions are given in normalized forms, but the graphical or chart presentations may make it appear that there are significant differences amongst the various solutions, whereas in fact, the solutions are quite similar. Mayne and Poulos (1999) provide an approximate solution for obtaining displacement influence factors using numerical integration, and illustrate compatibility with a number of well-known rigorous solutions that have been presented in differing formats.

3.3 Approximate Displacement Influence Factors

The displacement influence factor can be defined as summation of all vertical deflections occurring directly beneath the foundation and within the elastic medium. The maximum value is sought, as referenced to the center of the foundation base. The general derivation for the displacement influence factor is given by (Davis and Poulos, 1968):

$$I = \int_0^{h/d} \varepsilon_z \cdot dz^* \quad [3.4]$$

where $z^* = z/d =$ normalized depth and the vertical strains (ε_z) are summed from the base of the footing to some particular depth of interest, for instance, from $z^* = 0$ to $z^* = h/d$, where $h =$ depth to an incompressible layer such as bedrock. In the case of the flexible foundation, the unit strains may be calculated from the constitutive relationship of Hooke's Law:

$$\varepsilon_z = \frac{1}{E} [\Delta\sigma_z - \nu \cdot (\Delta\sigma_x + \Delta\sigma_y)] \quad [3.5]$$

where $\Delta\sigma_z$ = change in vertical stress at depth z and $\Delta\sigma_{x,y}$ = change in lateral stress in x and y directions at depth z . The incremental change of vertical stress with depth ($\Delta\sigma_z$) is well-known and derived by integrating the Boussinesq point load over a distributed surface area (Perloff and Baron, 1976):

$$\Delta\sigma_z/q = 1 - \frac{1}{\left[1 + \left(\frac{a}{z}\right)^2\right]^{3/2}} \quad [3.6]$$

where a is an equivalent radius of the footing under study.

The influence factors I_z for a uniform rectangular loading (q) is presented in **Figure 3.1**, specifically under the center, corner, far, and close edges (mid-center). The approximate spreadsheet solution is compared to the rigorous Giroud (1968) solution.

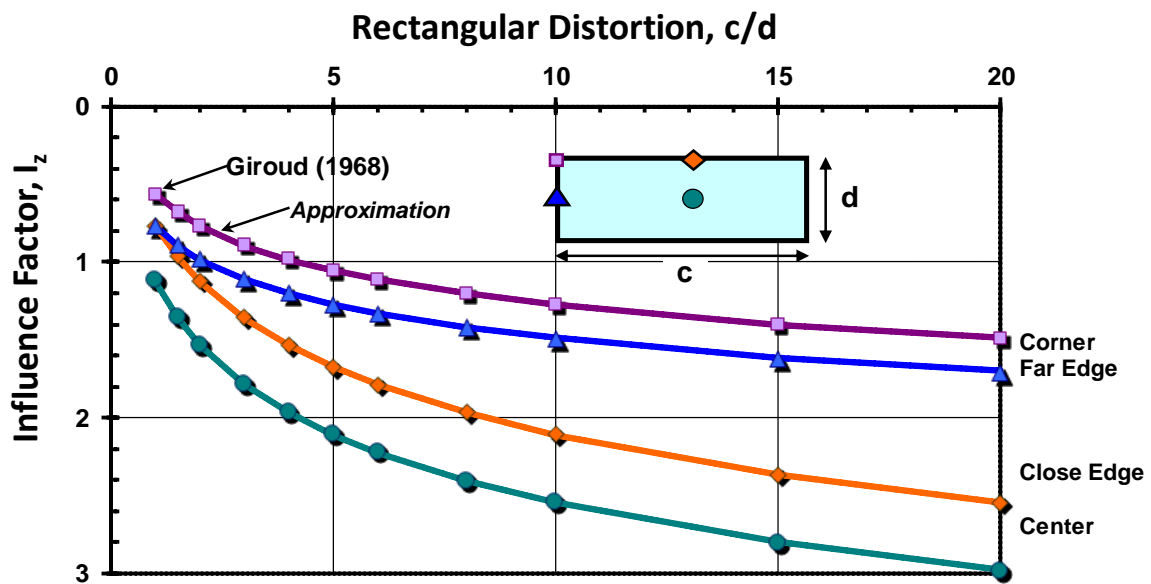


Figure 3.1 Displacement Influence Factors for Different Points (center, corner, edges) under a Uniform Rectangular Loading.

The vertical stress increase ($\Delta\sigma_z$) under the center of a uniform rectangular surface loading with length (c) and width (d) can be computed using (Harr 1977):

$$\text{Center} : \Delta\sigma_z / q = \frac{2}{\pi} \frac{mn}{\sqrt{1+m^2+n^2}} \frac{1+m^2+2n^2}{(1+n^2)(m^2+n^2)} + \frac{2}{\pi} \sin^{-1} \left(\frac{m}{\sqrt{m^2+n^2} \sqrt{1+n^2}} \right) \quad [3.7]$$

where $m = c/d$ and $n = 2z/d$

It is common geotechnical practice, in fact, to consider only vertical stress increases when calculating settlements of shallow foundations (Schmertmann 1986), and to use the results of one-dimensional consolidation tests to evaluate the compressibility characteristics of the various soil layers (Holtz and Kovacs 1981). In the one-dimensional uniaxial case, the lateral strains are neglected and the resulting vertical strains for the influence factor can be calculated from:

$$\varepsilon_z = \frac{\Delta\sigma_z}{D'} \quad [3.8]$$

For the special case with $\nu = 0$, the interrelationship is $D' = E'$. Using the calculated vertical stress changes with depth for a circular area of unit diameter ($d = 2a = 1$) under unit stress ($q = 1$) over a homogeneous elastic material of unit modulus ($D' = 1$), it is an easy matter to calculate the incremental strains via a spreadsheet and numerically integrate the results over a specified depth of interest. The distributions of unit vertical strains (ΔI_z) with depth are shown in **Figure 3.2**. The strains are summed over a large dimensionless depth ($z^* = z/d > 25$) on a spreadsheet to give a practical solution to the semi-infinite elastic half-space ($z^* = \infty$). For the case where $\nu = 0$, the integration of ΔI_z with depth gives a cumulative influence factor $I = 1$, corresponding to the general Boussinesq case. For the

more general case of triaxial stresses, the incremental increase in horizontal stress for axisymmetrical loading under a uniform circle is given by (Poulos and Davis, 1974):

$$\Delta\sigma_r/q = \frac{1}{2} + \nu' - \frac{(1+\nu')}{[1+(a/z)^2]^{0.5}} + \frac{1}{2 \cdot [1+(a/z)^2]^{1.5}} \quad [3.9]$$

For these situations ($\nu > 0$), the vertical strains ϵ_z can be calculated using both $\Delta\sigma_z$ (eqn 3.6) and $\Delta\sigma_r$ (eqn 3.9) with Hooke's Law (eqn 3.5), giving the other curves shown in **Figure 3.2**. These approximate the rigorous solutions for a rough or adhesive interface between the elastic compressible medium and underlying incompressible layer. In fact, these serve as the basis for the well-known footing settlement method using CPT results introduced by Schmertmann (1970) and revised method (Schmertmann et al. 1978).

Using a spreadsheet, the integral sign for calculating displacement influence factors is replaced by the summation over small layers. Thus, for a homogeneous soil, the influence factor is:

$$I_h = \sum \Delta I_z \cdot (\Delta z/d) \quad [3.10]$$

3.4 Poisson's Ratio

Recent research has shown that the drained value of Poisson's ratio (ν') corresponding to foundation settlements is less than earlier thought (Mayne and Poulos, 1999). The conventional external measurements of specimen strains in routine laboratory triaxial tests have been found to reflect difficulties due to end effects, stress nonuniformity, capping problems, and seating errors, resulting in the reporting of inappropriate values

of ν' on the order of 0.30 to 0.45 and measured soil stiffnesses that are too low (Jamiolkowski, et al., 1994, LoPresti, 1995).

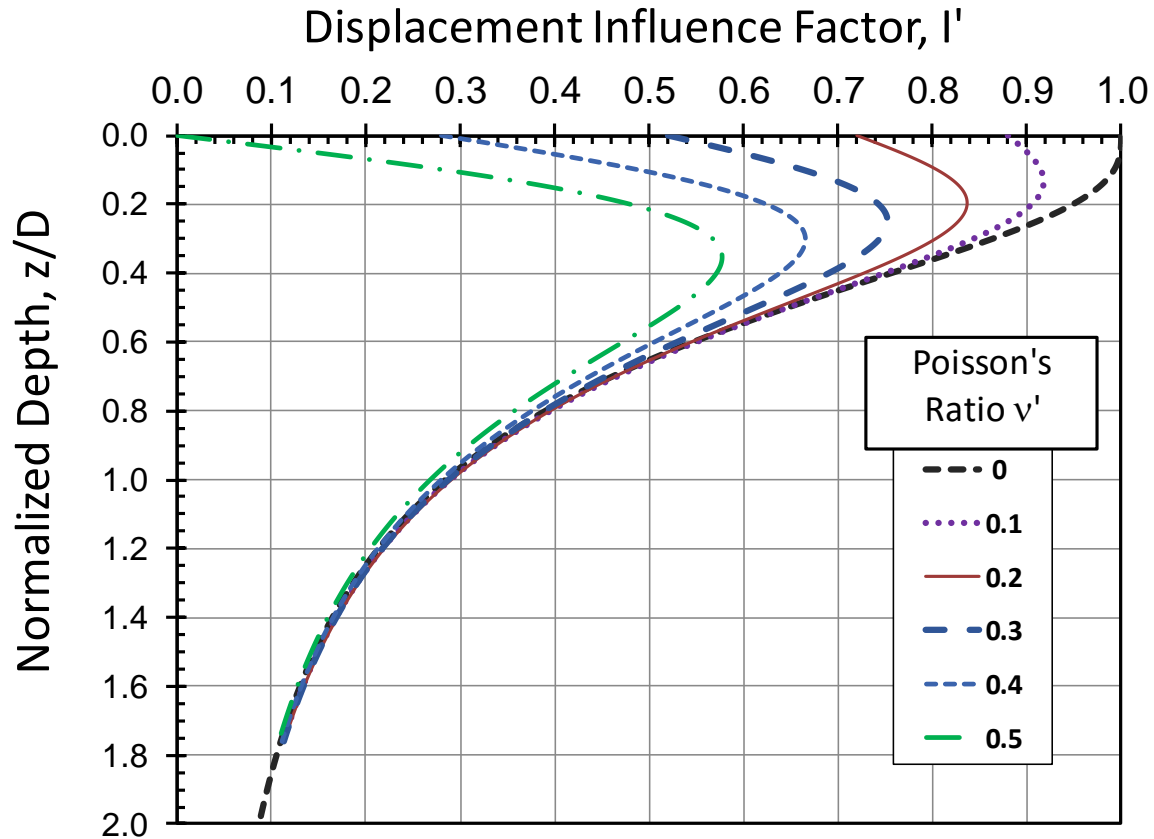


Figure 3.2 Strain Influence Factors from Elastic Theory for a Circular Foundation and Varying Soil Poisson's Ratio

Accurate measurements are now possible using local strain devices mounted midlevel on soil specimens and measured internally to the triaxial cell (e.g., Tatsuoka and Shibuya, 1992). The range of strain levels relevant to foundation deformation problems is between 0.01% and 0.2% (Jardine, et al. 1985; Burland, 1989), and therefore, the appropriate value of Poisson's ratio to use in elastic continuum solutions for drained loading is $0.1 < \nu' < 0.2$ for all soil types, including sands (Tatsuoka, et al., 1994; Lehane & Cosgrove 2000) and clays (Jamiolkowski et al., 1995; LoPresti et al., 1995).

For undrained conditions involving short-term loading of clays, it remains appropriate to use the value from elastic theory with $\nu_u = 0.5$. However, this case is not considered applicable to the method and procedures discussed in this report.

3.5 Finite Layer Thickness

For situations where the compressible geomaterial layer is of finite thickness (h) and underlain by an incompressible stratum (bedrock), spreadsheet integration is performed over a limited depth from $z = 0$ to $z = h$ (Széchy and Varga, 1978). The displacement influence factor (I_h) can be expressed in terms of the foundation geometry (expressed in the rectangular distortion ratio, c/d) and in terms of normalized layer thickness, h/d . An algorithm to fit the Harr (1966) solution can be expressed as:

$$I_h = \frac{1}{0.9 - \frac{1}{1.69 + 2.08 / [(c/d) - 0.8]} + [0.116 \cdot \ln(c/d) + 0.654] \cdot \frac{1}{(h/d) + 0.001}} \quad [3.11]$$

Results for the displacement influence factor (I_h) are shown in **Figure 3.3** for a uniformly-loaded (flexible) rectangular foundation with different distortion ratio (c/d) ranging from $c/d = 1$ for a square footing to $c/d > 10$ for a strip footing. The soil layer is finite and represented by the ratio of thickness to width (h/d).

3.6 Foundation Rigidity

The foundation stiffness affects the overall distribution of stresses and corresponding displacements. Analytical solutions for a infinitely thick layer indicate that the magnitude of deflection of a rigid circular footing is 0.785 times that of the centerpoint of a flexible

foundation. Thus, it is convenient to define a foundation flexibility factor (after Brown, 1969b):

$$K_F \approx \frac{E_{FDN}}{E_{s(av)}} \cdot \left(\frac{t}{a}\right)^3 \quad [3.12]$$

where a = foundation radius, E_{FDN} = elastic modulus of foundation material (reinforced concrete), $E_{s(AV)}$ = representative elastic soil modulus beneath the foundation base (i.e., value of E_s at depth $z = a$), and t = foundation thickness. If the percentage of concrete and reinforcing steel are known, the value of E_{FDN} may be calculated. Alternatively, for many reinforced concrete foundations, an approximate value may be assumed on the order of $E_{FDN} \approx 30 \text{ GPa} = 313,283 \text{ tsf}$.

The above definition of foundation flexibility is reasonable for footings and rafts, even though the nominal effects of ν' have been omitted (Horikoshi and Randolph, 1997). The variation of displacement influence factor for a circular foundation resting on an infinite elastic half-space has been previously evaluated in terms of the foundation flexibility factor, K_F , using finite element analysis (Brown, 1969b), as presented in **Figure 3.4**. The limiting values from analytical solutions for perfectly flexible and perfectly rigid are shown at $I_F = 1$ and $\pi/4$, respectively. According to **Figure 3.4**, the following categories can be made: (a) perfectly rigid with $K_F > 10$; (b) intermediate flexibility with $0.01 < K_F < 10$, and (c) perfectly flexible with $K_F < 0.01$. As an approximation, the aforementioned influence factor can be expressed as a correction factor for foundation flexibility (or rigidity):

$$I_F \approx \frac{\pi}{4} + \frac{1}{4.6 + 10 \cdot K_F} \quad [3.13]$$

Flexible Rectangular Footings

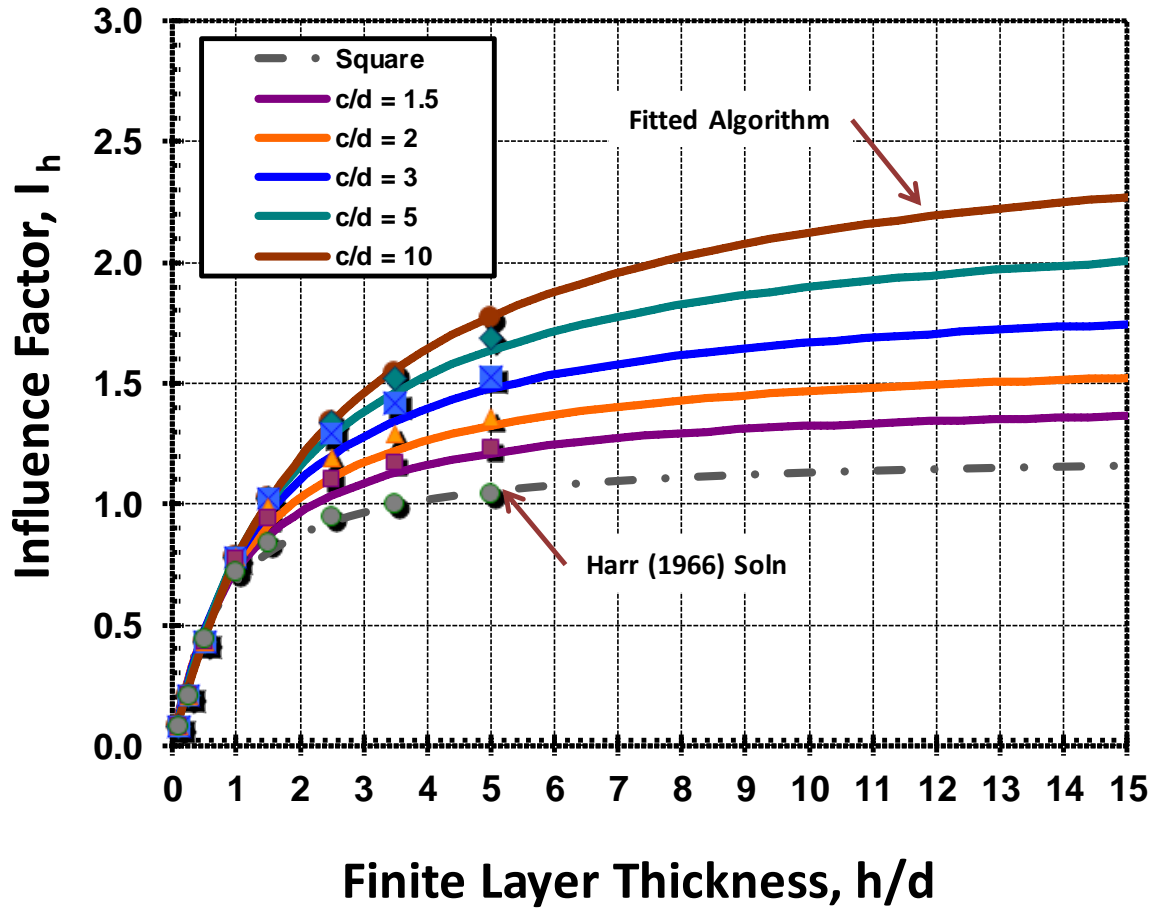


Figure 3.3 Displacement Influence Factors for Flexible Rectangular Footing of Different Geometries on Finite Elastic Layer.

For a rectangular raft or structural mat or footing, Horikoshi and Randolph (1997) discuss the expressions available for foundation flexibility. In order to be compatible for the expression for the circular foundation stiffness, the most rational definition for a rectangular foundation is given by:

$$K_F = 5.57 \cdot \frac{E_{mat}}{E_{soil}} \cdot \frac{(1 - \nu_s^2)}{(1 - \nu_{mat}^2)} \cdot \left(\frac{B}{L}\right)^{0.5} \cdot \left(\frac{t}{L}\right)^3 \quad [3.14]$$

where B = raft (mat) width, L = raft length, t = mat thickness. Here, $E_{mat} = E_{FDN}$ as detailed earlier.

Note that for a rigid circular footing, the magnitudes of settlements are equal at the center and edge, whereas for perfectly flexible circular mats, the edge settlements are about two-thirds the magnitude of the centerpoint settlement. Thus, the settlements at the edge of a circular foundation (ρ_{edge}) can be approximately given by:

$$\frac{\rho_{edge}}{\rho_{center}} \approx 1 - \frac{1.533}{4.6+10 \cdot K_F} \quad [3.15]$$

If analyzing a square or rectangular footing, a similar approach can be established because the corner settlements of a perfectly flexible foundation are about one-half those at the centerpoint, whereas for a rigid foundation all points are the same (Poulos and Davis, 1974). So, for square and rectangular foundations, the magnitude of corner settlements can be calculated from:

$$\frac{\rho_{corner}}{\rho_{center}} \approx 1 - \frac{2.3}{4.6+10 \cdot K_F} \quad [3.16]$$

A rigorous solution shows some slight dependency on the finite layer thickness (Fraser and Wardle, 1976). For consistent comparisons in results, the evaluation of foundation flexibility for slender rectangular rafts should be made using the procedure of Horikoshi and Randolph (1997).

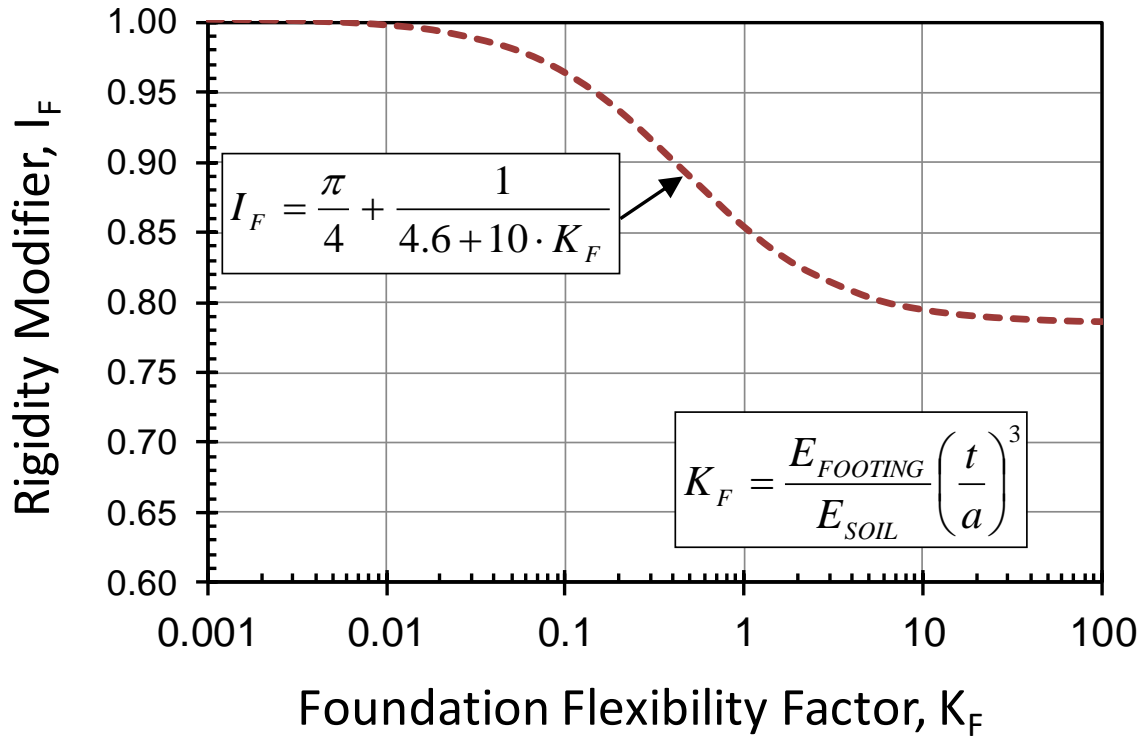


Figure 3.4 Effect of Foundation Rigidity on Centerpoint Settlement of Circular Foundation (after Mayne and Poulos, 1999)

3.7 Foundation Embedment

Most footings are embedded below grade in order to protect against frost heave, erosion, and facilitate construction. In many textbooks, the effect of foundation embedment on the settlement response has apparently been overestimated because of the erroneous mixing of various elastic solutions. A detailed discussion of this topic is given by Christian and Carrier (1978). A numerical assessment by finite elements (Burland, 1970) provides a more realistic evaluation of the problem. The correction factor (I_E , or originally designated μ_0) has been presented in terms of the ratio of embedment depth (z_e) to foundation diameter (d) and Poisson's ratio (ν) of the supporting soil medium, as shown in **Figure 3.5**. The effects of embedment can be seen to be relatively modest, unless the foundation

rests quite deep. The numerical results can be roughly expressed by the empirical formula:

$$I_E \approx 1 - \frac{1}{3.5 \cdot \exp(1.22\nu - 0.4) \cdot (1.6 + \frac{d}{z_e})} \quad [3.17]$$

3.8 Final Form of Settlement Equation

The final form of the settlement equation for shallow rectangular spread footing foundations that accounts for foundation dimensions, finite layer thickness, footing flexibility, and embedment is given by:

$$s_c = \rho_c = \frac{q \cdot B \cdot I_h \cdot I_F \cdot I_E \cdot (1 - \nu^2)}{E'} \quad [3.18]$$

where s_c = centerpoint settlement, q = uniform applied stress, B = the width (smaller dimension of rectangular footing), I_h = foundation geometry influence factor, I_F = foundation flexibility influence factor, I_E = embedment factor, and E' = representative elastic modulus of the supporting soil medium.

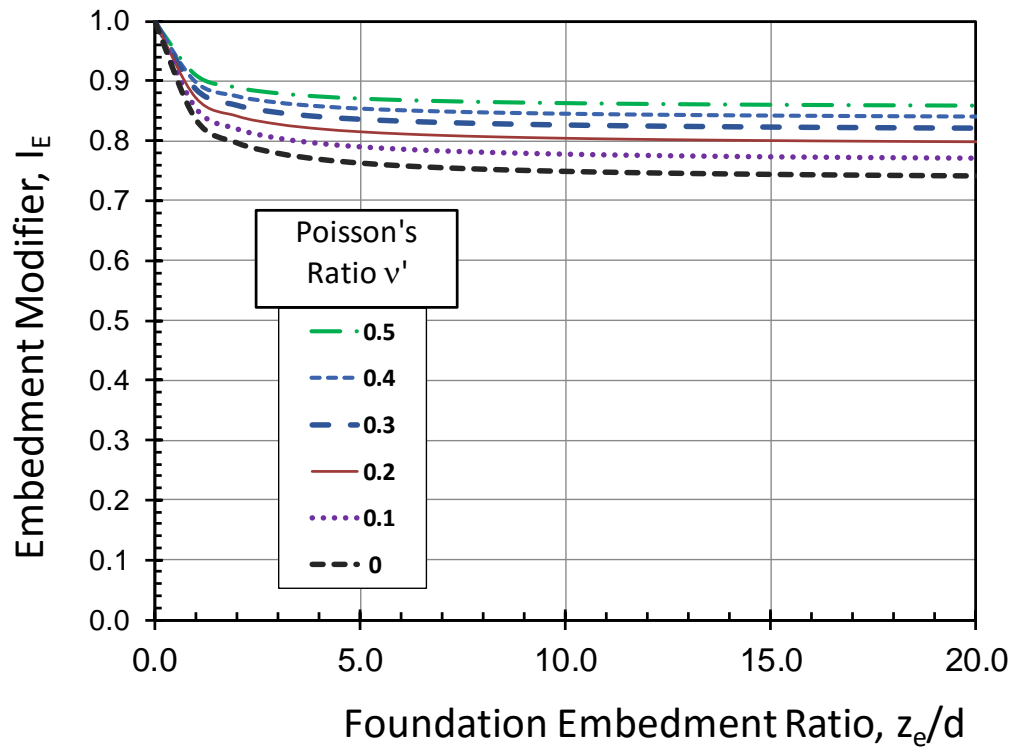


Figure 3.5 *Embedment Modifier Term for Shallow Foundation Settlements (after Mayne and Poulos, 1999)*

4. Input Parameters Using Standard Penetration Tests (SPT)

4.1 Overview of the Standard Penetration Test (SPT)

The standard penetration test (SPT) is performed during the advancement of a soil boring to obtain an approximate measure of the dynamic soil resistance, as well as a disturbed drive sample (split barrel type). The test was introduced by the Raymond Pile Company in 1902 and remains today as one of the most common in-situ test worldwide following AASHTO T206 and ASTM D 1586 standards. The main advantages of the SPT are obtaining both a sample and a number. The test is simple, rugged, and suitable in many soil types except for soft clays and coarse gravels. The SPT is usually performed using a conventional geotechnical drill rig and can provide a rough index of the relative strength and compressibility of the soil.

The SPT is conducted at the bottom of a soil boring that has been prepared using either flight augers or rotary wash drilling methods. At depth intervals of about 1.5 m (5 ft), the drilling process is interrupted to perform the SPT which involves driving a thick hollow open pipe at the bottom of the borehole during impacts from a drop hammer.

4.2 Equipment

Equipment necessary for performing a standard penetration test include a rotary drill rig, drilling rods, split-barrel (or split spoon) sampler, and a drop weight system. A truck-mounted drill rig is shown in **Figure 4.1) a** and track-mounted rig in **Figure 4.1) b**. Illustrative views of the split barrel sampler are presented in **Figure 4.2**. Over the past century, different types of SPT hammer systems have been used, including: pinweight,

donut, safety, and automatic free-fall versions. The SPT resistance is highly-dependent upon the type of hammer and energy efficiency, and also influenced by the borehole size, type of rods, length of rods, operator performing the test, and other factors (Skempton 1986; Kulhawy & Mayne 1990).



Figure 4.1 *Drilling Rigs for Conducting SPT: (a) CME truck rig (b) GeoProbe Systems*

4.3 Procedures

Test procedures for the SPT consist of repeatedly dropping a 63.5-kg (140 lb) hammer from a height of 760 mm (30 in) to drive a split-barrel sampler three successive vertical increments of 150 mm (6 in) each, as illustrated in **Figure 4.3**. The number of blows required to drive the sampler each increment and recorded. The initial increment is considered a seating drive. The blows required for the second and third increments are totaled to provide number of blows/300 mm (i.e., blows/foot), referred to as the measured SPT resistance or “N-value” (Sabatini et al., 2002).



Figure 4.2 *Split-Barrel Samplers used in SPT: (a) closed and (b) open*

Since the SPT is highly dependent upon the equipment and operator performing the test, it is often difficult to obtain repeatable results, particularly amongst different drillers and rigs at the same site. The factors affecting the SPT results include energy inefficiency, type of hammer, number of rope turns, conditions of sheaves and rotating cathead (e.g., lubricated, rusted, bent, new, old), age of rope, actual drop height, vertical plumbness, weather moisture conditions (wet, dry, freezing), inadequate cleaning of hole, careless measure of drop, inaccurate hammer weight, eccentricity of drop, and other issues (Skempton 1986; Sabatini et al. 2002).

When performing an SPT and recording information on the field log, the following items are of note: (1) N is always recorded as an integer; (2) a test is ended and noted as SPT “refusal” if driving resistance is recorded as 50 blows over a 25-mm increment or less (e.g. $N > 50/1''$); and (3) if the N-value is less than one, then the geoenvironmental or engineering geologist should record the actual penetration that occurred. For instance, in very soft clays, a value of 1 blow could drive the split barrel sampler the entire vertical distance (i.e., 1/18"), or no driving performed whatsoever, but merely the full or partial

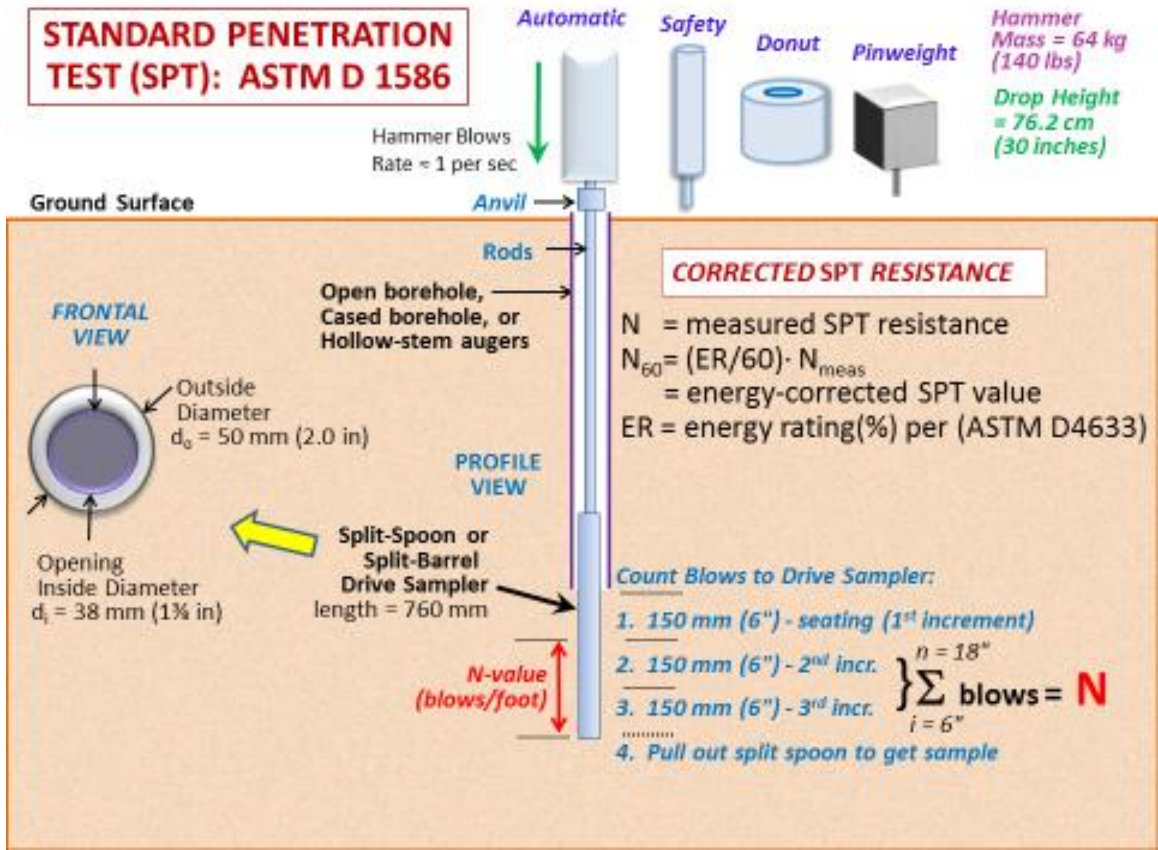


Figure 4.3 Illustration of Setup and Procedure for the Standard Penetration Test (SPT)

penetration occurred due to the added weight of the hammer (WOH) or even just the weight of the rods (WOR).

In the USA, for the most part, many drilling and field testing firms have upgraded to an auto-hammer system in order to facilitate the operations and obtain more consistent results. **Figure 4.4** shows a selection of auto-hammers available for commercial SPT work.

SPT AutoHammers

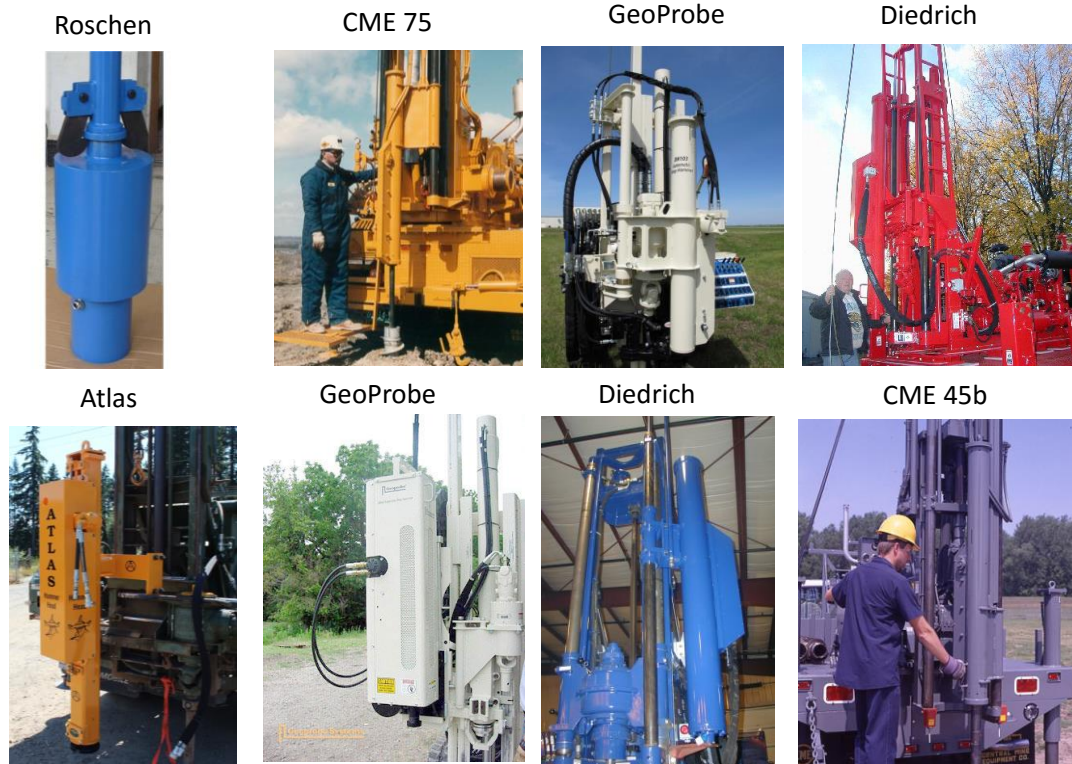


Figure 4.4 Various AutoHammers from Different Manufacturers

4.4 Corrections to the SPT N-value

Numerous correction factors to the measured N-value are necessary because of energy inefficiencies and procedural variation in practice. When all factors are applied to the field recorded N-value (N_{meas}), the corrected SPT-N value is calculated as:

$$N'_{60} = C_E \cdot C_B \cdot C_S \cdot C_R \cdot N_{\text{measured}} \quad [4.1]$$

where the approximate magnitude of corrections for energy efficiency (C_E), borehole diameter (C_B), sampling method (C_S), and rod length (C_R) as presented in **Table 4.1** are discussed elsewhere (Skempton 1986, Kulhawy & Mayne 1990, Youd et al. 2001, Boulanger & Idriss 2014). The most important factor is the energy efficiency which is

obtained by a one time calibration using the procedures outlined in ASTM D 4633. Note, in some instances, such as nuclear power plant investigations, the calibration must be checked annually.

The efficiency of the system can be obtained by comparing the kinetic energy, KE, ($KE = \frac{1}{2}mv^2$), with the potential energy, PE, of the system, ($PE = mgh$), where m = mass, v = impact velocity, $g = 9.8 \text{ m/s}^2 = 32.2 \text{ ft/s}^2$ = gravitational constant, and h = drop height. The energy ratio (ER) is defined as KE/PE . The theoretical energy of a free-fall system is 4200 in-lb (140 lb falling 30 inches), but is always less due to frictional losses, eccentric loading, wear, and other factors. Calibration of energy efficiency recommended by ASTM D-4633 with strain gages and accelerometer measurements (usually not done by commercial firms). Standard of practice varies from about 35% to 85% with cathead system, but averages about 60%. Newer automatic trip-hammers are available that provide consistent results, however the energy efficiencies still may range from 45% to 97% and depend upon the specific system.

When the necessity for correcting SPT values for energy inefficiency were finally acknowledged circa 1985, a mean $ER \approx 60\%$ was the average standard of practice based on the 1902 to 1985 timeframe (Skempton 1986; Kulhawy & Mayne 1990). The N-values had been primarily obtained from safety and donut hammers, with some data from older pinweight types. Unfortunately, the reference value was established for that timeset (1985) and raw SPT resistances must now always be corrected to N_{60} , corresponding to an energy efficiency of 60%.

Table 4.1 Definition of different correction factors: depth effect (C_N), energy efficiency (C_E), borehole diameter (C_B), sampling method (C_S), and rod length (C_R)

Factor	Influencing Variable	Field Case	Factor Values
C_N	Depth effect due to increasing effective overburden stress (σ_{vo}')	Note: $\sigma_{atm} = 1$ atmosphere = 1.013 bars = 101.3 kPa = 1.058 tsf	$C_N = (\sigma_{atm}/\sigma_{vo}')^{0.5} \leq 2$
C_E	$C_E = ER/60$ where ER = hammer energy ratio (ASTM D 4633)	Hammer Type: <i>Automatic:</i> <i>Safety:</i> <i>Donut:</i> <i>Pinweight:</i>	Range of Factor C_E 1.0 to 1.6 0.8 to 1.3 0.6 to 0.8 0.5 to 0.7
C_B	Borehole diameter, b (mm)	$65 < b \leq 115$ b = 150 mm b = 200 mm	$C_B = 1.00$ $C_B = 1.05$ $C_B = 1.15$
C_S	Split-barrel sampler	With liner: No liner:	$C_S = 1.0$ $C_S = 1.2$
C_R	Drill rod length, L (meters)	L > 10 m 6 < L < 10 m 4 < L < 6 m 3 < L < 4 m L < 3 m	$C_R = 1.00$ $C_R = 0.95$ $C_R = 0.85$ $C_R = 0.80$ $C_R = 0.75$

*Note: common US practice is no liner.

Figure 4.5 shows results from two side-by-side borings with SPTs at the same site in Vermont, as conducted for the Vermont Department of Transportation (VTRANS). This case exemplifies the need for correcting N-values to a common reference energy level. The energies were measured for each strike of the hammer and gave an average ER of 81 % for the CME auto hammer and an average ER of 48 % for the safety hammer at this site. The individual trends for the measured N-values from CMR auto and safety hammers are

quite apparent in **Figure 4.5a** whereas a consistent profile is obtained in **Figure 4.5b** once the data have been corrected to ER = 60%. The N values corresponding to 60 % efficiency are termed N_{60} and are given by:

$$N_{60} = (ER/60) \cdot N_{\text{measured}} \quad [4.2]$$

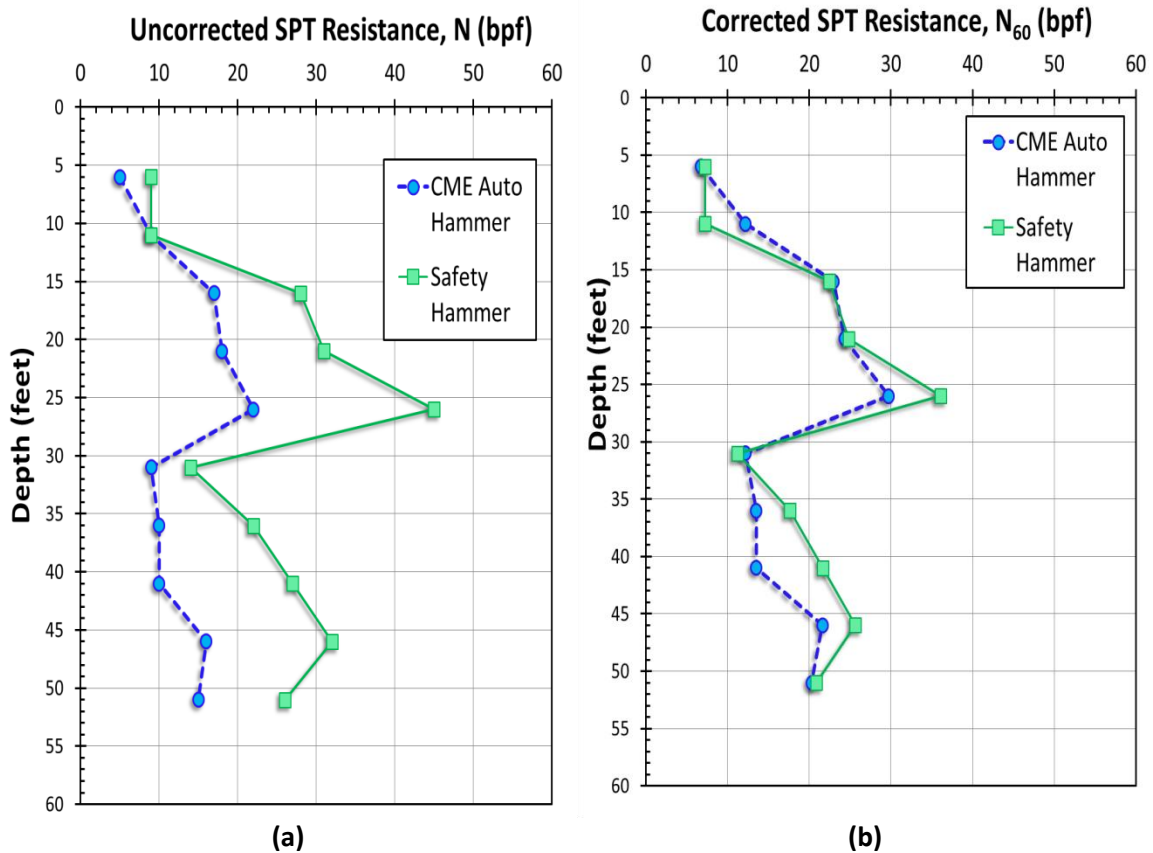


Figure 4.5 SPT- N values from Vermont: (a) Uncorrected data; and (b). Corrected data to 60 % efficiency. (Data from VTRANS, 2008)

A second example of the large differences in N -values obtained from two different hammer systems is presented in **Figure 4.6**. The SPTs have been performed at the national geotechnical experimentation site (NGES) at Northwestern University, Evanston, Illinois. The results are from tests in a fine sand layer ($0.15 \text{ mm} < D_{50} < 0.30 \text{ mm}$) that extends to a depth of around 6.7 m (22 ft). The two sets of N -values were obtained using a safety hammer and an auto hammer.

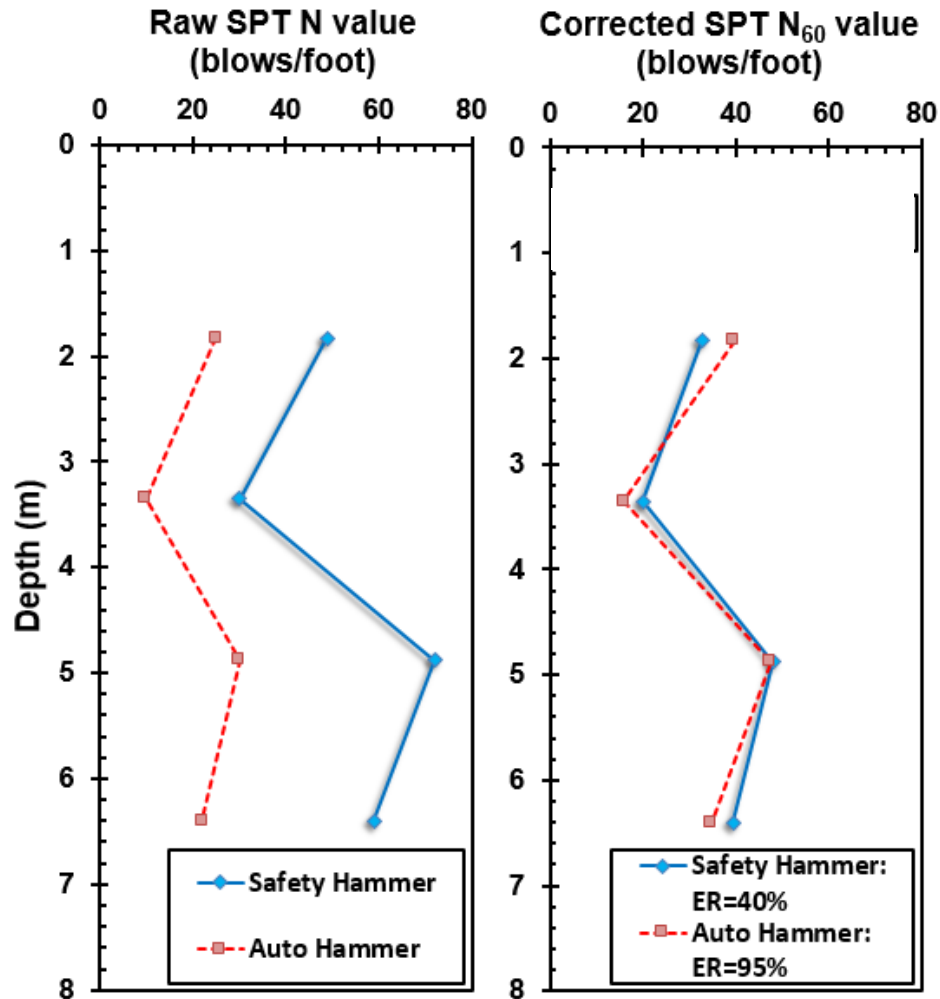


Figure 4.6 SPTs at Northwestern University: (a) Uncorrected N values; (b) Energy-Corrected N_{60} values.

Using the above energy corrections, it is evident that the corrected N_{60} profiles are in good agreement for both hammer systems. However, without the ER correction, the SPT resistances from the auto hammer are too low ($C_E = 1.58$), while those from the safety hammer are too high ($C_E = 0.67$). Both require significant corrections.

Table 4.2 Summary of Energy Ratios (ER) Measured from AutoHammers in USA

AutoHammer System	Mean Energy Ratio (ER) %	Standard Deviation of ER (%)	Location or Agency
Diedrich D-120	46	± 8.7	UDOT
Diedrich D-50	56	± 2	TN
CME 850	62.7	± 4.0	UDOT
BK-81 w/ AW-J rods	68.6	± 7.5	ASCE/WA
Mobile B-80	70.4	± 4.6	UDOT
CME hammer w skid	72.9	± 4.2	Washington
Diedrich D50	76	± 5.3	FDOT
CME 45c Skid	77.4	± 5	VTRANS
Diedrich D-120	78	± 4	TN
CME 55	78.4	± 8.2	FDOT
CME 850	79	± 2	TN
CME 45c Track	80.6	± 3.9	VTRANS
CME 45	80.7	± 10.1	FDOT
CME 45c Track	81.1	± 5.8	VTRANS
CME 85	81.2	± 3.9	FDOT
CME 75 w/ AW-J rods	81.4	± 4.7	ASCE/WA
CME 75	83.1	± 5.1	FDOT
CME 75 Track	84	± 5.3	VTRANS
CME 55 Track	85	± 4.9	VTRANS
CME 750	86.6	± 6.2	UDOT
CME 55 Track	87.4	± 5.4	VTRANS
Mobile B-57	88	± 3	TN
Mobile B-57	93	± 3	TN
CME 75 rig	94.6	± 2.1	UDOT

NOTE: Range is factor of 2.1

There is a general misconception by geotechnical engineers that if the SPT is performed using an autohammer, the results do not need to be corrected for energy content. **Table 4.2** shows a compilation of energy measurements by different organizations at different sites in the USA, all using automatic hammers. These ER data represent thousands of field measurements (ASTM D 4633) for each hammer strike and indicate a documented range of ER from 45% to 95% for autohammer efficiencies. Therefore, one cannot assume a value of ER for a valid correction of energy on a particular system. Interestingly, the state-of-the-practice using autohammers has now risen to a mean value \pm one standard deviation of $ER_{ave} \approx 82\% \pm 7\%$ based on some 17,825 ER measurements taken in the past five years (Honeycutt et al. 2014). Unfortunately, the correction reference value remains stuck to the value from 1985 vintage, i.e. N_{60} .

Since SPT N-values in the same geomaterial will increase with increasing effective overburden stress, the energy-corrected blowcount (N_{60}) is often stress-normalized to an equivalent effective overburden stress of 1 atmosphere (≈ 100 kPa ≈ 1 tsf), also called an overburden correction. The stress-normalized and energy-corrected blowcount is referred to as $(N_1)_{60}$, and is equal to:

$$(N_1)_{60} = C_N \cdot N_{60} \quad [4.3]$$

where C_N is the stress normalization parameter calculated as:

$$C_N = \left(\frac{P_a}{\sigma'_{v0}} \right)^n \quad [4.4]$$

where P_a is atmospheric pressure in the same units as σ'_{v0} (i.e., 1 atm ≈ 1 bar ≈ 100 kPa ≈ 1 tsf), and n is a stress exponent typically equal to 0.5 in clean sands (Liao & Whitman, 1986; Kulhawy & Mayne 1990) and increases to 1 in clays (Mayne & Kemper, 1988).

4.5 Soil Unit Weight from SPT

The soil unit weight (γ_t) is needed in the calculation of overburden stresses. The unit weight relates to the more fundamental mass density (ρ_t):

$$\gamma_t = \rho_t \cdot g_a \quad [4.5]$$

where g_a = gravitational constant (= 9.8 m/s² = 32.2 ft/s²).

Unit weights are best obtained by securing "undisturbed" samples (thin-walled Shelby tubes; piston samples) and weighing a known volume of soil. The ratio of weight to volume is the unit weight.

Soil identity relationships provide information about the initial state of the soil. One primary identity is:

$$G_s \cdot w_n = S \cdot e_0 \quad [4.6]$$

where G_s = specific gravity of solids (for "normal" soils: $G_s = 2.70 \pm 0.1$), w_n = natural water content, S = degree of saturation (S ranges from zero in dry soil to 100% in fully saturated soils), and e_0 = initial void ratio.

A second identity for the general case of unit weight is:

$$\gamma_t = \frac{1+w}{1+e} \cdot G_s \cdot \gamma_w \quad [4.7]$$

where γ_t = unit weight of water (= 9.8 kN/m³ = 62.4 pcf for freshwater). Depending upon the water content and degree of saturation, two boundary cases are commonly taken in soil mechanics: (a) dry soil (with $w = 0$); and (b) fully-saturated soil with $S = 1$ (and then: $e = G_s \cdot w$). This gives:

$$\text{Dry unit weight: } \gamma_{\text{dry}} = \frac{G_s \cdot \gamma_w}{1+e} \quad [4.8]$$

$$\text{Saturated unit weight: } \gamma_{\text{sat}} = \frac{G_s + e}{1 + e} \gamma_w \quad [4.9]$$

For solid rock (no voids), the unit weight is simply: $\gamma_{\text{rock}} = G_s \cdot \gamma_w$. Thus, for $G_s = 2.7$: $\gamma_{\text{rock}} = 27 \text{ kN/m}^3 = 172 \text{ pcf}$. Thus for practical use, the hierarchy for assignment of unit weights would be: $\gamma_{\text{dry}} \leq \gamma_t \leq \gamma_{\text{sat}} < \gamma_{\text{rock}}$.

For soils above the groundwater table, a dry unit weight would apply for no capillarity (i.e., clean sands), while if full capillarity exists (e.g., clays), then a saturated unit weight would be appropriate. If the soil is partially saturated, the total unit weight will depend upon the ambient degree of saturation, likely a value that changes with the weather, humidity, and temperature. For soils below the water table, it is often taken that the total unit weight is equal to the saturated unit weight. In some cases, calculations involve the effective unit weight ($\gamma' = \gamma_{\text{sat}} - \gamma_w$), also referred to as the buoyant unit weight or submerged unit weight.

When undisturbed samples or natural water contents are not available, the unit weight can be estimated from the shear wave velocity (V_s in m/s) and depth (z in meters):

$$\gamma_t \text{ (kN/m}^3\text{)} = 8.31 \log(V_s) - 1.61 \log(z) \quad [4.10]$$

The relationship is shown in **Figure 4.7** and applies to particulate geomaterials that are not cemented or bonded, thus would not be applicable to saprolites, rocks, cemented or structured diatomaceous or calcareous or carbonate soils.

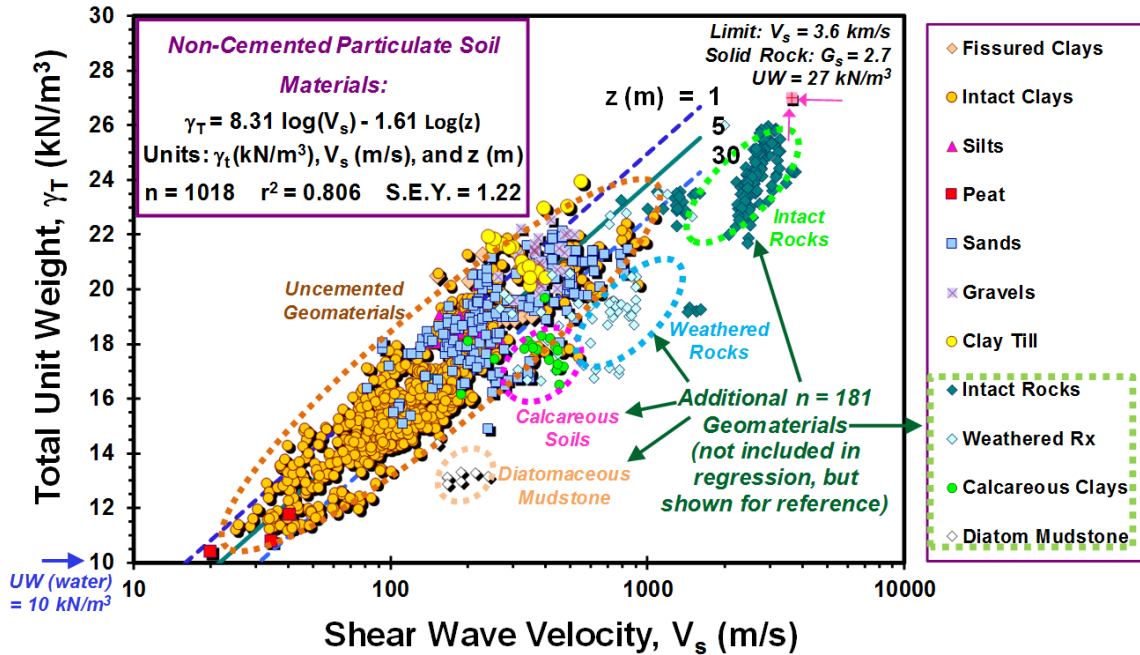


Figure 4.7 Relationship for unit weight in terms of shear wave velocity and depth (Mayne, 2001)

A more fundamental trend is derived in terms of effective overburden σ_{vo}' (in kPa) rather than depth z where γ_t is expressed:

$$\gamma_t \text{ (kN/m}^3\text{)} = 8.64 \log(V_s) - 0.74 \log(\sigma_{vo}') - 0.40 \quad [4.11]$$

where V_s (m/s) and $\sigma_{vo}' = \sigma_{vo} - u_0 =$ effective vertical overburden stress (kPa), $\sigma_{vo} = \int \gamma_t dz$ = total overburden stress, $u_0 =$ hydrostatic porewater pressure = $h_w \cdot \gamma_w$, and $h_w =$ height of the water table at that elevation.

As these estimated unit weights are in terms of saturated values, a relationship between dry and saturated unit weights can be developed from [4.8] and [4.9] to allow the evaluation of dry unit weights for those conditions (Figure 4.8).

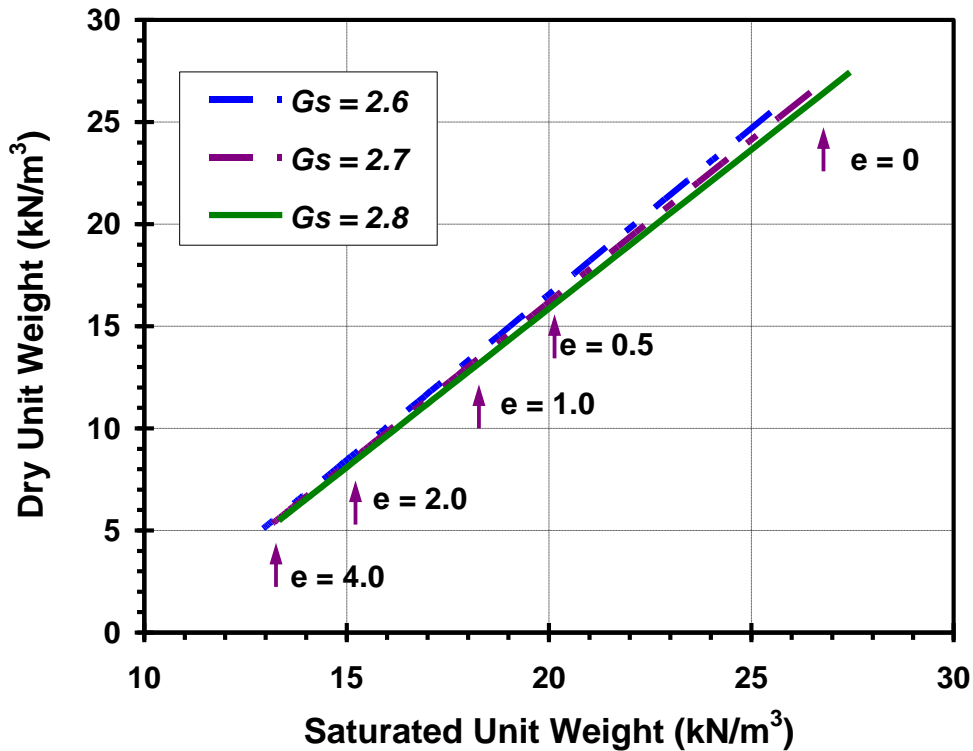


Figure 4.8 Interrelationship between dry unit weight and wet unit weight.

By using the measured in-situ SPT resistance (N value), one can estimate the corresponding shear wave velocity (V_s) value to be used in estimating in the unit weight of the soil following Equations [4.10] and [4.11].

Imai and Tonouchi (1982) compiled a database of a variety of ground conditions through Japan where they collected data points from over 400 boreholes covering different soil types ranging from alluvial to diluvial clays, gravels, peats, and sands, in addition to special soils such as loam, fill, and sirasu. The database included 1654 measured SPT resistance N values with an average energy rating of 78 % with corresponding shear wave velocity (S-wave) measured mainly using a suspension logging method. **Figure 4.9** illustrates the

direct relationship between the measured shear wave velocity (V_s) and the SPT (N-value)

and the relationship can be expressed as:

$$V_s \left(\frac{m}{s}\right) = 97.0 N^{0.314} \quad [4.12]$$

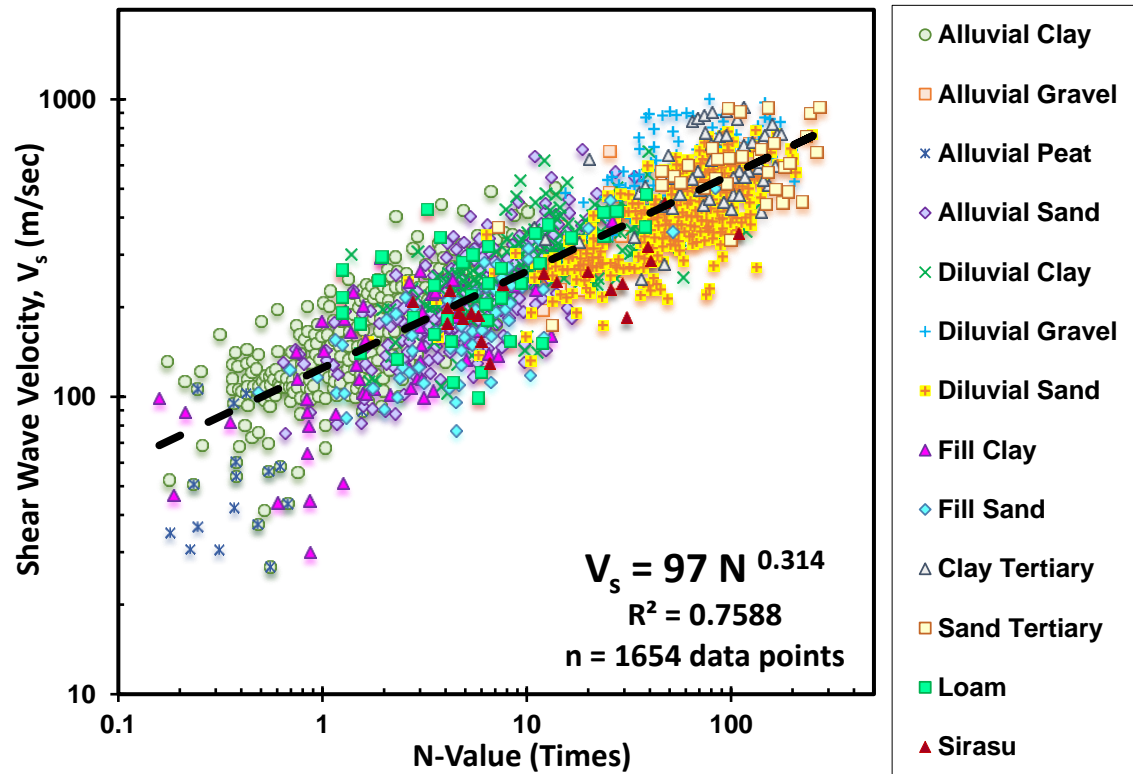


Figure 4.9 Relationship between shear wave velocity V_s and SPT N-value (data after Imai & Tonouchi, 1982)

4.6 Effective Friction Angle from SPT

In-situ penetration tests can be used to relate the effective stress friction angle (ϕ') of granular materials to the penetration resistance, which is N_{60} value for the SPT. Meyerhof (1956) presented baseline relationships for evaluating the drained friction angle of cohesionless soils, where he considered the state of packing of the granular soil

(expressed in terms of relative density) and presented typical ranges for the standard penetration resistance, N and the corresponding friction angle, ϕ' .

A more reliable correlation between ϕ' and stress-normalized SPT resistance, $(N_1)_{60}$, was derived by Hatanaka and Uchida (1996) where high quality undisturbed samples of natural sands were obtained by special freezing method. Once mounted in the triaxial cell and allowed to thaw, specimens permitted direct measurements of ϕ' in triaxial compression tests. Corresponding field SPT data were obtained at the same elevations as the undisturbed samples using a Japanese automatic trip hammer system where energy efficiency is reported as 78 percent. For an reference 60% efficiency in the U.S., the expression for peak ϕ' is presented in **Figure 4.10** and is given as:

$$\phi^\circ = \sqrt{15.4 (N_1)_{60}} + 20^\circ \quad [4.13]$$

It is important to recognize that these correlations have been developed for relatively clean sands. Some limited experience with this expression in residual silty fine sands (Mayne & Harris 1993) and fine sandy silts of the Appalachian Piedmont geology (Mayne et al. 2000) have shown good agreement with laboratory triaxial tests on undisturbed samples.

The SPT should not be used to estimate the drained friction angle of gravelly soils, unless the correlations are verified and/or modified based on local experience. The size of gravel particles can be larger than the inner diameter of the split sampler used in the SPT test, thus affecting the penetration resistance in gravelly geomaterials.

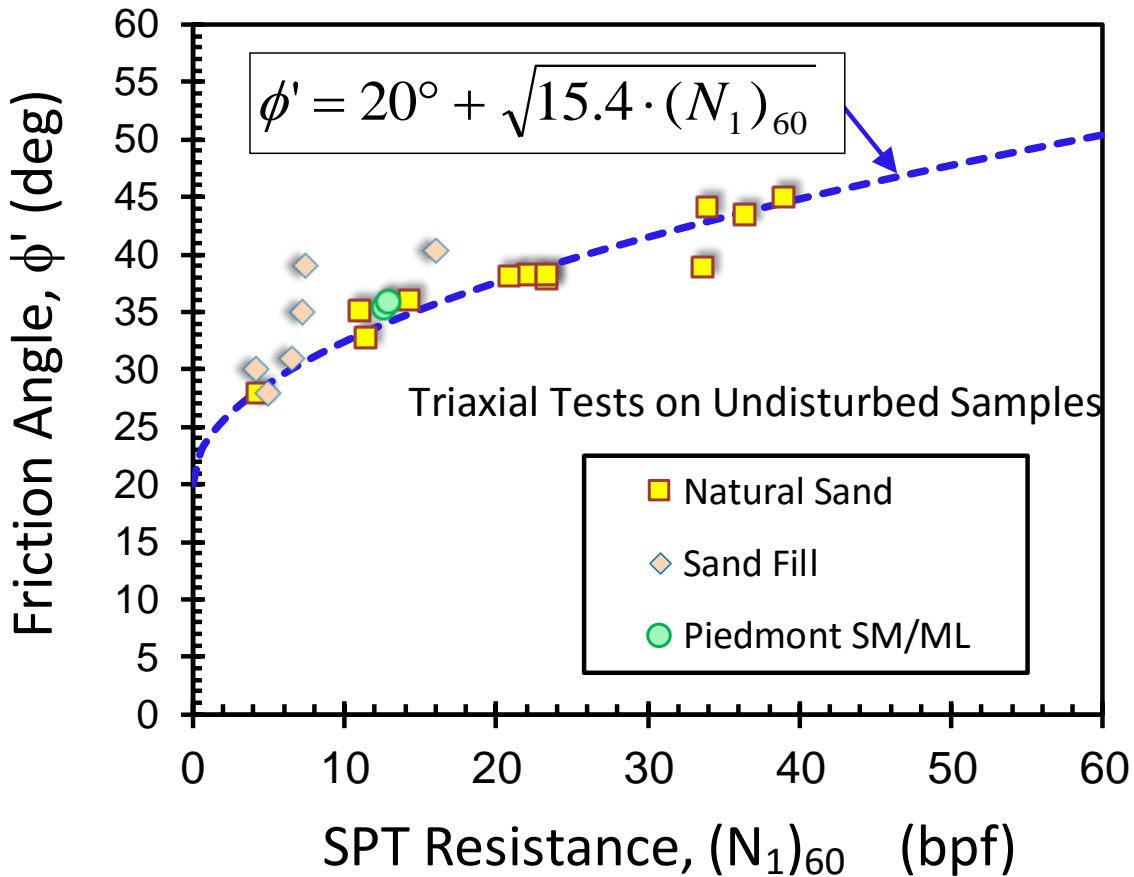


Figure 4.10 Peak friction angle of sands from SPT resistance (data from Hatanaka & Uchida, 1996; Mayne & Brown, 2003)

In the case of clays, there is no direct relationship between the SPT resistance and the effective stress friction angle. A review of compiled data for clay effective friction angle values (ϕ') from approximately 200 different clays versus their plasticity index values ($n = 453$ data points); as collected from Diaz-Rodriguez et al. (1992); Terzaghi, et al. (1996); Locat, Tanaka, and Lee (2003); Kulhawy and Mayne (1990); and Bhandari and Yatabe (2007); as presented in **Figure 4.11**, it can be seen that the clay friction angle exhibits a mean value of $\phi' = 28.6$ degrees with a standard deviation of about 5 degrees (Mayne 2013). Contrary to some claims, no correlation for ϕ' with PI exists for natural clays.

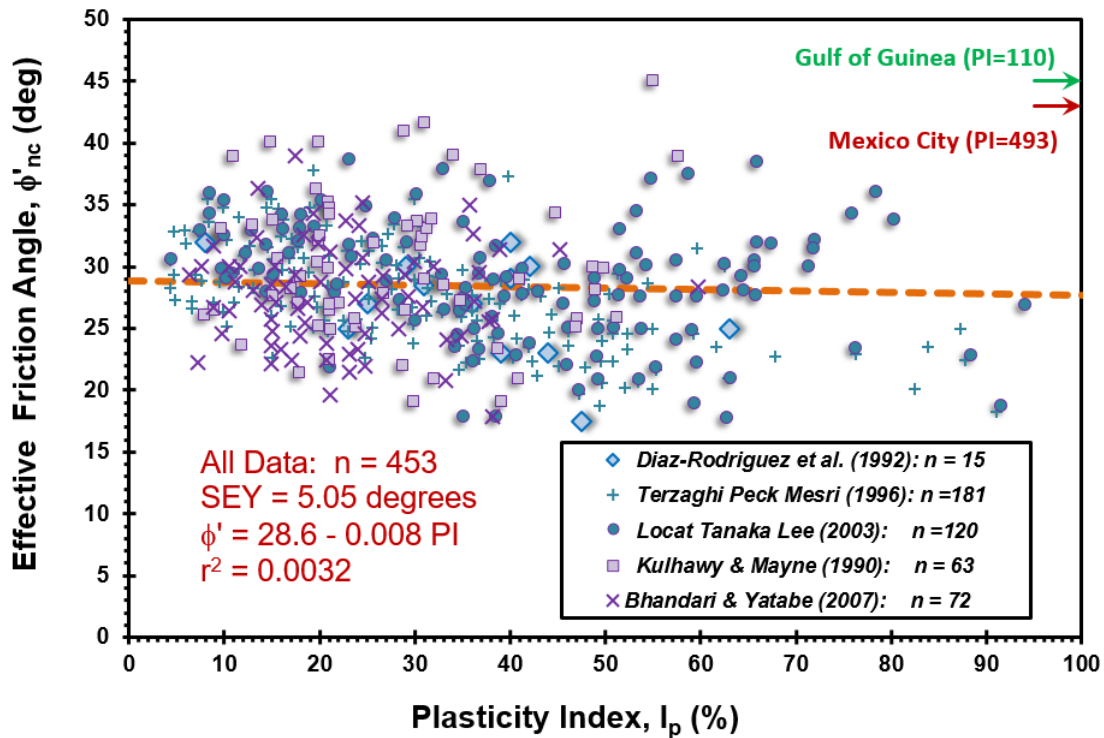


Figure 4.11 Effective stress friction angle of clays versus Plasticity Index

4.7 Soil Modulus of Elasticity from SPT

Elasticity theory can be used to represent the stiffness of soil where it allows for interrelationships between the equivalent elastic Young's modulus (E'), shear modulus (G'), and constrained modulus (D') in terms of the Poisson's ratio (ν'). In-situ methods such as the flat dilatometer test (DMT) and pressuremeter test (PMT) can be directly used to measure an elastic modulus (E') which in turn can be related to corrected penetration resistance (N_{60}) measured at the same location.

For the Piedmont residual soils, Mayne & Frost (1988) compiled over 160 flat dilatometer tests with supplementary routine soil borings and cone penetrometer soundings in the vicinity of Washington DC, VA, and MD. The DMT elastic moduli were compared with

values obtained from laboratory tests and backcalculated moduli from field performance of full-scale foundation measurements. By considering the SPT penetration resistance measured at the same testing locations which had an average energy rating of 60 % in the late 1980s, a direct relationship between the derived elastic modulus (E') obtained from flat dilatometer tests (DMT) assuming $\nu' = 0.2$ and corrected SPT penetration resistance (N_{60}) was developed, as shown in **Figure 4.12** and expressed by:

$$E_D \text{ (bars)} = 22 \cdot \sigma_{atm} \cdot (N_{60})^{0.82} \quad [4.14]$$

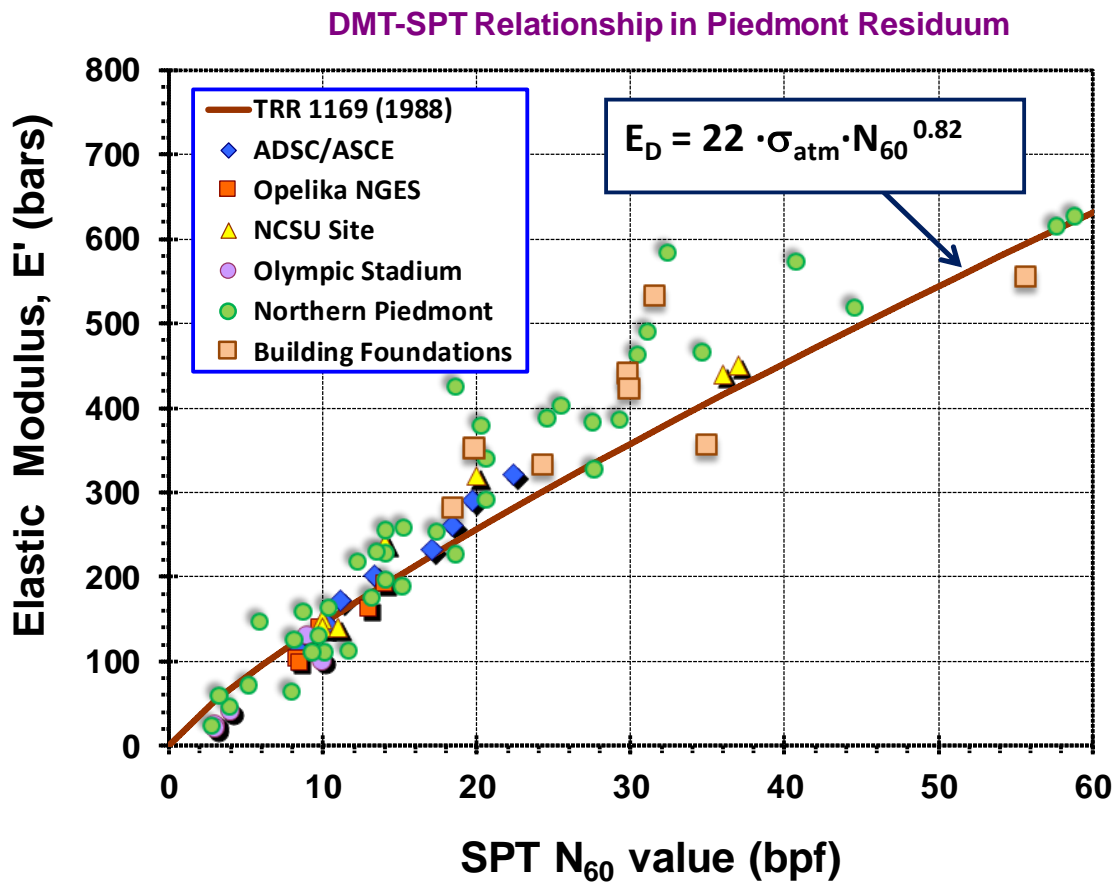


Figure 4.12 DMT modulus versus SPT relationship in Piedmont Residuum (data from Mayne & Frost, 1988)

The database was expanded to include more soil types such as silty sands and clayey sands (Atlantic Coastal Plain) and plotting them with the residual silts and sands of the Piedmont geology as presented in **Figure 4.13**. It can be seen that Equation 4.14 is still valid and applicable, yet can be considered on the conservative side for some of the sands.

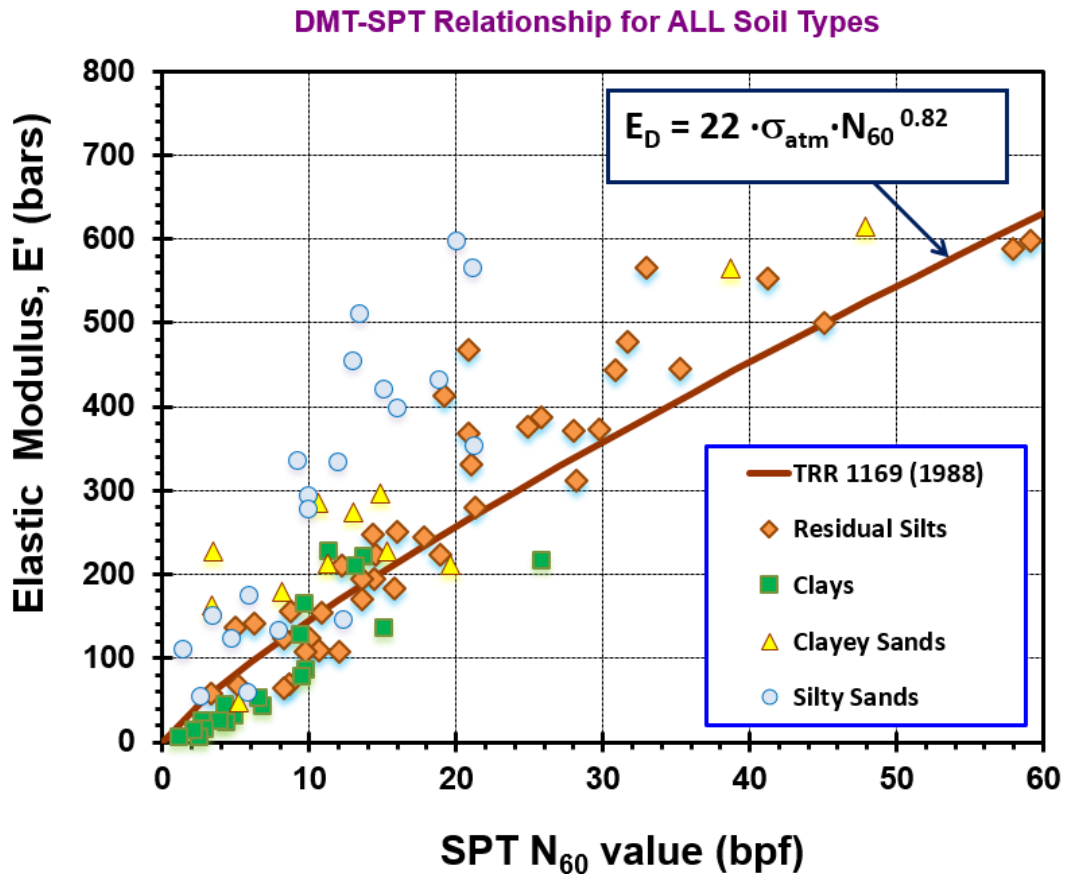


Figure 4.13 *DMT modulus versus SPT N_{60} relationship for a variety of soil types (modified after Gordon & Mayne 1986).*

4.8 Stress History from SPT

The stress history of a soil can be used to represent the geological conditions and evolutionary changes that the soil has undergone over the years and thus be considered as the focal point for geotechnical design applications since it relates to many

fundamental aspects of the soil behavior in terms of strength, stiffness, and compressibility. The preconsolidation stress (σ_p') can be defined as the maximum effective overburden stress experienced by the soil during its stress history. Soils are often prestressed because of overburden removal, erosion, glaciation, and/or excavation, which are mechanical means. Also, soils can develop a pseudo-preconsolidation due to effects of ageing, desiccation, groundwater changes, exposure to wet-dry cycles, and repeated freezing-thawing. The overconsolidation ratio (OCR) is a classic normalized and dimensionless parameter based on the σ_p' and effective vertical stress (σ_{v0}'), such that:

$$\text{OCR} = \sigma_p' / \sigma_{v0}' \quad [4.15]$$

The most basic and conventional means to determine stress history is via laboratory one-dimensional consolidation testing per ASTM D2435. The specimens are subjected to constrained compression in either a mechanical oedometer, electro-pneumatic or hydraulic consolidometer, or automated constant rate of strain (CRS) device. On the basis of the consolidation test, many methods have been proposed to delineate σ_p' from the compression measurements. However, the results are dependent on the plotting methods and curve-fitting procedures. Laboratory based techniques are associated with many issues, including: disturbance which can be attributed to the sampling process, specimen handling, and stress relief due to removal of the sample from depths beneath the ground surface. To overcome issues associated with laboratory methods, σ_p' can be determined using direct correlations with in-situ test measurements such as standard

penetration, cone penetration, flat dilatometer, and/or vane shear tests that are faster, more economical, and productive than laboratory tests.

Kulhawy and Mayne (1990) investigated the relationship between the SPT resistance (N) and the effective preconsolidation stress (σ_p') for 51 fine-grained soils. These were mainly firm to stiff to hard clays which were not sensitive nor structured, resulting in the following expression:

$$\sigma_p' \approx 0.47 \cdot \sigma_{atm} \cdot N \quad [4.16]$$

Although the reported penetration resistance values were not specifically corrected for energy efficiency, the SPT data were obtained primarily using safety hammers for which the average ER \approx 60%. Later, a more detailed study investigated the relationship between energy-corrected standard penetration resistance (N_{60}) and the preconsolidation stress for different soil types as presented in **Figure 4.14** and as expressed:

$$\sigma_p' \approx 0.47 \cdot \sigma_{atm} \cdot (N_{60})^m \quad [4.17]$$

where m is an exponent that depends on the soil type: m = 0.6 for clean quartzitic sands and gravels, m = 0.7 for silty or clayey sands, m = 0.8 for sandy silts (e.g., Piedmont), m = 0.9 for silts to clayey silts, and m = 1.0 for intact “vanilla” clays (Mayne 1992). Fissured clays may exhibit an exponent value with 1.1 or higher, depending upon the extent and frequency of the discontinuities and joints.

The OCR can then be calculated from eqn [4.15]. For clays and silts where the $OCR < 1$, an underconsolidated state is identified. This is a very precarious and unstable condition and should be reviewed by the chief engineer and/or senior geotechnical engineer.

Clays and silts with $1 < OCR < 2$ are normally consolidated to lightly overconsolidated deposits that are prone to problems of instability, bearing capacity, and high compressibility problems, and these too should be reviewed by senior geotechnical staff. Since there is some uncertainty in the correlative trends, a value of $OCR < 3$ has been used to conservatively identify these soft clays and silts. Additional laboratory and/or in-situ testing may be warranted before proceeding forward with foundations in these geomaterials.

Soils exhibiting a range: $2 < OCR < 10$ are moderately overconsolidated and generally do not exhibit difficulties during construction and not normally associated with issues of strength, compressibility, and stiffness.

Finally, fine-grained soils that have very high OCRs > 30 are often cracked and fissured and have discontinuities which may present issues in slopes, drainage, walls below grade, and foundations. If heavily overconsolidated and highly plastic, these may also be prone to swelling problems and exhibit characteristics of expansive clays and other concerns.

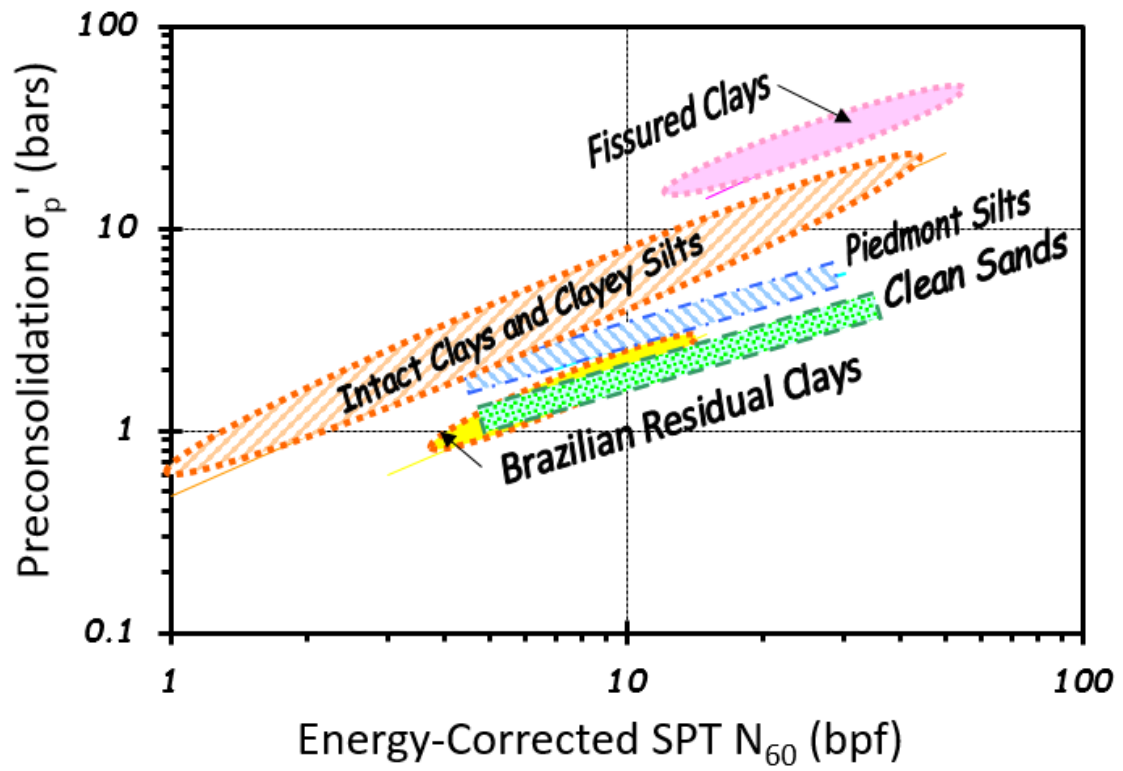


Figure 4.14 Effective preconsolidation stress versus N_{60} for soils (after Mayne 2007b).

5. Input Parameters Using Cone Penetration Tests (CPT)

5.1 Overview of the Cone Penetration Test (CPT)

The cone penetration test (CPT) involves the hydraulic pushing of an instrumented steel probe at a constant rate to obtain continuous vertical profiles of stress, friction, and pressure with depth. Cone penetration testing can be conducted for measurement of tip and sleeve resistances (i.e., CPT) or the additional readings of penetration porewater pressures using a piezocone (i.e., CPTu). Some equipment includes the ability to measure shear wave velocities, called a seismic piezocone test and designated SCPTu.

By recording continuous measurements vertically with depth, the CPT is an excellent tool for profiling strata changes, delineating the interfaces between soil layers, soil consistency, and detecting small lenses, inclusions, and stringers within the ground. The data presentation from a CPT sounding includes cone resistance (q_t), sleeve friction (f_s), and porewater pressures (u_2) plotted with depth in side-by-side graphs. The records are stored digitally and can be post-processed to interpret a number of geotechnical engineering parameters that relate to unit weight, soil strength, preconsolidation, stiffness, stress state, and permeability (Lunne, et al. 1997; Mayne, 2007).

5.2 Equipment

Equipment necessary for performing a cone penetration test includes a penetrometer, set of cone rods or drill rods, electrical cable, a data acquisition system, and hydraulic actuator with sufficient reaction mass to advance the penetrometer. This can be a conventional drilling rig or a CPT truck weighing 20 to 25 tons.

A standard cone penetrometer is a 35.7-mm diameter cylindrical probe with a 60° apex at the tip, 10-cm² cross-sectional area, and a 150-cm² sleeve surface area. More robust penetrometers are available with a 44-mm diameter body, a 15-cm² projected tip area, and 200- to 225-cm² sleeve surface area. **Figure 5.1** shows a number of different cone penetrometers and piezocones. Standard cone rod is typically 1 m in length with a 35.7 mm outer diameter and a 22 mm inner diameter opening. An electronic cable runs through the hollow rods and attaches to a data acquisition system at the ground surface. The newest data acquisition systems are digital types, yet many older systems consist of a signal conditioner, an analog to digital (A-D) converter, and computer processor. Data are typically recorded every 2 to 5 cm of vertical penetration (Sabatini et al., 2002).

For a piezocone penetration test (CPTu), the penetration porewater pressures are monitored using a transducer and porous filter element. Porewater readings can be taken at the apex or mid-face (designated u_1), shoulder (just above the cone tip, or u_2), or behind the sleeve (u_3). The standard required position per ASTM D 5778 is the shoulder position (type 2) because the u_2 value is required for the correction of tip resistance. Filter elements consist of high-density polypropylene, ceramic, or sintered metal. Fluids for saturation include: water, glycerine, or silicone.

For the seismic piezocone test, a geophone is located approximately 500 mm uphole from the cone tip. The geophone detects shear waves generated at the ground surface at depth intervals of approximately 1-meter, corresponding to successive rod additions.



Figure 5.1 *Different cone penetrometers and piezocones used in production testing and research*

5.3 Procedures

Test procedures for the CPT consist of hydraulically pushing the cone at a rate of 20 mm/s in accordance with ASTM D 5778 using either a standard drill rig or specialized cone truck. The advance of the probe requires the successive addition of rods at approximately 1 m intervals. Readings of measured tip resistance (q_c), sleeve friction (f_s), inclination (i), and pore pressure (u_2) are taken at least every 5-cm, as illustrated in **Figure 5.2**.

Careful saturation of the porous filter and transducer ports is paramount for piezocone testing. Poor saturation will lead to a compressible measurement system, and thus the full magnitude of the penetration pore pressure response will not be recorded. If water or water mixtures are used as the saturation fluid, a fluid filled membrane should be wrapped around the element to maintain saturation until the probe enters the ground. Glycerin and silicon oil are typically viscous enough to prevent desaturation of the element before penetration into the ground. Typically a pause in penetration will occur

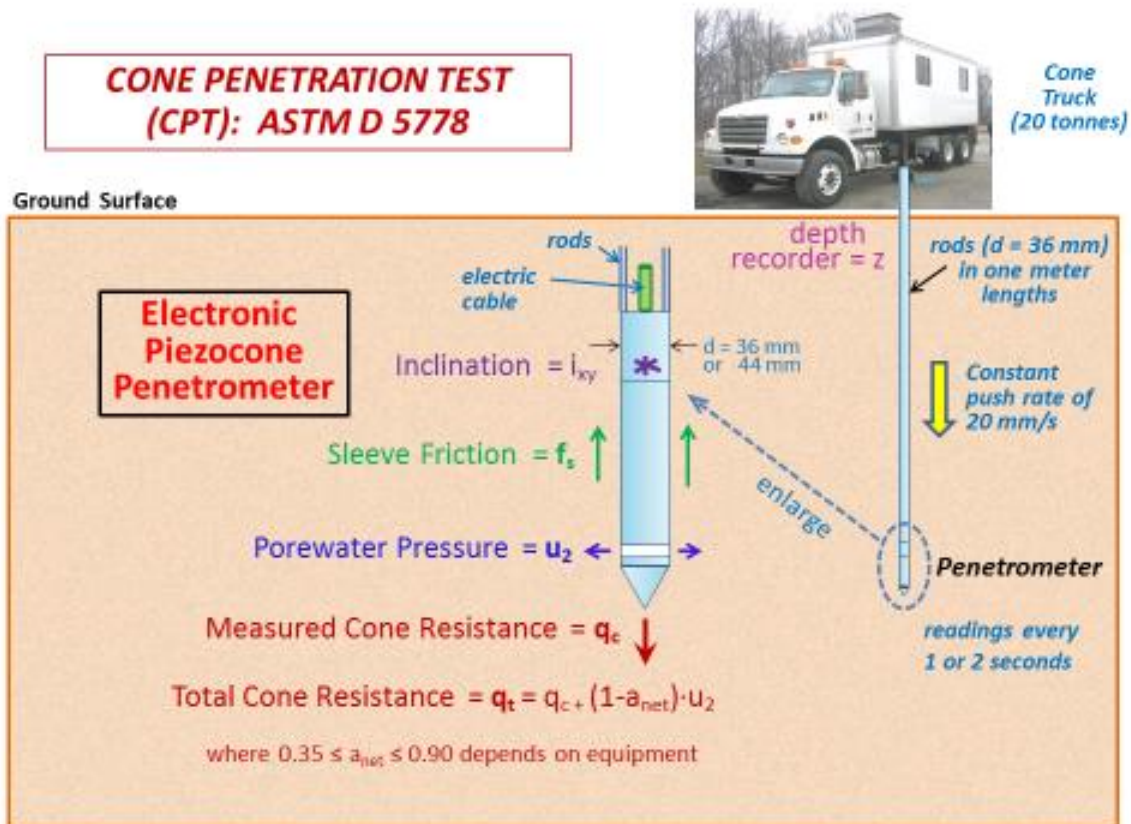


Figure 5.2 Depiction of Cone Penetration Testing (CPT) Setup and Procedures

to add new rods. This is referenced as the rod break. The depth at each rod break should be recorded and compared to the expected depth.

For the seismic piezocone (SCPTu), downhole shear wave velocity tests are performed at each 1-m rod break. A special instrumented hammer is used to trigger a surface source rich in shear waves (typically a horizontal steel beam). The steel beam is coupled to the ground under a hydraulic outrigger of the cone truck or drill rig, or under the tire of a support vehicle. The horizontal distance between the source beam and cone rod should be minimized (typically < 1 m) to ensure a relatively vertically-propagating shear wave. A

horizontal geophone located within the penetrometer serves as a receiver for the signal, which is displayed on the screen of an oscilloscope. First arrival times for shear waves are recorded with respect to depth, to provide interpretations of shear wave velocity of the overlying soil material (Sabatini et al., 2002).

5.4 Parameters Measured

Electric and electronic penetrometers have standard readings of measured cone tip resistance (q_c) and sleeve friction (f_s), as shown in **Figure 5.3 (a)**. Piezocone penetrometers obtain penetration porewater pressures using filters located at the shoulder (u_2 ; **Figure 5.3 (b)**) or the midface (u_1 ; **Figure 5.3 (c)**). A horizontal geophone in the seismic piezocone (**Figure 5.3 (d)**) can be used to record mechanically induced shear waves from the surface, leading to determination of shear wave arrival time (t_s) and shear wave velocity (V_s).

The cone tip resistance (q_c) is the measured axial force over the projected tip area. It is a point stress related to the bearing capacity of the soil. In sands, the tip resistance is primarily controlled by the effective stress friction angle, relative density, and effective horizontal stress-state. For intact clays, the tip resistance is primarily controlled by the undrained shear strength and preconsolidation stress. Particularly in clays and silts, the measured q_c must be corrected for porewater pressures acting on the cone tip geometry, thus obtaining the corrected or total cone tip resistance, q_t (Lunne et al., 1997):

$$q_t = q_c + (1 - a_n) \cdot u_2 \quad [5.1]$$

where a_n is the net area ratio determined from laboratory calibration and u_2 is the shoulder penetration porewater pressure. The net area ratio is approximated as the ratio

of the unequal end areas of the cone (see Figure 5.4). The net area ratio (a_n) is penetrometer-specific and is obtained by isotropic pressurization of the cone in a triaxial cell. It is best to use penetrometers with a value of net area ratio $a_n \geq 0.80$ to minimize the necessary correction. Contract specifications should always request the actual calibration curves and clear indication that q_c readings have been adjusted to provide the proper q_t values. Notedly, the correction is paramount for intact clays and silts where excess porewater pressures will occur ($q_t > q_c$), while in clean sands, the correction is negligible and thus $q_t \approx q_c$.

Because soil samples are not normally taken during CPT, soil types must be deduced or inferred from the measured readings. As a general rule of thumb, measured cone tip resistances in sands are rather high ($q_t > 5$ MPa or 50 tsf), reflecting the prevailing drained strength conditions, whereas measured values in clays are low ($q_t < 5$ MPa or 50 tsf) and indicative of undrained soil response owing to low permeability.

The sleeve friction (f_s) is a shear stress determined as the axial side load acting along the cylindrical surface area of a smooth sleeve. This value is often expressed as the Friction Ratio (FR) which is defined as the ratio of the sleeve friction to cone tip resistance, designated $FR = R_f = 100 \cdot f_s / q_t$, thus reported in percent. The friction ratio is generally indicative of soil type (Lunne et al., 1997). In clean quartz sands to siliceous sands, it is observed that friction ratios are low: $R_f < 1\%$, whereas in clays and clayey silts of low sensitivity, $R_f > 4\%$. However, in soft sensitive to quick clays, the friction ratio can be quite low, approaching zero in many instances.

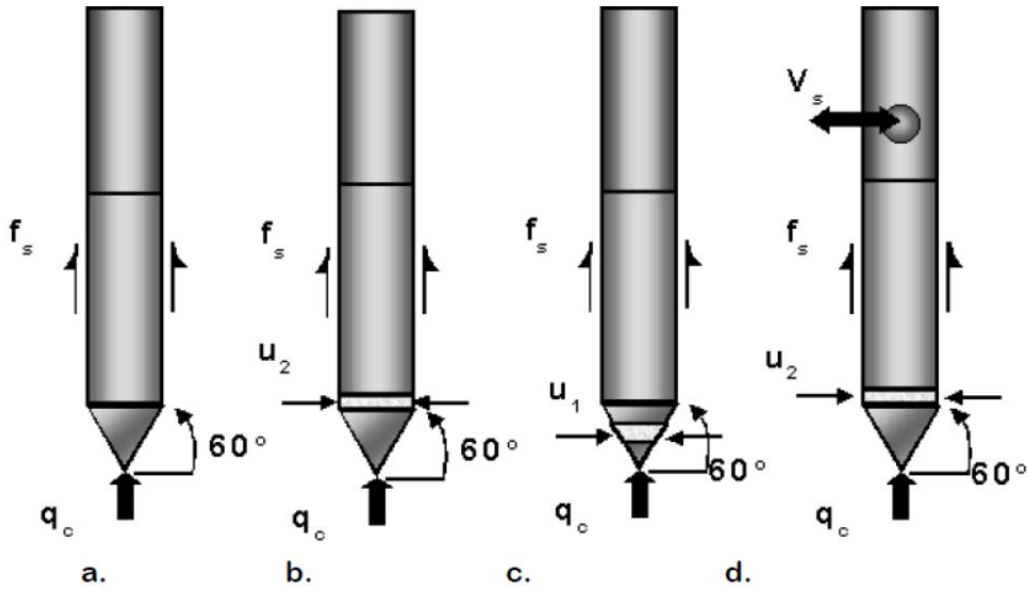


Figure 5.3 Measurement locations on cone penetrometers: a. Electric Cone Penetrometer, CPT; b. Piezocone Penetrometer with filter behind tip, CPTu₂; c. Piezocone with mid-face filter, CPTu₁; d. Seismic Piezocone, SCPTu₂

The penetration porewater pressures are monitored using a pressure transducer and porous filter element. These readings represent the fluid pressures between the soil particles during penetration. At the shoulder position, the pressures are near hydrostatic in sands ($u_2 \approx u_0$) whilst considerably higher than hydrostatic ($u_2 > u_0$) in soft to firm to stiff intact clays. Using values for total stress, σ_{vo} , and hydrostatic pore pressure, u_0 , the pore pressure parameter, $B_q = (u_2 - u_0) / (q_t - \sigma_{vo})$, is used as a means to normalize CPTu data for the purpose of soil classification and undrained shear strength estimation. At the mid-face location (u_1), penetration porewater pressures are always positive, while at the u_2 location measurements range from positive in intact (i.e., nonfissured) geomaterials to as low as negative one atmosphere (-100 kPa) in fissured clays and dense silts. The data

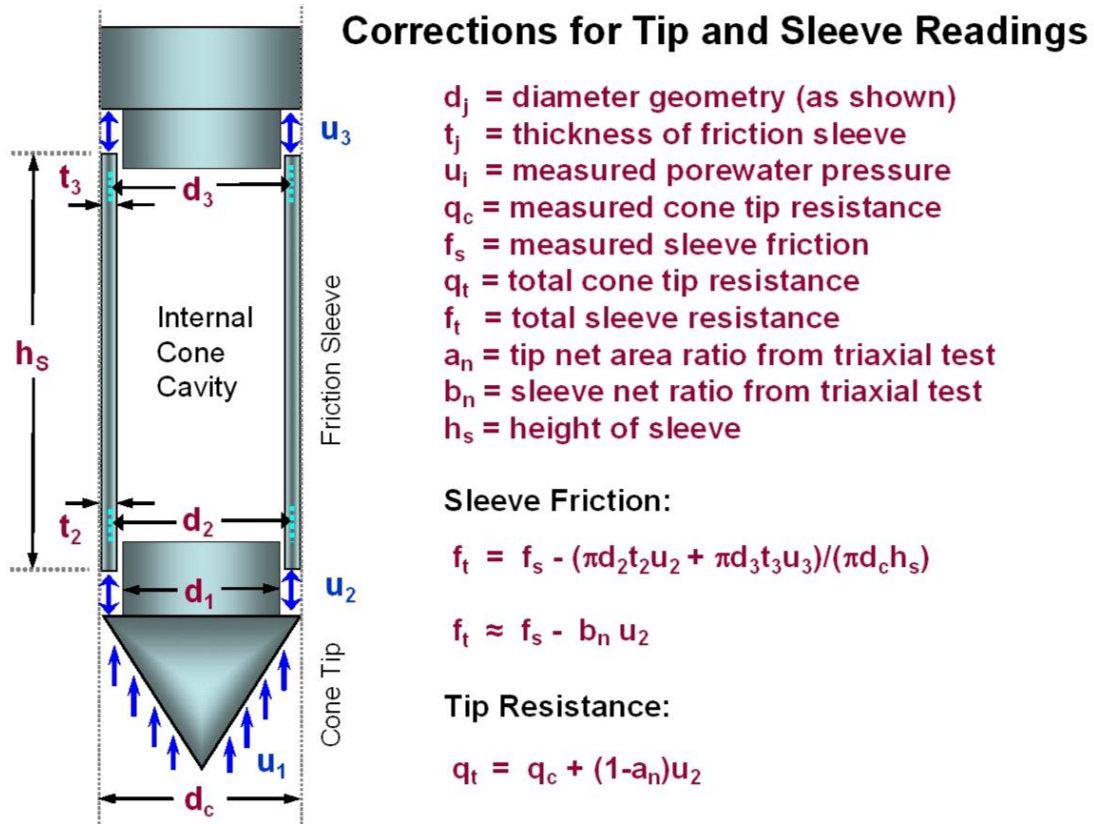


Figure 5.4 Illustration of unequal end areas of CPT (after Jamiolkowski et al. 1985)

resulting from a CPT, CPTu, or SCPTu are combined to provide several useful index and performance parameters.

5.5 Soil Identification and Classification from CPT

Since soil samples are not normally taken during cone penetration testing, then indirect methods must be utilized in evaluating various soil types of the strata encountered. Different approaches can be used: (a) correlation with adjacent boreholes and recovered samples; (b) rules-of-thumb; (c) empirical soil behavioral type (SBT) charts; (d) probabilistic methods.

The simple rules of thumb rely on one or more of the cone readings, where a reference cone tip value $q_t = 5 \text{ MPa}$ (50 tsf) should be identified, whereby measured $q_t > 5 \text{ MPa}$ imply clean "hourglass" sands and $q_t < 5 \text{ MPa}$ suggest "vanilla" clays. For the friction sleeve, it is convenient to plot this in terms of friction ratio, $FR = f_s/q_t$ (%). As such, clean sands are identified by $FR < 1\%$, whereas fine-grained soils (silts and clays) exhibit $FR > 1\%$. Lastly, using the porewater pressure channel, it is advantageous to plot the hydrostatic porewater pressure line as a reference:

$$u_0 = h_w \gamma_w \quad [5.2]$$

where h_w = height of the water (depth less groundwater table) and γ_w = unit weight of water (freshwater: $\gamma_w = 9.81 \text{ KN/m}^3 = 62.4 \text{ pcf}$).

Above the groundwater table, the ambient hydrostatic u_0 is taken equal to zero in clean sands; however, in clays and fine-grained materials, u_0 can be negative to account for capillarity effects depending upon the degree of saturation, recent rainfall, and other site features. In clean "hourglass" sands, the measured porewater pressures are often close to hydrostatic ($u_2 \approx u_0$). However, if the sands are very dense, dilatancy may result in u_2 readings below u_0 . Below the groundwater table, intact clays can be found by examining where $u_2 \gg u_0$.

To facilitate the identification of soil types by computer software, a number of empirical soil behavioral type (SBT) charts have been proposed. Robertson, et al. (1986) presented a 12-zone SBT system that uses a three-axes plot of cone tip resistance (q_t), friction ratio (FR), and normalized porewater pressure (B_q). Due to the inconvenience of working with 3-d graphs directly, the system is usually presented in two matched graphs: (a) q_t vs. FR

(%); and (b) q_t vs B_q . Other system are also in use for particular geologies (Kulhawy & Mayne 1990)

In order to account for depth effects on the readings, stress-normalized CPT parameters have been defined by Lunne, et al. (1997) as follows:

$$Q = (q_t - \sigma_{vo}) / \sigma_{vo}' \quad [5.3]$$

$$F = 100 \cdot f_s / (q_t - \sigma_{vo}) \quad [5.4]$$

For automation in a spreadsheet or software, it is convenient to use the CPT material index, I_c which is defined (Robertson & Wride, 1998):

$$I_c = \sqrt{\{3.47 - \log(Q)\}^2 + \{1.22 + \log(F)\}^2} \quad [5.5]$$

The aforementioned stress normalization for tip resistance directly with effective overburden stress works well in soft clays and silts, however in sands the stress normalization is proportional to the square root of effective stress, probably due to particle grain crushing effects. In this case, a modified normalized cone tip resistance has been defined as (Robertson, 2004; 2009):

$$Q_m = \frac{(q_t - \sigma_{vo})}{\sigma_{atm}} \cdot \left(\frac{\sigma_{atm}}{\sigma_{vo}'} \right)^n \quad [5.6]$$

where $\sigma_{atm} = 1$ atmosphere ≈ 1 bar = 100 kPa and the exponent n is varies with soil type, with typical values of 1.0 in the general case of clays ($I_c > 2.95$), $n = 0.75$ for silty soils, and $n = 0.5$ for clean sands ($I_c < 2.05$). Since the exponent n is a function in the material index I_c which is a function in the modified normalized cone tip resistance Q_{tn} which is also a

function in the same exponent n then an iterative approach is needed to find the appropriate exponent n to identify the SBT zone number for mixed soil types.

$$n = 0.381 \cdot (I_c) + 0.05 \cdot \left(\frac{\sigma_{vo}'}{\sigma_{atm}} \right) - 0.15 \quad [5.7]$$

By plotting the data in terms of Q_{tn} versus F_r , a modified 9-zone SBT system has been developed (Robertson, 2009), as presented in **Figure 5.5**. In this system, basic "vanilla" clay is found in zone 3 while "hourglass" sands form zone 6. The SBT classifications can be identified as per Robertson (2009) following **Table 5.1** and as plotted in **Figure 5.6**.

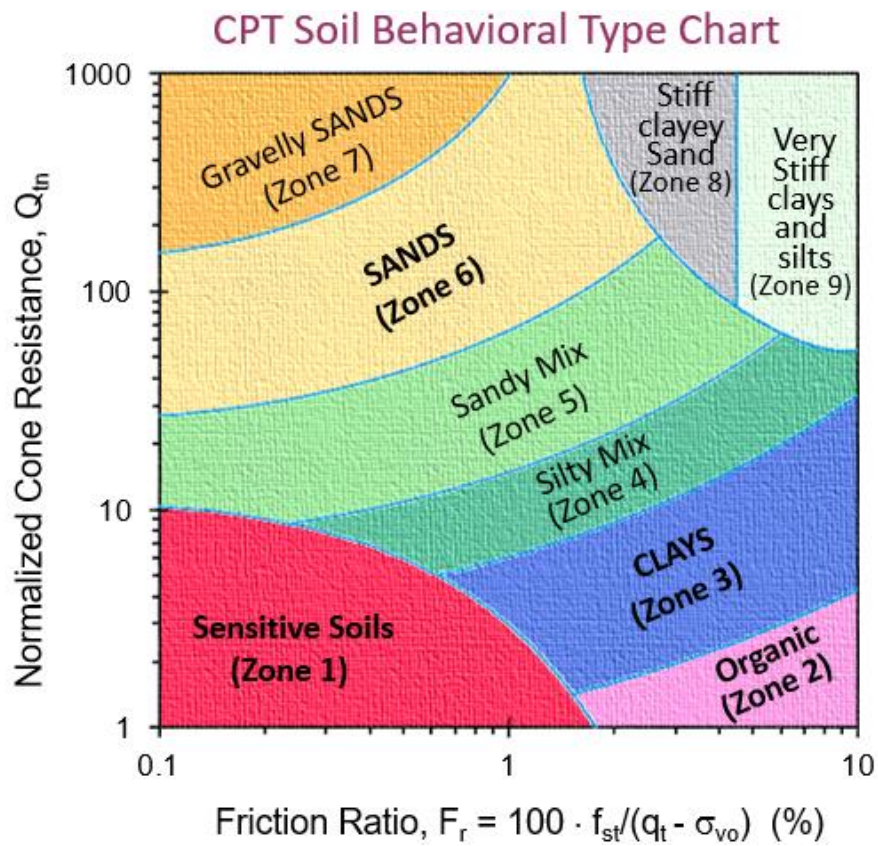


Figure 5.5 Colorized Soil Behavioral Type (SBTn) Chart for normalized CPT readings (after Robertson 2009)

Table 5.1 Soil Behavioral Type and Zone Number as defined by CPTu Material Index, I_c

Soil Classification	SBT Zone	Range CPT Material Index I_c
Stiff sands and clays	8 and 9	(see note 1)
Sands with gravels	7	$I_{cRW} < 1.31$
Sands: clean to silty	6	$1.31 < I_{cRW} < 2.05$
Sandy mixtures	5	$2.05 < I_{cRW} < 2.60$
Silty mixtures	4	$2.60 < I_{cRW} < 2.95$
Clays	3	$2.95 < I_{cRW} < 3.60$
Organic soils	2	$I_{cRW} > 3.60$
Sensitive soils	1	(see note 2)

Notes: 1. Zone 8 ($1.4 < F < 4.5\%$) and Zone 9 ($F > 4.5\%$) and following criterion:

$$Q_m \geq \frac{1}{0.006 \cdot (F - 0.9) - 0.0004 \cdot (F - 0.9)^2 - 0.002}$$

2. Sensitive soils of zone 1 identified when $Q < 12 \exp(-1.4 F)$

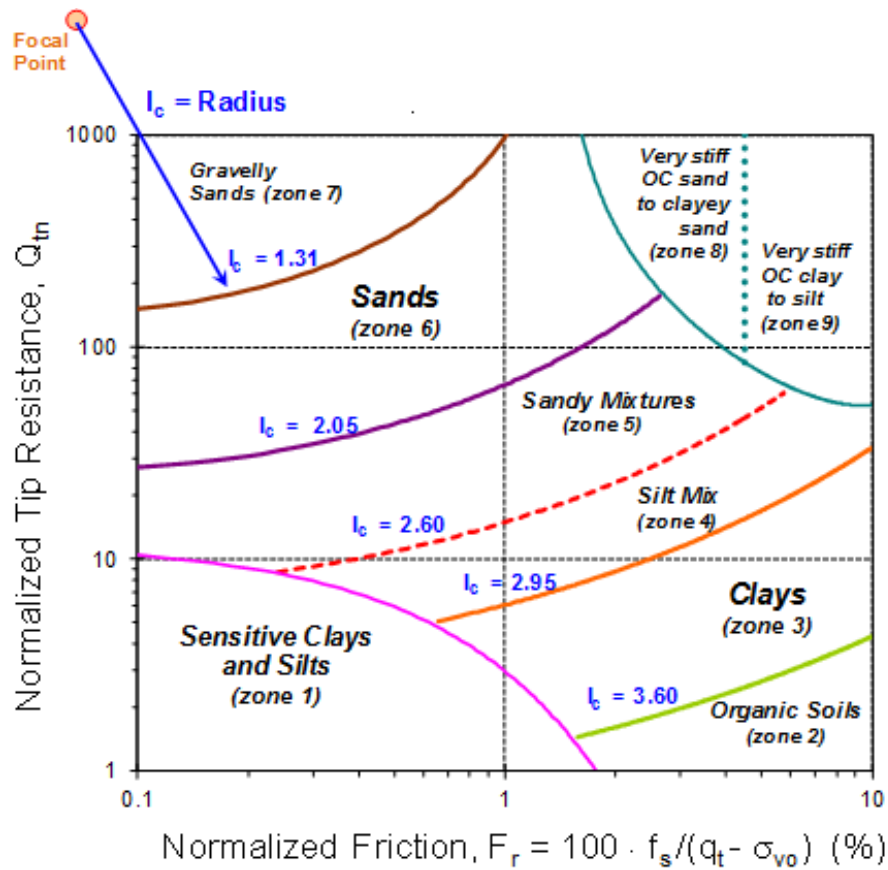


Figure 5.6 CPT Soil Classification Zones Using Nine-Part Soil Behavioral Type (after Robertson 2009)

5.6 Soil Unit Weight from CPT

A direct relationship for unit weight from CPT resistances has been sought (Mayne, et al. 2010). The findings are given in **Figure 5.7** and indicate that the sleeve friction provides a reasonable first-order estimate on γ_t . An initial value is assumed in order to process the first results using σ_{vo}' and then later adjusted based on the derived profile of γ_t from the CPT readings. The expression for total unit weight in terms of sleeve friction is:

$$\gamma_t = 1.95 \gamma_w (\sigma'_{vo}/\sigma_{atm})^{0.06} (f_s/\sigma_{atm})^{0.06} \quad [5.8]$$

where $\sigma_{atm} = 1$ atmosphere = 1 bar = 100 kPa \approx 1 tsf. The expression works well in normal "vanilla-flavoured" clays and "hourglass quartz" sands, but is not applicable to highly plastic and diatomaceous soils, such as Japanese mudstone or infamous Mexico City clays.

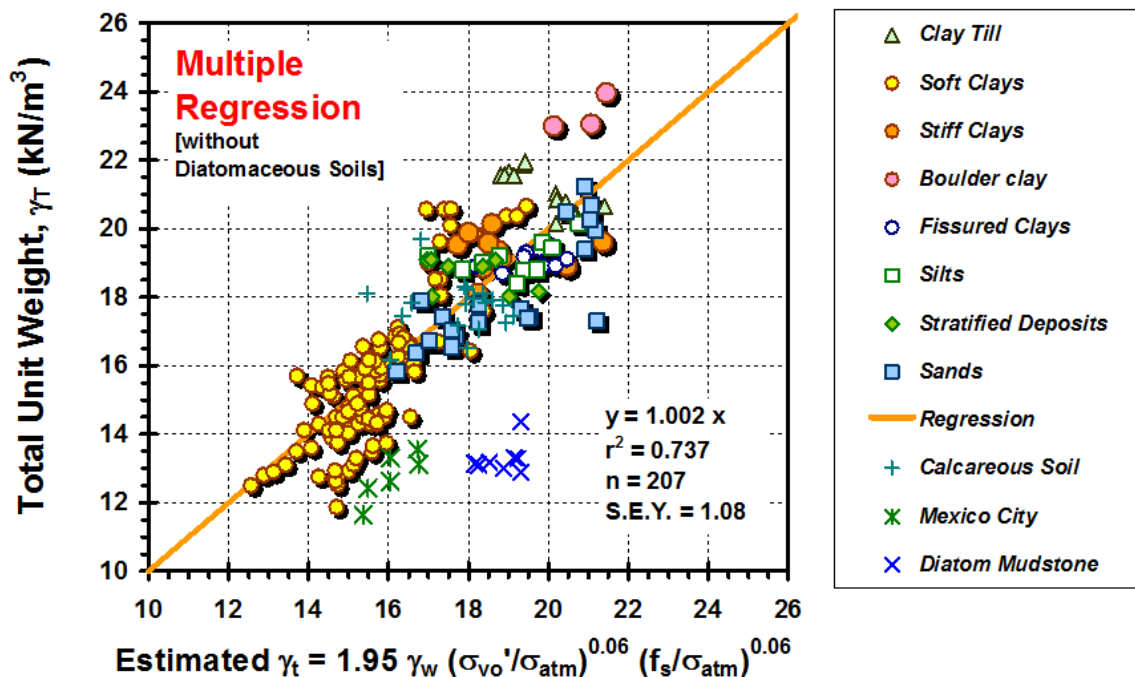


Figure 5.7 Unit weight directly estimated from CPT sleeve resistance and effective stress (Mayne et al., 2010).

A direct unit weight relationship with the sleeve friction is also observed, as presented in

Figure 5.8:

$$\gamma_t = 26 - \frac{14}{1 + [0.5 \cdot \log(f_s + 1)]^2} \quad [5.9 a]$$

where the specific units include: γ_t (kN/m³) and f_s (kPa). Alternatively, a simpler expression for the majority of sleeve reading ranges is given by:

$$\gamma_t = 12 + 1.5 \ln(f_s + 0.1) \quad [5.9 b]$$

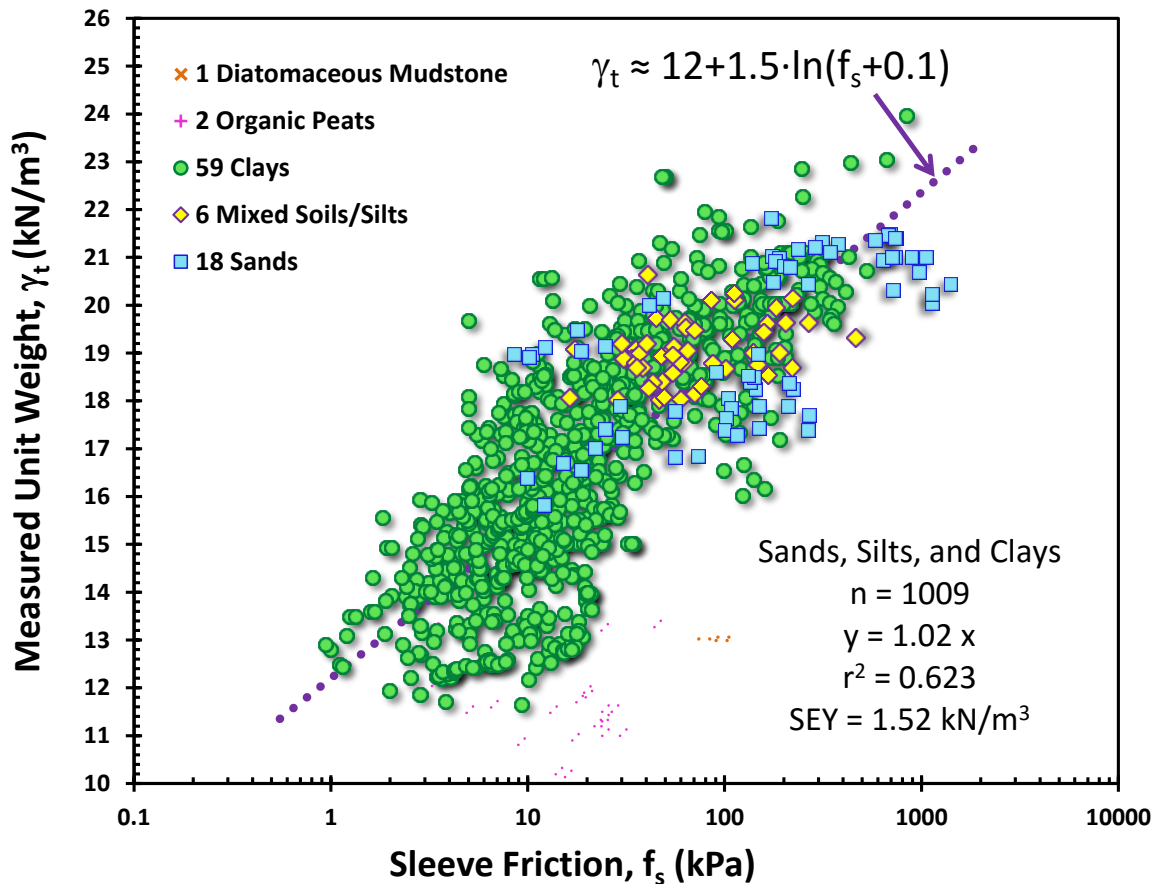


Figure 5.8 Unit weight directly estimated from CPT sleeve resistance (Mayne, 2014)

5.7 Effective Friction Angle from CPT

The drained (effective stress) friction angle (ϕ') of soils is a fundamental property that controls the strength, behavioral response to loading, and initial stress state. The effective friction angle of sands (also termed angle of internal friction) represents the strength of the material in stability analyses and is often required for assessing the coefficient of lateral stress (K_0), footing bearing capacity, pile end-bearing resistance, and side resistance in deep foundations. In terms of the commonly-adopted Mohr-Coulomb strength criterion, the shear strength (τ_{\max}) is expressed:

$$\tau = c' + \sigma'_n \tan \phi' \quad [5.10]$$

where c' = effective cohesion intercept (generally: $c' = 0$ for unbonded geomaterials). In most cases, the normal stress can be taken equal to the effective vertical overburden stress: $\sigma'_n = \sigma_{v0}'$.

For granular soils, the peak friction angle (ϕ'_p) of sands is composed of two components: (1) a basic frictional value (designated ϕ'_{cs} for critical state) that is due to particle grain shape, compressibility characteristics and mineralogy; and (2) a dilatancy term (quantified by ψ , the dilatancy angle) which reflects the relative packing of particles (e_0 or D_R) and ambient stress level (σ_{v0}' or p'). Together, the two components combine to produce a peak friction angle:

$$\phi'_p \approx \phi'_{cs} + \psi' \quad [5.11]$$

Characteristic values of ϕ'_{cs} are on the order of 32° for quartz sands, 33° for silty quartz sands with up to 20% fines content, 34° for siliceous sands (approx. half quartz-half

feldspar), 39° for calcareous sands, and 40° for feldspathic sands (Bolton 1986; Salgado et al. 2000; Jamiolkowski et al. 2001). The friction angle also depends upon mode of testing (i.e., plane strain vs. triaxial) and direction of loading (compression vs. extension). For the assessment of ϕ_p' of sands from CPT, there are several approaches: (a) use of a dilatancy framework where q_c provides the input value of D_R (Bolton, 1986); (b) inverse bearing capacity, such as from cavity expansion or limit plasticity theories (Yu & Mitchell, 1998; Schnaid 2009); (c) numerical simulation by finite elements, finite differences, and/or discrete elements (e.g., Salgado et al. 1998); or (d) direct CPT methods (Lunne et al. 1997). Because of the difficulties in procuring intact samples of natural sands, many early approaches were either benchmarked to or based on reconstituted samples where small triaxial specimens were prepared at similar relative densities and confining stress levels to those of larger calibration chamber tests subjected to CPTs. The methods of reconstitution, however, were not standardized (pluviation, compaction, vibration, sedimentation, moist tamping, slurry). Furthermore, the CPT data were not corrected for boundary conditions from limited size chambers.

Towards an improved solution, an elite database was compiled from special and expensive undisturbed samples of clean sands (Mayne 2006). Primarily, these sands were initially frozen in-place using one-dimensional thermal technologies. After careful mounting of specimens in triaxial apparatuses with membranes and confinement, they were allowed to thaw, and then sheared to failure to derive ϕ_p' corresponding to undisturbed intact sands. The sites for these sands were subjected to SPT, CPT, and V_s measurements, as well as other lab and field testing.

The triaxial data from undisturbed sands can be seen to fit nicely with the expression derived by Kulhawy & Mayne (1990) that was developed on the basis of CPT calibration chamber data that have been corrected for boundary effects and stress-normalized:

$$\phi^{\circ} = 17.6^{\circ} + 11 \cdot \log \left(\frac{(q_t / \sigma_{atm})}{\sqrt{(\sigma'_{vo} / \sigma_{atm})}} \right) \quad [5.12]$$

The relationship in **Figure 5.9** primarily applied to clean quartz to siliceous sands, yet there is some evidence it has applicability in natural sands with up to 30 percent silt content.

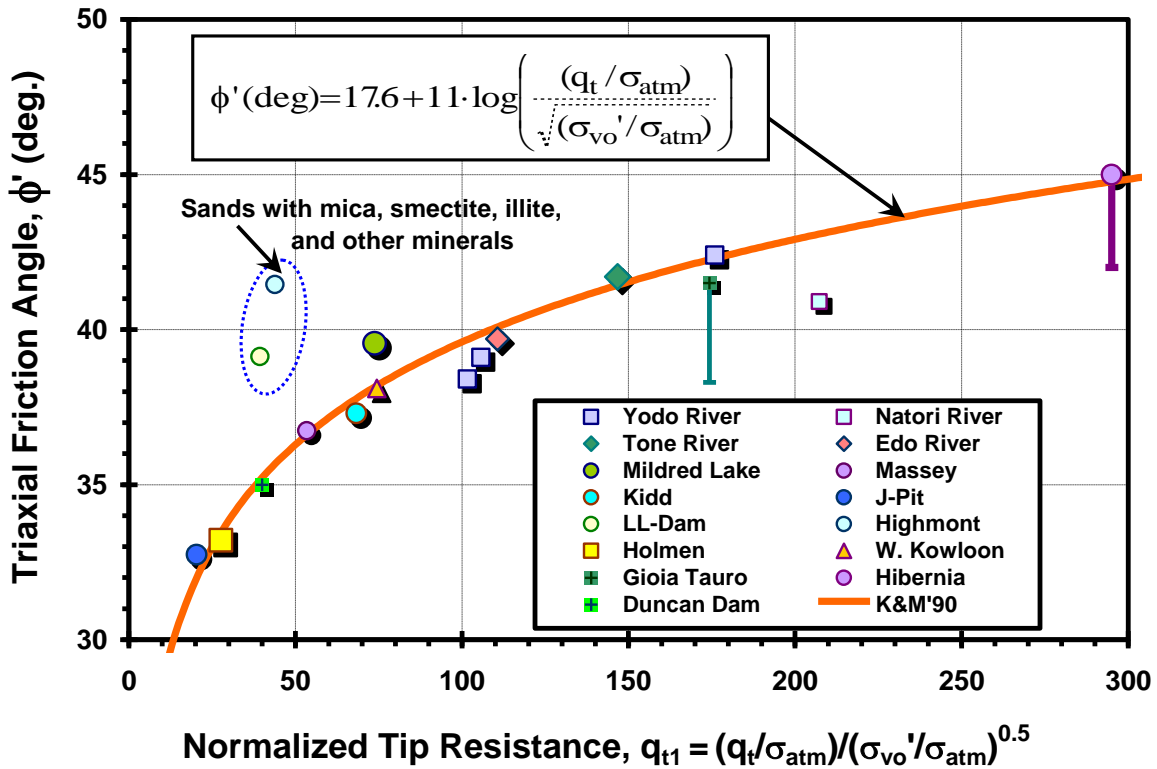


Figure 5.9 Direct CPT approach for evaluating ϕ' in clean sands (Mayne, 2006)

As for clays an average approximate friction angle value of 28 degrees is assigned following **Figure 4.11**.

5.8 Modulus of Elasticity from CPT

Deformation of the ground is an important facet that must be addressed during analysis and design of the proposed construction. Many office type buildings are built towards tolerable settlements of less than 25 mm (1 inch), while open structures such as parking garages are able to withstand up to 50 mm (2 inches) of vertical movement. Large bridge structures can sustain up to 75 mm (3 inches) displacements, yet earthen embankments may undergo deflections of 100 to 1000 mm during initial loading, primary consolidation, and long-term secondary compression (creep). For the latter, the full consideration of deformations can be expressed:

$$S_{\text{total}} = S_{\text{initial}} + S_{\text{consolidation}} + S_{\text{creep}} \quad [5.13]$$

as detailed earlier in Section 3.1.

Elastic theory allows for interrelationships between the equivalent elastic Young's modulus (E), shear modulus (G), and constrained modulus (D) in terms of the Poisson's ratio, such that:

$$E = 2 \cdot G \cdot (1 + \nu) \quad [5.14]$$

$$D' = E' \cdot \frac{(1 - \nu')}{(1 + \nu')(1 - 2\nu')} \quad [5.15]$$

Note that the constrained modulus (designated by the symbol D', but also by the nomenclature M') takes on only a drained value as it is measured directly in a one-

dimensional consolidation test (oedometer), while the moduli E and G can have drained (E' and G') as well as undrained values (E_u and G_u). At the value of $\nu' \approx 0$, elastic theory states that the constrained modulus equals the Young's modulus, thus $D'/E' = 1$. At a value $\nu' \approx 0.2$ that is characteristic of sands and granular soils (Jamiolkowski et al. 1994; Lehane & Cosgrove 2000), the ratio $D'/E' = 1.1$ and therefore the constrained modulus and drained Young's modulus are often used somewhat interchangeably. In terms of the compressibility parameters from consolidation testing, the constrained modulus can be expressed:

$$\text{OC Soils: } D' = \frac{1+e_0}{C_s} \cdot \ln(10) \cdot \sigma_v' \quad [5.16]$$

$$\text{NC Soils: } D' = \frac{1+e_0}{C_c} \cdot \ln(10) \cdot \sigma_v' \quad [5.17]$$

where D' corresponds to the current effective stress state (σ_{v0}'). For an approximate evaluation of the constrained modulus (and drained Young's modulus) from CPT results, the common approach is expressed in the form:

$$D' \approx \alpha_D \cdot (q_T - \sigma_{v0}') \quad [5.18]$$

where α_D is an empirical scaling factor that has been shown to depend upon soil type, confining stress level, overconsolidation, and other factors (Kulhawy & Mayne, 1990).

Figure 5.10 shows that for wide range of soil types: $\alpha_D \approx 5$ is an approximate starting place, excepting soft plastic organic clays and cemented geomaterials. The original database for this compilation was based on laboratory consolidometer data to provide the corresponding D' for clays and silts, while the consolidation phase of calibration chamber tests were used to obtain D' for clean quartz sands (Mayne 2007b).

For Piedmont residual soils, Mayne & Liao (2004) showed a direct relationship between the elastic modulus (E') obtained from flat dilatometer tests (DMT) and cone resistance (q_t) from CPT. This is quite compatible with the aforementioned study for sediments reported in terms of constrained modulus (D'). Revisiting those data, the net cone resistance can be used to show the relationship in **Figure 5.11**.

$$E' \text{ (DMT)} = 5 (q_t - \sigma_{vo}) \quad [5.19]$$

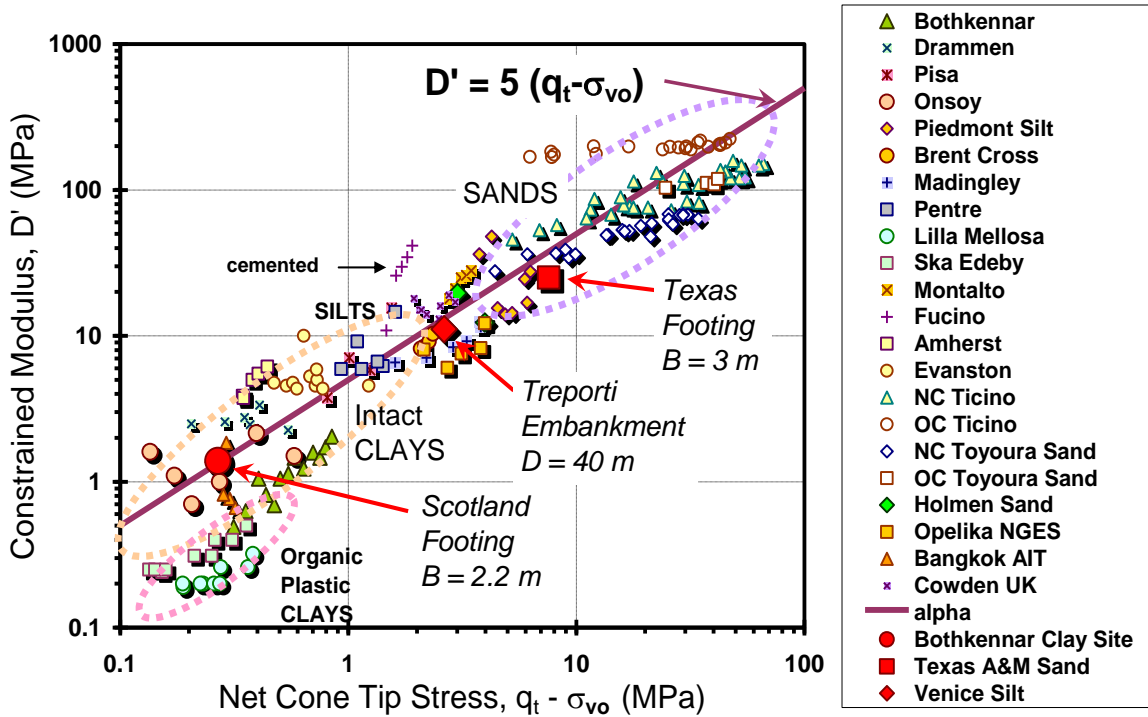


Figure 5.10 Overall trend between drained constrained modulus and net cone tip resistance in various soils, including three case studies with backfigured moduli

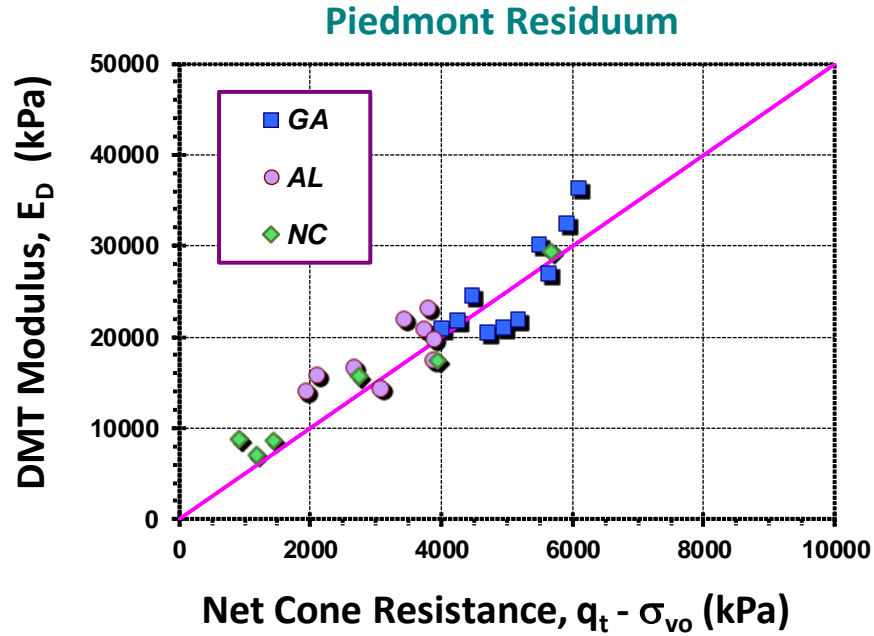


Figure 5.11 Relationship between the DMT elastic modulus and the net cone tip resistance in Piedmont soils (modified after Mayne and Liao, 2004)

5.9 Stress History from CPT

For estimating the effective preconsolidation stress using the cone penetrometer readings, a general equation for all types of natural soils, including sands, silts, clays, and mixed soil types has been introduced by Mayne et al. (2009) as presented in **Figure 5.12**.

The generalized expression is expressed as:

$$\sigma_p' = 0.33 \cdot (q_t - \sigma_{vo})^{m'} \cdot (\sigma_{atm}/100)^{1-m'} \quad [5.20]$$

where the *exponent* m' is a parameter that increases with fines content and decreases with mean grain size. The approximate value of parameter $m' \approx 0.72$ in clean quartz sands, 0.8 in silty sands, up to $m' = 1.0$ in intact clays of low sensitivity, and may even take greater values in fissured geomaterials. Using the CPT material index I_c one can identify the magnitude of the parameter m' for general profiling of σ_p' in homogeneous or

heterogeneous deposits, as well as mixed soils. **Figure 5.13** shows the concluded trends, based on a review of the investigated data. For basic uncemented and non-structured soils, the exponent m' can be estimated as follows:

$$m' = 1 - \frac{0.3}{1 + (I_c / 2.65)^{20}} \quad [5.21]$$

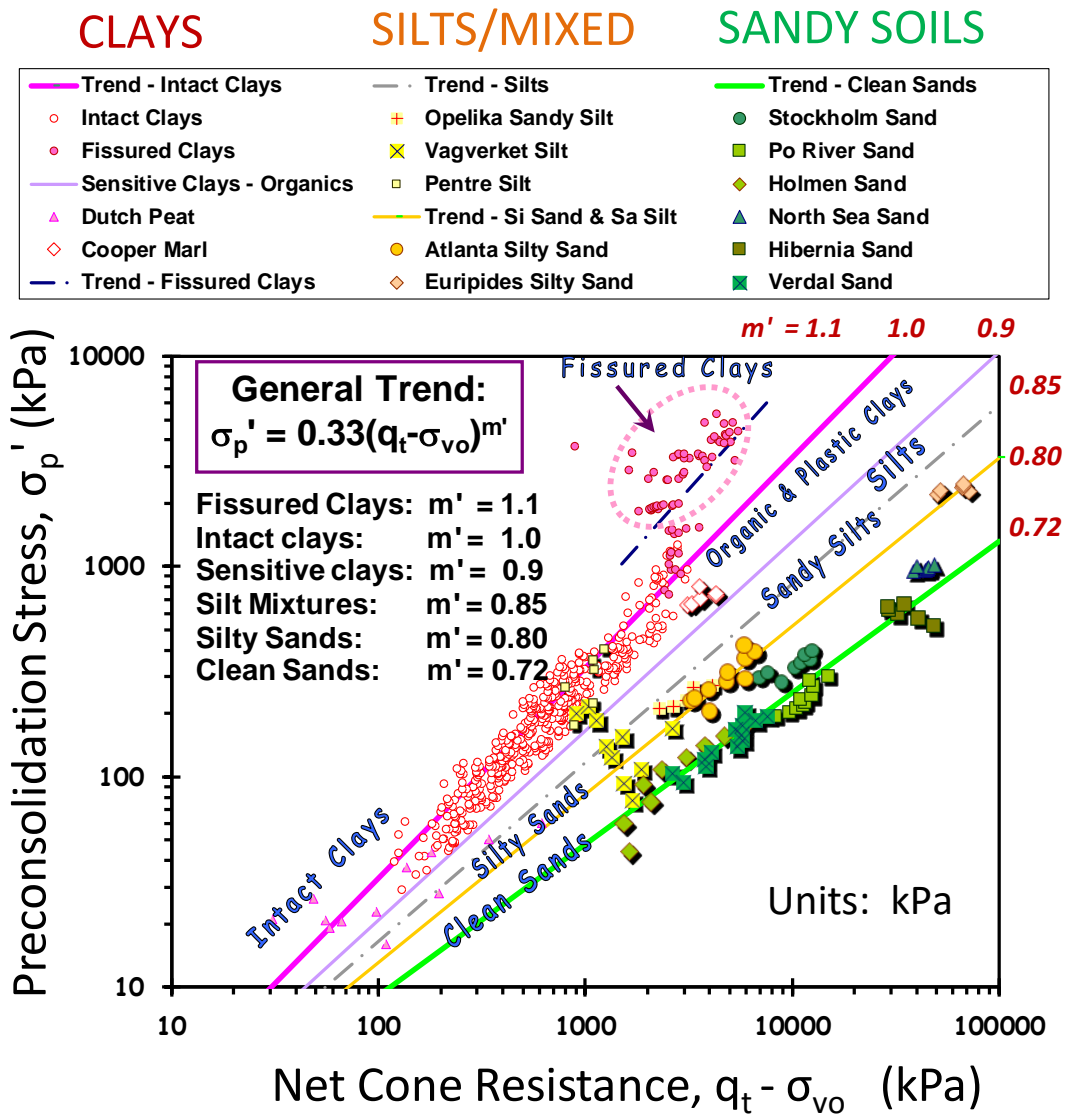


Figure 5.12 General Approach to σ_p' interpretation of soils by CPT net cone resistance. (Mayne, et al. 2009)

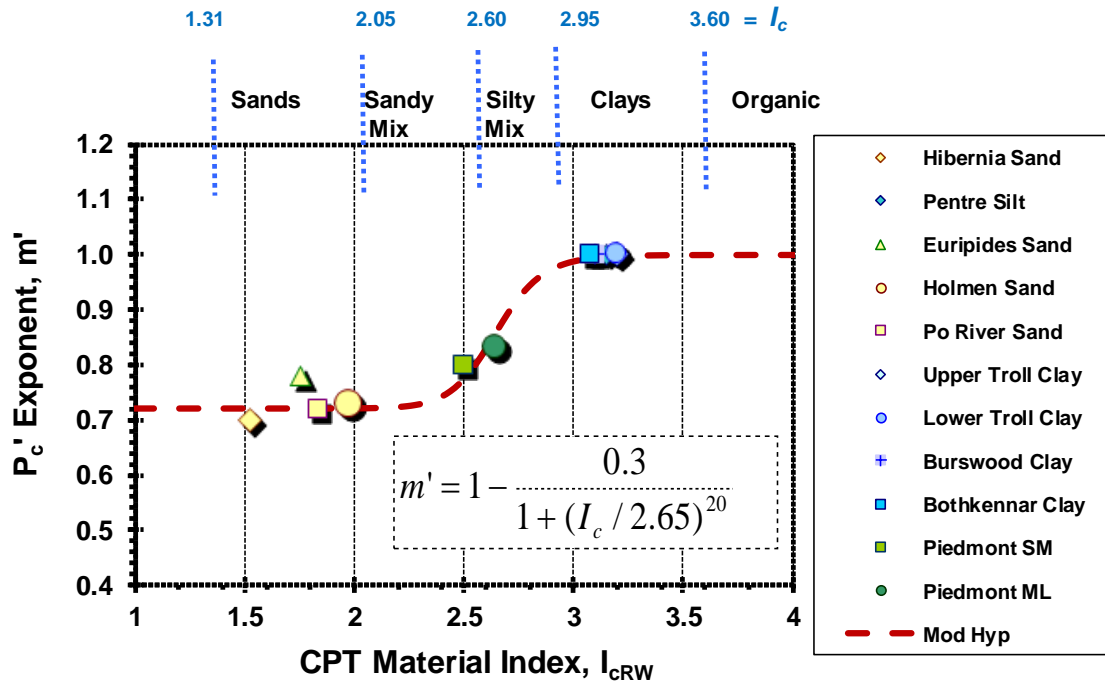


Figure 5.13 Preconsolidation exponent parameter m' versus CPT material index, I_c

6. Input Parameters Using the Flat Dilatometer Tests (DMT)

6.1 Overview of the Flat Dilatometer Test (DMT)

The flat plate dilatometer test (DMT) is an in-situ method that involves pushing an instrumented flat steel blade into soils and recording two horizontal pressures at each test depth. The specific pressure measurements are utilized to obtain stratigraphy and estimates of geoparameters, including: unit weight, at-rest lateral stresses, elastic modulus, stress history, and shear strength. The flat dilatometer test (DMT) was developed in Italy and then introduced in North America and Europe (Marchetti, 1980).

The flat dilatometer test is simple, robust, repeatable, quick, economic, and operator-independent. The field of application of the DMT is very wide, ranging from extremely soft soils to dense sands. However, the DMT is difficult to push in very dense and hard materials and not applicable to gravels. The DMT analyses primarily relies on correlative relationships and requires calculations for local geologies. No borehole cuttings or spoil are generally produced by this test, although it is possible to advance a conventional soil boring and then perform the DMT downhole within the borehole.

6.2 DMT Equipment

The device consists of a tapered stainless steel blade with 18° wedge tip that is vertically advanced into the ground at 20-cm or 30-cm intervals per ASTM D 6635. The blade has a cutting edge to penetrate the soil. The steel blade has nominal dimensions of 240 mm length, 95 mm width, and 15 mm thickness and is connected to a readout pressure gauge.

The steel blade is connected to a control unit on the ground surface by a pneumatic-electrical tube (transmitting gas pressure and electrical continuity) running through the insertion rods. A nitrogen gas tank, connected to the control unit by a pneumatic cable, supplies the gas pressure required to expand the membrane. The control unit is equipped with a pressure regulator, pressure gauges, audio-visual signal, and vent valves. A circular 60-mm diameter flexible steel membrane that is located on one side of the blade is inflated pneumatically to give the pressure readings (Sabatini et al., 2002) . **Figure 6.1** shows a flat plate dilatometer blade and the associated control unit.

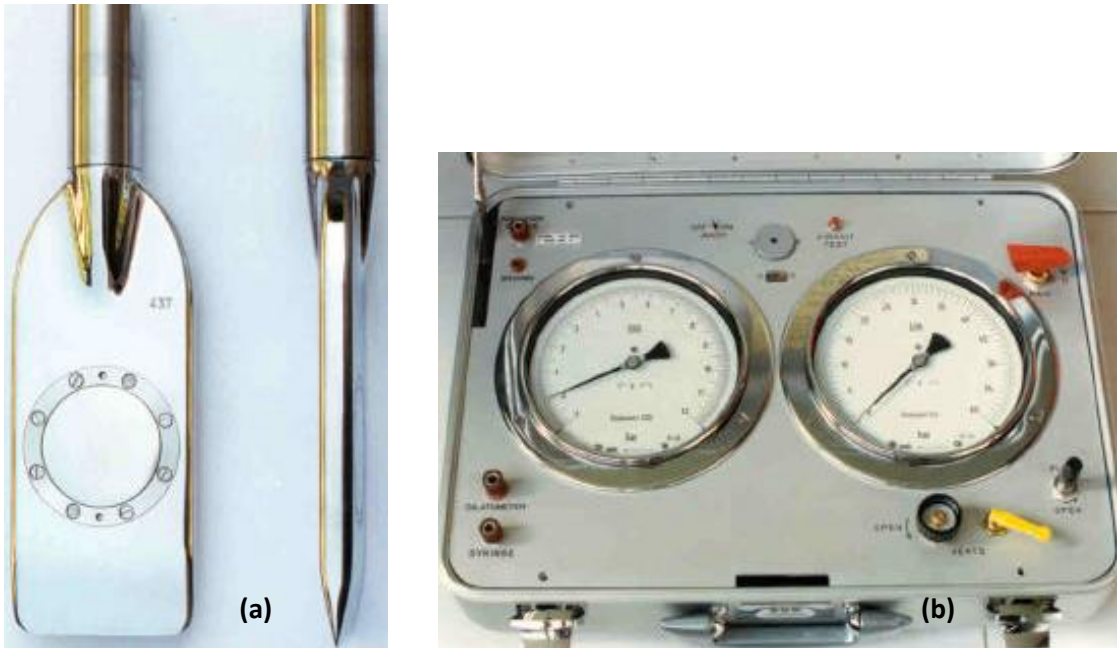


Figure 6.1 Main Components of the Flat Dilatometer Test: a. Steel DMT blade with inflatable membrane; and b. Pressure Control Unit

6.3 Procedures for the DMT

Procedures for the test are given by ASTM D 6635 and Schmertmann (1986). **Figure 6.2** provides an overview of the DMT test and its setup. Two calibrations (ΔA and ΔB) are taken before the sounding to obtain corrections for the membrane stiffness in air. The test starts by advancing the steel blade into the ground at 20 mm/s using common field equipment such as drill rigs, cone trucks, or hydraulic ram systems. Discrete tests are performed typically at 200-mm (8-in) depth intervals, or in US practice at 300-mm (1 foot) intervals.

After blade penetration, the membrane is inflated using nitrogen pressure to obtain two readings: (a) A-pressure reading, required to make the membrane flush with the flat blade, and (b) B-pressure reading, required to move the center of the membrane 1.1 mm into the soil. The membrane is deflated just after the B-reading. The blade is then advanced to the next test depth and the procedure repeated to obtain another A and B at each depth. Each depth is accomplished in about 1 minute.

Two calibration readings are taken for membrane stiffness: ΔA = pressure required in air to move the flexible membrane inward a distance 0.05 mm; ΔB = pressure required in air to move membrane outward a distance 1.1 mm. Each of the pressure readings A and B are then converted into p_0 (contact pressure) and p_1 (expansion pressure), respectively per Figure 6.2. Additional details on the operations and mechanics of the DMT are given elsewhere (Marchetti and Crapps, 1981; Marchetti 1999; and Marchetti et al. 2001).

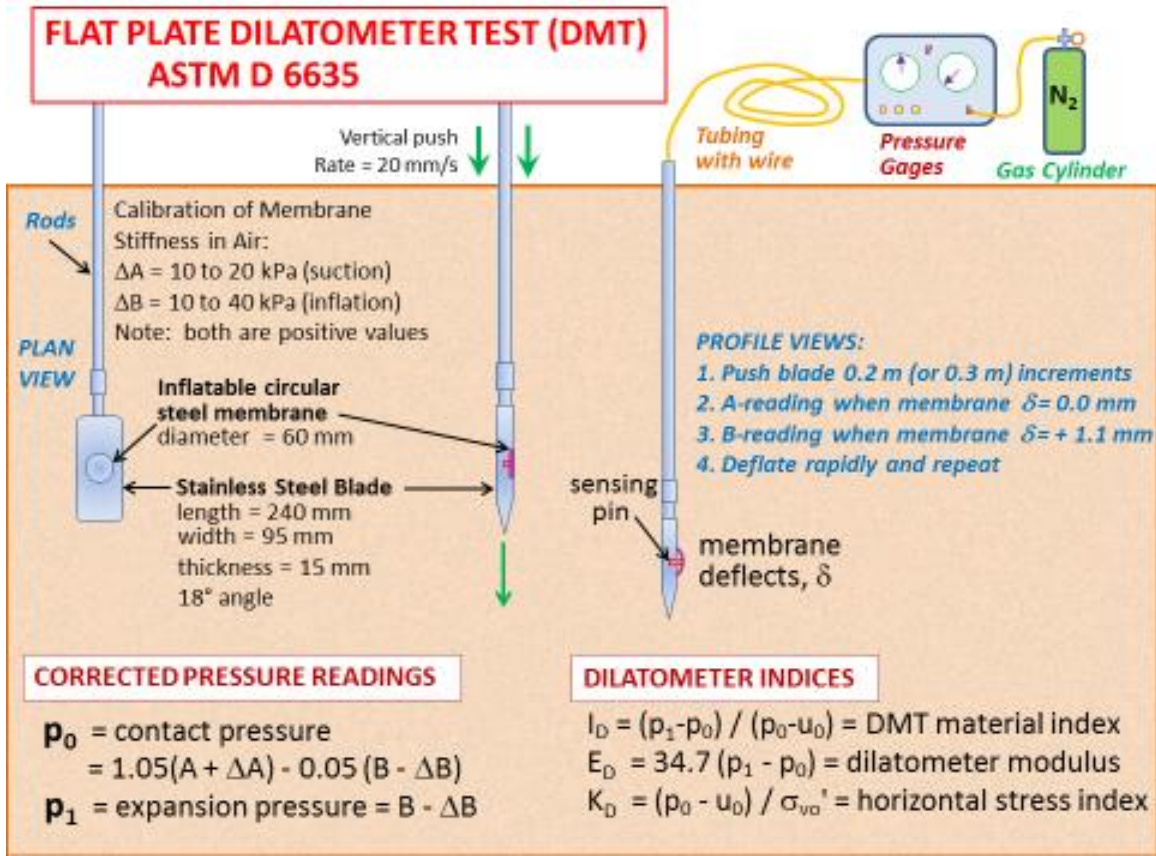


Figure 6.2 Illustration of Setup and Procedure for the Flat Dilatometer Test (DMT)

6.4 DMT Index Parameters

The field A- and B- readings need to be corrected for membrane stiffness effects to obtain the liftoff pressure, p_0 , and expansion pressure, p_1 . Correction of the readings has been presented by Schmertmann (1986):

$$p_0 = 1.05 (A + \Delta A - z_m) - 0.05 (B - \Delta B - z_m) \quad [6.1]$$

$$p_1 = B - \Delta B - z_m \quad [6.2]$$

where ΔA and ΔB reported as positive absolute values are the calibration factors for applied suction and expansion of the membrane in air, respectively, and z_m is the gage

offset zero reading when vented to atmospheric pressure and it is typically set to zero for a new gage.

The two dilatometer pressures, p_0 and p_1 , are combined with the hydrostatic water pressure, u_0 , to provide three index parameters: (a) material index I_D , (b) horizontal stress index K_D , and (c) dilatometer modulus E_D . These were developed by Marchetti (1980) to provide information on the stratigraphy, soil types, and the evaluation of soil parameters. Hydrostatic water pressure (u_0) can be evaluated based on available groundwater table information. If not available, then a special "C" reading can be made in clean sands to evaluate the u_0 value at that elevation and determine the groundwater table.

The material index, I_D , is related to the soil classification and is presented as:

$$I_D = (p_1 - p_0)/(p_0 - u_0) \quad [6.3]$$

The above definition of I_D was introduced having observed that the p_0 and p_1 profiles are systematically "close" to each other in clay and "distant" in sand. According to Marchetti (1980), the soil type can be identified: clay: $0.1 < I_D < 0.6$, silt: $0.6 < I_D < 1.8$, and sand: $1.8 < I_D < 10$. In general, I_D provides an expressive profile of soil type, and for normal soils, a reasonable soil description.

The horizontal stress index, K_D , is related to the in-situ horizontal stress-state of the soil. The index K_D will always be greater than K_0 due to disturbance caused during insertion of the blade. This parameter is presented as:

$$K_D = (p_0 - u_0)/\sigma'_{v0} \quad [6.4]$$

K_D provides the basis for several soil parameter correlations and is a key result of the dilatometer test. The horizontal stress index K_D can be regarded as K_0 amplified by the

penetration (Marchetti et al., 2001). In NC clays; with no aging, structure, cementation; the value of $K_D \approx 2$. The K_D profile is similar in shape to the OCR profile with depth, hence can be used to better understand the soil deposit and its stress history (Marchetti 1980, Jamiolkowski et al. 1988).

6.5 Soil Unit Weight from DMT

The total soil unit weight (γ_t) can be evaluated from the material index and dilatometer modulus as presented in **Figure 6.3**. For spreadsheet use, the approximate expression is:

$$\gamma_t = 1.12 \gamma_w (E_D / \sigma_{atm})^{0.1} (I_D)^{-0.05} \quad [6.5]$$

where γ_w = unit weight of water and σ_{atm} = atmospheric pressure. For each successive layer, the cumulative total overburden stress (σ_{vo}) can be calculated, as this is needed for the determination of the effective vertical overburden stress ($\sigma_{vo}' = \sigma_{vo} - u_o$) and the evaluation of the K_D parameter (Mayne et al., 2002).

6.6 Effective Friction Angle from DMT

The peak friction angle in sands can be assessed using the flat plate dilatometer test. A wedge plasticity solution for the CPT was presented by Marchetti (1985) that was later cross-correlated for CPT-DMT relationships by Campanella & Robertson (1991). The wedge solutions relate the DMT lateral stress index (K_D) as a function of ϕ' and lateral stress state including active, at-rest (NC), and passive conditions. The passive case provides a generally conservative evaluation of peak friction angle and gives a good

agreement with field data from different sand sites (Mayne, 2001). The expression for the passive case as presented in **Figure 6.4** can be approximated by a hyperbola in the form:

$$\phi' = 20^\circ + \frac{1}{0.04 + 0.06/K_D} \quad [6.6]$$

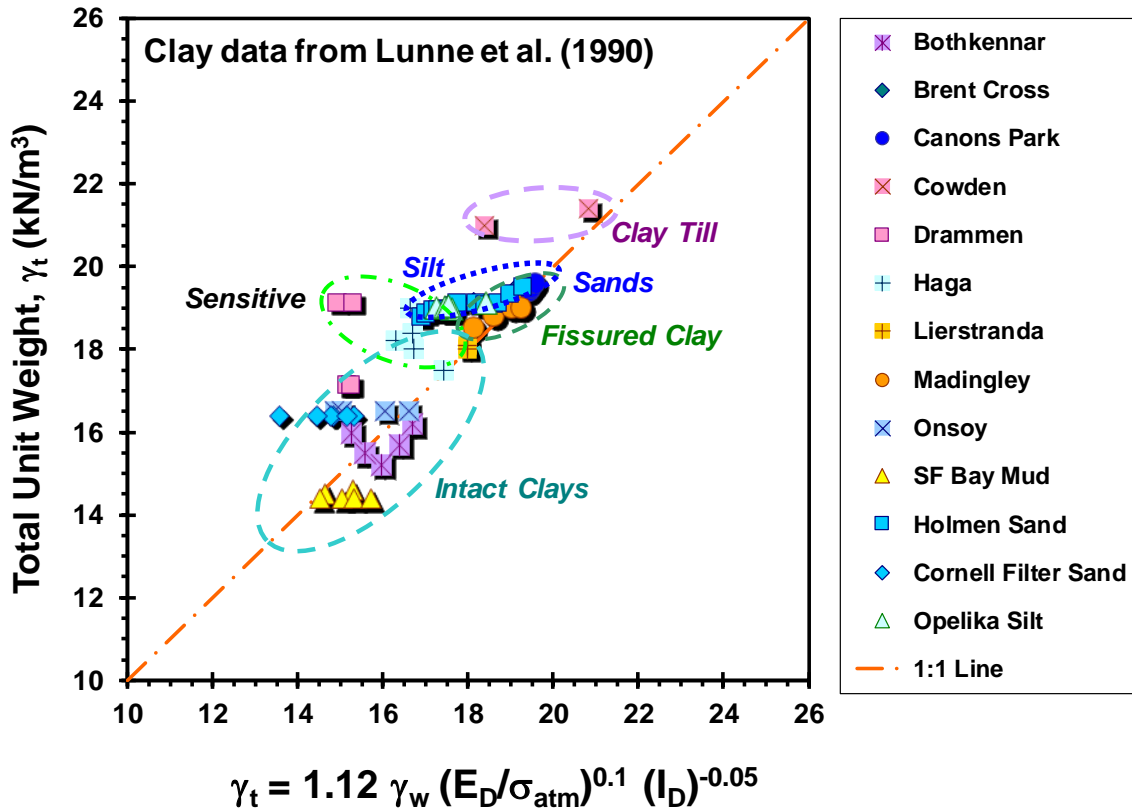


Figure 6.3 Total Unit Weight in terms of DMT Index Parameters (Mayne et al., 2002)

6.7 Modulus of Elasticity from DMT

The dilatometer modulus E_D is obtained from p_0 and p_1 from the theory of elasticity (Gravesen 1960). For the 60 mm membrane diameter and required 1.1 mm displacement, it is found (Marchetti 1980):

$$E_D = 34.7 (p_1 - p_0) \quad [6.7]$$

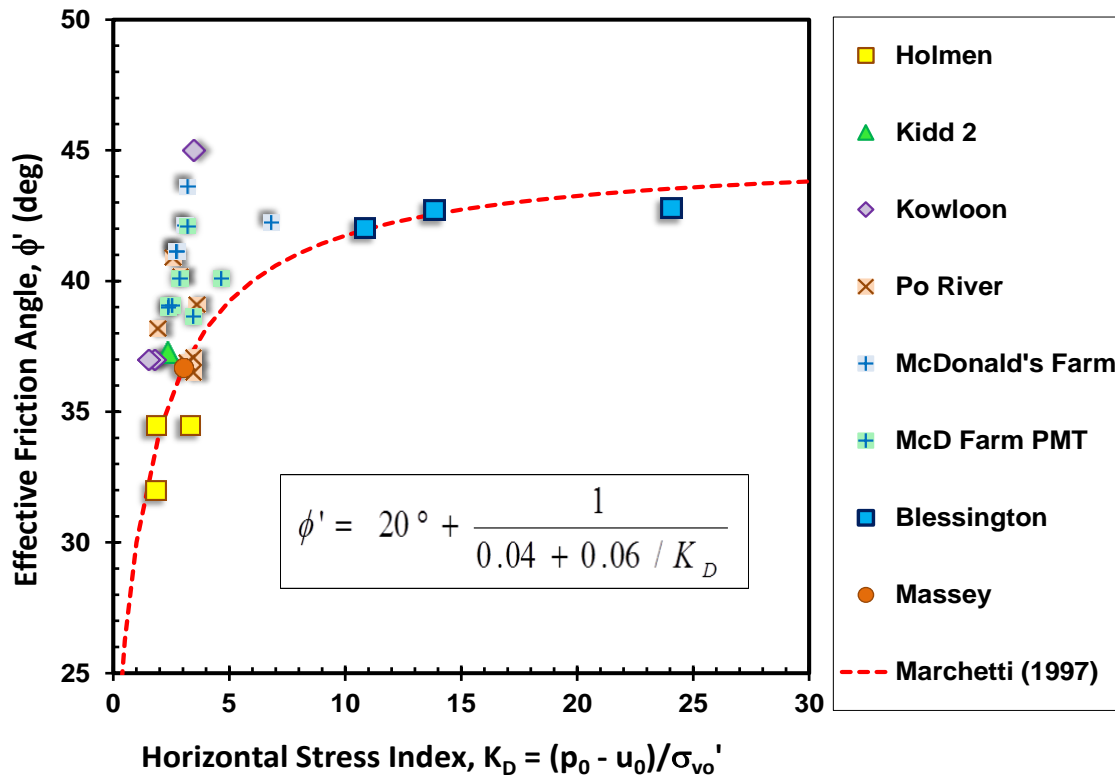


Figure 6.4 *Effective Friction Angle of Sands in terms of DMT Horizontal Stress Index (modified after Mayne 2015)*

An example illustrating the evaluation of the dilatometer material index and modulus from the p_0 and p_1 readings is illustrated in **Figure 6.5** for a local test site in Cherokee County, GA. The constrained modulus M determined from the flat dilatometer test (designated as M_{DMT}) is the drained tangent modulus at σ'_{v0} and is conceptually equivalent to the oedometer modulus obtained in the laboratory ($E_{oed} = 1/m_v$). M_{DMT} can be evaluated using a correction factor R_M to the dilatometer modulus E_D using an adjustment factor R_M :

$$M_{DMT} = R_M \cdot E_D \tag{6.8}$$

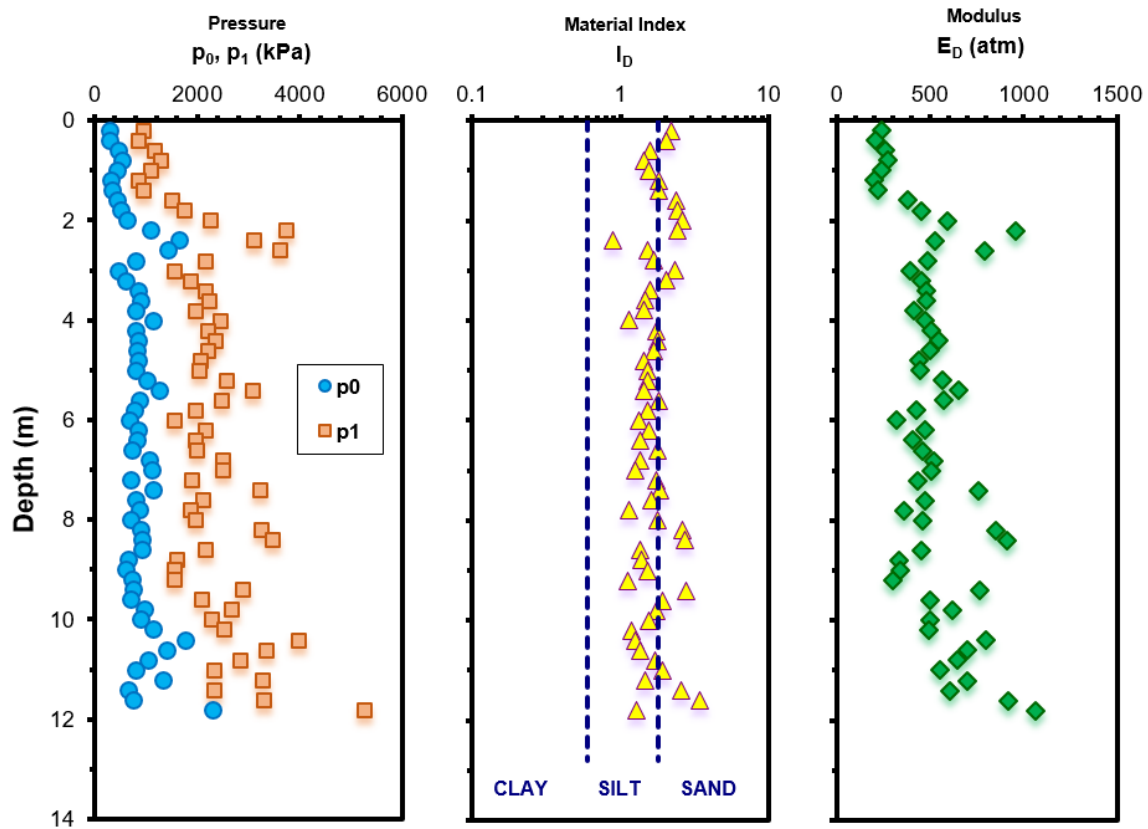


Figure 6.5 Illustration of direct evaluation of E_D from DMT readings (P_0 and P_1) at site in Cherokee County, GA within the Blue Ridge-Piedmont geology

The equations defining R_M as a function of both I_D and K_D are described by (Marchetti 1980) and are given in **Table 6.1**.

Table 6.1 Equations defining correction factor $R_M = M_{DMT}/E_D$

For $I_D < 0.6$	$R_M = 0.14 + 2.36 \log K_D$
For $I_D > 3$	$R_M = 0.5 + 2 \log K_D$
For $0.6 < I_D < 3$	$R_M = R_{M,0} + (2.5 - R_{M,0}) \log K_D$ with $R_{M,0} = 0.14 + 0.15 (I_D - 0.6)$
For $K_D > 10$	$R_M = 0.32 + 2.18 \log K_D$
If $R_M < 0.85$	Set $R_M = 0.85$

The Young's modulus E' of the soil skeleton can be derived from M_{DMT} using the theory of elasticity equation:

$$E' = \frac{(1 + \nu')(1 - 2\nu')}{(1 - \nu')} M_{DMT} \quad [6.9]$$

In sands, using a typical value for Poisson's ratio $\nu' = 0.2$, then $E' = 0.9 M_{DMT}$.

6.8 Stress History from DMT

Initial studies by Marchetti (1980) investigated the relationship between the overconsolidation ratio (OCR) and the DMT horizontal stress index, K_D . The correlation was based on the results of database from only five clays that was later investigated by Mayne (1995) to include data from 24 clays ranging from intact to calcareous to fissured clays as presented in **Figure 6.6**. The correlation is expressed in terms of net contact pressure ($p_0 - u_0$):

$$\sigma_p' \approx 0.5 \cdot (p_0 - u_0) \quad [6.10]$$

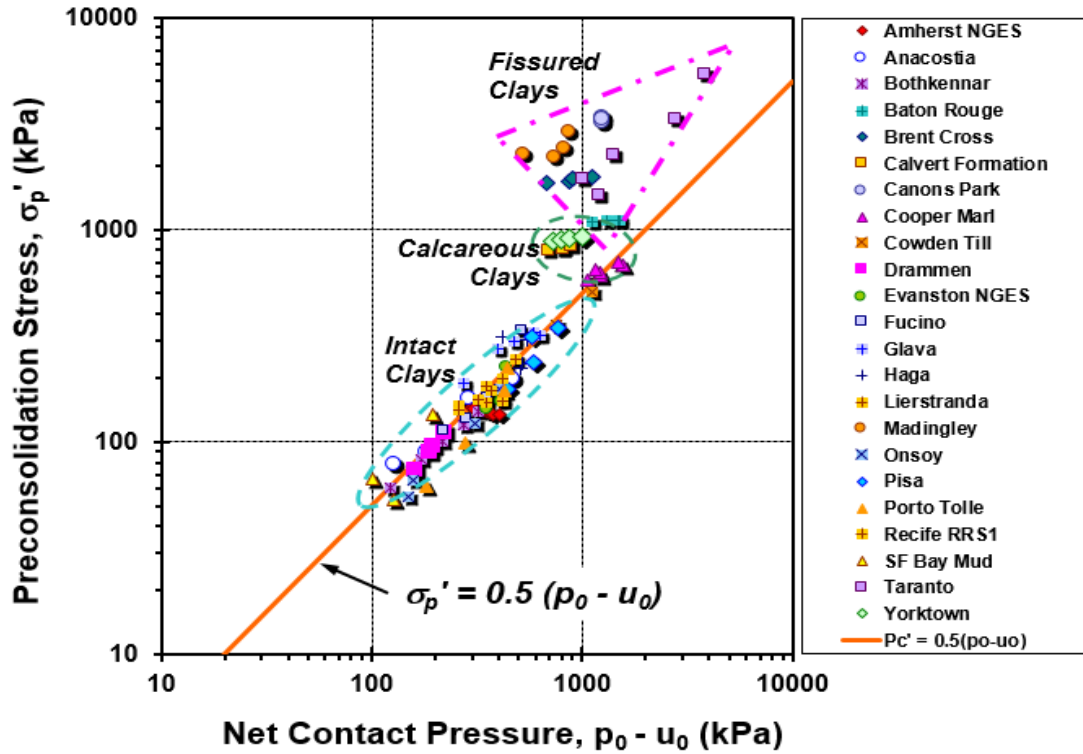


Figure 6.6 Relationship between effective preconsolidation stress and dilatometer net contact pressure ($p_0 - u_0$) for clays

The database was expanded to include other soil types such as sands and silts (including Appalachian Piedmont silts and sands) as shown in **Figure 6.7**. It can be seen that **Equation 6.10** is generally applicable for all soil types and can be used to provide an estimate for effective preconsolidation stress.

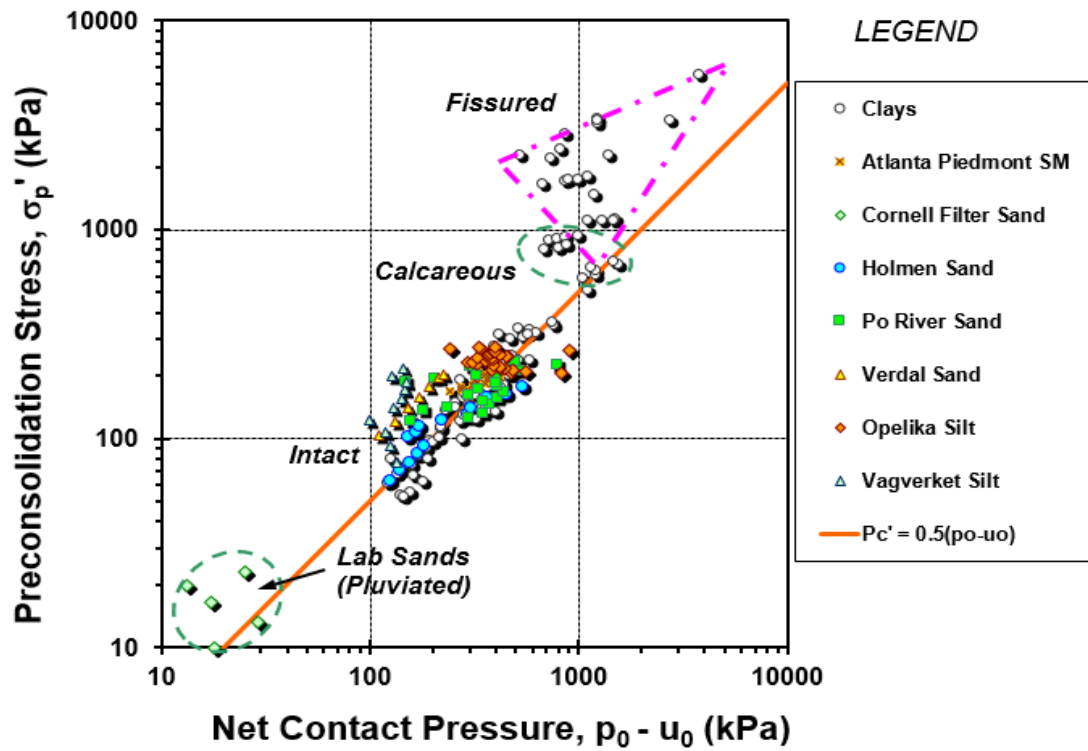


Figure 6.7 Relationship between effective preconsolidation stress and dilatometer net contact pressure ($p_0 - u_0$) for all soil types

7. References

- AASHTO (2008). Interim Revisions to *AASHTO LRFD Bridge Design Specifications*, 4th Edition, 2007. American Association of State Highway and Transportation Officials, Washington, DC.
- AASHTO (2014). *AASHTO LRFD Bridge Design Specifications*, 7th Edition, with 2015 and 2016 Interim Revisions, LRFDUS-7-M. American Association of State Highway and Transportation Officials, Washington, DC. www.transportation.org
- ADOT SF-2 (2010). Limiting Eccentricity Criteria for Spread Footings based on Load and Resistance Factor Design (LRFD) Methodology. *Memorandum* from N.H. Wetz, J.D. Wilson, A. Islam and N. Viboolmate to J. Lawson and J. Nehme, Dated December 1, 2010, Arizona Department of Transportation. Phoenix, AZ. Download document from: www.azdot.gov/Highways/Materials/Geotech_Design/Policy.asp
- Beradi, R., Jamiolkowski, M., and Lancellotta, R. (1991). "Settlement of shallow foundations in sands: Selection of stiffness on the basis of penetration resistance". *Geotechnical Engineering Congress 1991*, Vol. 1 (GSP No. 27), ASCE, Reston, Virginia: 185-200.
- Bhandary, N. P., & Yatabe, R. (2007). "Ring shear tests on clays of fracture zone landslides and clay mineralogical aspects". *Landslide risk and sustainable disaster management. Proceedings of first general assembly of Internal Consortium on Landslides*. Springer, Germany, 183-192.
- Bolton, M.D. (1986). The strength and dilatancy of sands. *Geotechnique* 36 (1): 65-78.
- Boswell, L.F. and Scott, C.R. (1975), "A flexible circular plate on a heterogeneous elastic half-space: influence coefficients for contact stress and settlement". *Geotechnique* 25 (3), 604-610.
- Boulanger, R.W. and I.M. Idriss, *CPT and SPT Based Liquefaction Triggering Procedures*, Report No. UCD/CGM-14/01, Center for Geotechnical Modeling, Univ. California-Davis, 138 pages; 2014.
- Brown, D.A. and Mayne, P.W. (2012). Piedmont residual soils and rocks. *GeoStrata* Vol. 16 (issue 6), ASCE, Reston, Virginia: 18-22.
- Brown, P.T. (1969a). "Numerical analyses of uniformly loaded circular rafts on elastic layers of finite depth". *Geotechnique* 19 (2), 301-306.
- Brown, P.T. (1969b). "Numerical analyses of uniformly loaded circular rafts on deep elastic foundations". *Geotechnique* 19 (3), 399-404.
- Burland, J.B. (1970). Discussion of Session A, *Proceedings, Conference on In-Situ Investigations in Soils and Rocks*, British Geotechnical Society, London, 61-62.
- Burland, J.B. (1989). Ninth Bjerrum Memorial Lecture: "Small is beautiful: the stiffness of soils at small strains". *Canadian Geotechnical Journal* 26 (4), 499-516.

Burns, S.E., Mayne, P.W., and Santamarina, J.C., editors (2008). *Deformational Characteristics of Geomaterials*, Vol. 2 (Proceedings 4th International Symposium on Deformation Characteristics of Geomaterials, Atlanta), Millpress/IOS Press, Amsterdam: Vols. 1 and 2: total 953 pages.

Campanella, R.G. and Robertson, P.K. (1991). "Use and interpretation of a research dilatometer." *Canadian Geotechnical Journal* 28 (1), 113-126.

Carrier, W.D., III, and Christian, J.T. (1973). "Rigid circular plate resting on a non-homogeneous elastic half-space". *Geotechnique* 23 (1), 67-84.

Christian, J.T. and Carrier, W.D., III (1978). "Janbu, Bjerrum, and Kjaernsli's chart reinterpreted". *Canadian Geotechnical Journal* 15 (1), 123-128.

D'Appolonia, D.J., Poulos, H.G., and Ladd, C.C. (1971), "Initial settlement of structures on clay". *ASCE Journal of the Soil Mechanics and Foundations Division* 97 (SM10), 1359-1377.

Das, B. (2011). *Principles of Foundation Engineering, Seventh Edition*, Cengage Learning, Stamford, Conn., 794 pages.

Davis, E.H. and Poulos, H.G. (1968). "The use of elastic theory for settlement prediction under three-dimensional conditions". *Geotechnique* Vol. 18 (1), 67-91.

Diaz-Rodriguez, A., Leroueil, S. and Aleman, J. (1992). "Yielding of Mexico City clay and other natural clays". *Journal of Geotechnical Engineering* 118 (7): 981-995.

Elhakim, A.F. and Mayne, P.W. (2008). Footing stress-displacement response using small-strain modulus. *Deformational Characteristics of Geomaterials*, Vol. 2 (Proc. 4th Intl. Symposium DCG, Atlanta), Millpress/IOS Press, Amsterdam: 937-944.

Fellenius, B.H. (1996; 2009). *Basics of Foundation Design: A geotechnical textbook and a background to the UniSoft programs*. BiTech Publishers, Richmond, British Columbia, 134 pages: www.fellenius.net

Foott, R. and Ladd, C.C. (1981), "Undrained settlement of plastic and organic clays". *ASCE Journal of Geotechnical Engineering Division (ASCE)*, Vol. 107 (GT8), 1079-1094.

Fraser, R.A. and Wardle, L.J. (1976). "Numerical analysis of rectangular rafts on layered foundations". *Geotechnique* Vol. 26 (4), 613-630.

Gibson, R.E. (1967), "Some results concerning displacements and stresses in a nonhomogeneous elastic half-space". *Geotechnique* Vol. 17 (1), 58-67.

Gordon, D. and Mayne, P.W. (1986). Geotechnical report at Surry Power Station, Virginia, submitted to Virginia Power, Richmond VA by Law Engineering Associates, McLean, VA.

Gravesen, S. (1960). "Elastic Semi-Infinite Medium Bounded by a Rigid Wall with a Circular Hole". Laboratoriet for Bygningsteknik, Danmarks Tekniske Højskole, *Meddelelse No. 10*, Copenhagen.

Harr, M.E. (1966), *Foundations of Theoretical Soil Mechanics*, McGraw-Hill, New York, 81-100.

- Harr, M.E. (1977), *Mechanics of Particulate Media*, McGraw-Hill, New York, 330-342.
- Hatanaka, M. and Uchida, A. (1996). "Empirical correlation between penetraion resistance and effective friction of sandy soil.", *Soils & Foundations*, Vol. 36 (4), Japanese Geotechnical Society, 1-9.
- Hegazy, Y.A. and Mayne, P.W. (1995). Statistical correlations between V_s and CPT data for different soil types. *Proceedings, Intl. Symp. on Cone Penetration Testing*, Vol. 2, Swedish Geotechnical Society, Linköping: 173-178. Download from: www.usucger.org
- Holtz, R.D. and Kovacs, W.D. (1981). *An Introduction to Geotechnical Engineering*, Prentice-Hall, Englewood Cliffs, NJ, 733 p.
- Honeycutt, J.N., Kiser, S.E. and Anderson, J.B. (2014). "Database Evaluation of Energy Transfer for CME Automatic Hammer SPT", *Journal of Geotechnical & Geoenvironmental Engineering* Vol. 140 (1): 194-200.
- Horikoshi, K. and Randolph, M.F. (1997). "On the definition of raft-soil stiffness ratio for rectangular rafts". *Geotechnique* Vol. 47 (5), 1055-1061.
- Imai, T., and Tonouchi, K. (1982). "Correlation of N-value with S-wave velocity and shear modulus." *Proceedings of the 2nd European Symposium on Penetration Testing*, Vol. 1, Amsterdam: pp. 67 – 72.
- Jamiolkowski, M., Ghionna, V., Lancellotta, R. and Pasqualini, E. (1988). "New Correlations of Penetration Tests for Design Practice". *Penetration Testing 1988* (Proc. ISOPT-1, Orlando), Vol. 1, Balkema Publishers, Rotterdam: 263-296.
- Jamiolkowski, M., Ladd, C.C., Germaine, J.T., and Lancellotta, R. (1985). "New Developments in Field and Lab Testing of Soils." *Proceedings 11th International Conference on Soil Mechanics and Foundation Engineering*, Vol. 1, San Francisco, Calif. pp. 57–154.
- Jamiolkowski, M., Lancellotta, R., and LoPresti, D.C.F. (1995). "Remarks on the stiffness at small strains of six Italian clays". *Pre-Failure Deformation of Geomaterials*, Vol. 2 (Proc. Sapporo), Balkema, Rotterdam, 817-836.
- Jamiolkowski, M., Lancellotta, R., LoPresti, D.C.F., and Pallara, O. (1994), "Stiffness of Toyoura sand at small and intermediate strain". *Proceedings, 13th Intl. Conf. on Soil Mechanics and Foundation Engineering* (3), New Delhi, India, 169-173.
- Jamiolkowski, M., LoPresti, D.C.F., and Manasserro, M. (2001). Evaluation of relative density and shear strength of sands from CPT and DMT. *Soil Behavior and Soft Ground Construction*, GSP 119, ASCE, Reston, Virginia: 201-238.
- Janbu, N. (1969). "The resistance concept applied to deformations of soils.", *Proceedings, 7th International Conference on Soil Mechanics and Foundation Engineering* (1), Mexico City, 191-196.
- Jardine, R.J., Fourie, A., Maswoswe, J., and Burland, J.B. (1985). "Field and lab measurements of soil stiffness." *Proceedings, 11th International Conference on Soil Mechanics and Foundation Engineering* (2), San Francisco, 511-514.

Kulhawy, F. H., O'Rourke, T. D., Stewart, J. P., and Beech, J. F. (1983). *Transmission Line Structure Foundations for Uplift-Compression Loading*, EPRI Final Report EL-2870. Electric Power Research Institute, Palo Alto: www.epri.com.

Kulhawy, F.H. and Mayne, P.W. (1990). "Manual on Estimating Soil Properties for Foundation Design.", *Report EL-6800*, Electric Power Research Institute, Palo Alto, 306 p. www.epri.com

Lambe, T.W. and Whitman, R.V. (1979). *Soil Mechanics, SI Version*, John Wiley & Sons, New York, 153-158.

Larsson, R. and Mulabdić, M. (1991). Piezocone Tests in Clays. *Report No. 42*, Swedish Geotechnical Institute, Linköping, 240 p.

Lehane, B.M. and Cosgrove, E. (2000). Applying triaxial compression stiffness data to settlement prediction of shallow foundations on cohesionless soil. *Proc. Institution of Civil Engineers, Geotechnical Engineering*, Vol. 143 (4), London: 191-200.

Liao, S.S., and Whitman, R.V. (1986). "Overburden Correction Factors for SPT in Sand." *Journal of Geotechnical Engineering*, ASCE, Vol. 112, No. 3, pp. 373-377.

Locat, J., Tanaka, H., Tan, T.S., Dasari, G.R. and Lee, H. (2003). "Natural soils: geotechnical behavior and geological knowledge". *Characterisation & Engineering Properties of Natural Soils*, Vol. 1 (Proc. Singapore Workshop), Swets & Zeitlinger, Lisse: 3–28.

LoPresti, D.C.F. (1995). "General report: measurement of shear deformation of geomaterials". *Pre-Failure Deformation of Geomaterials*, Vol. 2 (Proc. Sapporo), Balkema, Rotterdam, 1067-1088.

LoPresti, D.C.F., Pallara, O., and Puci, I. (1995). "A modified commercial triaxial testing system for small strain measurements". *ASTM Geotechnical Testing Journal* 18 (1), 15-31.

Lunne, T., Powell, J.J.M., Hauge, E.A., Mokkelbost, K.H., and Uglow, I.M. (1990). "Correlation for dilatometer readings with lateral stress in clays." *Transportation Research Record* 1278, National Academy Press, Washington, D.C., 183-193.

Lunne, T., Robertson, P.K. and Powell, J.J.M. (1997). *Cone Penetration Testing in Geotechnical Practice*. EF Spon/Blackie Academic, Routledge Publishers, London, 312 p.

Marchetti, S. (1980). "In-situ tests by flat dilatometer." *Journal of the Geotechnical Engineering Division (ASCE)*, Vol. 106 (3), 299-321.

Marchetti, S. (1985). "On the field determination of K_0 in sand." *Proceedings, 11th International Conference on Soil Mechanics & Foundation Engineering (ICSMFE, San Francisco)*, Vol 5, Balkema, Rotterdam: 2667-2672.

Marchetti, S. (1997). "The flat dilatometer: design applications." *Proceedings of the 3rd Geotechnical Engineering Conference*, Cairo University, 1-25.

Marchetti, S. (1999). "On the calibration of the DMT membrane." L'Aquila Univ., *Unpublished report*, March. <http://marchetti-dmt.it/>

- Marchetti, S. and Crapps, D.K. (1981). "Flat Dilatometer Manual." *Internal Report* of G.P.E. Inc., Gainesville, Florida. www.gpe.org
- Marchetti, S., Monaco, P., Totani, G., and Calabrese, M. (2001). "The flat dilatometer test (DMT) in soil investigations—A report by the ISSMGE committee TC16." *Proceedings of the 2nd International Flat Dilatometer Conference*, Arlington, VA: pp. 7-48. www.usucger.org
- Massarsch, K.R. (1994). "Settlement Analysis of Compacted Granular Fill". *Proc. XIII Intl. Conf. Soil Mechanics & Foundation Engineering*, New Delhi, Vol. 1, 325- 328.
- Mayne, P.W. (1992). "In-situ characterization of Piedmont residuum in Eastern US". *Proc. National Science Foundation (NSF) US-Brazil Geo-Workshop: Application of Classical Soil Mechanics to Structured Soils*, Belo Horizonte: 89–93.
- Mayne, P.W. (2001). Invited Keynote: "'Stress-Strain-Strength-Flow Parameters from Enhanced In-Situ Tests".", *Proceedings, International Conference on In-Situ Measurement of Soil Properties & Case Histories* (In-Situ 2001), Bali, Indonesia, 27-47.
- Mayne, P.W. (2005). "'Unforeseen large settlements of mat foundation on Piedmont residuum".", *International Journal of Geoengineering Case Histories*: Vol. 1 (1): 5-17. Online GeoEngineer journal at: <http://casehistories.geoengineer.org/contents.html>
- Mayne, P.W. (2005). Invited Keynote: "Integrated Ground Behavior: In-Situ and Lab Tests.", *Deformation Characteristics of Geomaterials*, Vol. 2 (Proc. IS Lyon'03), Taylor & Francis Group, London: 155-177.
- Mayne, P.W. (2006). "In-situ test calibrations for evaluating soil parameters." *Characterisation and Engineering Properties of Natural Soils*", Vol. 3, (Proc. Singapore), Taylor & Francis Group, London: 1602-1652.
- Mayne, P.W. (2006). "The 2006 James K. Mitchell Lecture: Undisturbed sand strength from seismic cone tests." *Geomechanics & Geoengineering*: Vol. 1 (4): 239-257.
- Mayne, P.W. (2007). *NCHRP Synthesis 368 on Cone Penetration Test*. Transportation Research Board, National Academies Press, Washington, D.C., 118 pages. Download from: www.trb.org
- Mayne, P.W. (2007b). Invited Overview Paper: In-situ test calibrations for evaluating soil parameters, *Characterization & Engineering Properties of Natural Soils*, Vol. 3 (Proc. Singapore 2006), Taylor & Francis Group, London: 1602-1652.
- Mayne, P.W. (2013). Updating our geotechnical curricula via a balanced approach of in-situ, laboratory, and geophysical testing of soil. *Proceedings, 61st Annual Geotechnical Conference*, Minnesota Geotechnical Society, University of Minnesota, St. Paul: 65-86.
- Mayne, P.W. (2014) "Interpretation of geotechnical parameters from seismic piezocone tests." In *Proceedings 3rd International Symposium on Cone Penetration Testing, (CPT'14*, Las Vegas): 47-73. Download from: www.cpt14.com
- Mayne, P.W. (2015). Peak friction angle of undisturbed sands using DMT. *Proceedings, Third International Conference on Flat Dilatometer, (DMT'15, Rome)*, paper ID 20: pp. 237-

242: www.dmt15.com

Mayne, P.W. and Brown, D.A. (2003). "Site characterization of Piedmont residuum of North America." *Characterization and Engineering Properties of Natural Soils*, Vol. 2, Swets & Zeitlinger, Lisse, 1323-1339.

Mayne, P.W. and Frost, D.D. (1988). "Dilatometer Experience in Washington, DC and Vicinity", *Transportation Research Record 1169*, National Academy Press, Washington, DC, pp. 16-23

Mayne, P.W. and Harris, D.E. (1993). *Axial Load-Displacement Behavior of Drilled Shaft Foundations in Piedmont Residuum*. FHWA Reference No. 41-30-2175 Report to ADSC/ASCE by Georgia Tech, School of Civil & Environmental Engineering, Atlanta, GA: 172 p. Download: <http://geosystems.ce.gatech.edu/Faculty/Mayne/papers/index.html>

Mayne, P.W. and Kemper, J.B. (1988). "Profiling OCR in Stiff Clays by CPT and SPT." *ASTM Geotechnical Testing Journal*, Vol. 11, No. 2, pp. 139-147.

Mayne, P.W. and Liao, T. (2004). "CPT-DMT interrelationships in Piedmont residuum.", *Geotechnical & Geophysical Site Characterization*, Vol. 1, (Proc. ISC-2, Porto), Millpress, Rotterdam, 345-350.

Mayne, P.W. and Poulos, H.G. (1999). "Approximate Displacement Influence Factors for Elastic Shallow Foundation Systems", *ASCE Journal of Geotechnical & Geoenvironmental Engineering*, Vol. 125, No. 6: 453-460.

Mayne, P.W. and Woeller, D.J. (2014). Direct CPT method for footings on sands, silts, and clays. *Geocharacterization for Modeling and Sustainability* (GSP 235: Proc. GeoCongress 2014, Atlanta), ASCE, Reston, Virginia: 1983-1997.

Mayne, P.W., Brown, D., Vinson, J., Schneider, J.A., and Finke, K.A. (2000). "Site characterization of Piedmont residual soils at the NGES, Opelika, Alabama", *National Geotechnical Experimentation Sites*, (GSP No. 93), American Society of Civil Engineers, Reston/VA: 160-185.

Mayne, P.W., Christopher, B., Berg, R., and DeJong, J. (2002). "Subsurface Investigations - Geotechnical Site Characterization." Publication No. FHWA-NHI-01-031, National Highway Institute, Federal Highway Administration, Washington, D.C., 301 pages

Mayne, P.W., Coop, M.R., Springman, S., Huang, A-B., and Zornberg, J. (2009). State-of-the-Art Paper (SOA-1): Geomaterial Behavior and Testing. *Proc. 17th Intl. Conf. Soil Mechanics & Geotech. Engrg.*, (ICSMGE, Alexandria, Egypt), Vol. 4, Millpress/IOS Press Rotterdam: 2777-2872.

Mayne, P.W., Peuchen, J., and Bouwmeester, D. (2010). Estimation of soil unit weight from piezocone readings in onshore soils. *Proc. 2nd Intl. Symposium on Cone Penetration Testing*, Vol. 2, Huntington Beach, CA: 169-176. www.cpt10.com

Mayne, P.W., Uzielli, M. and Illingworth, F. (2012). Shallow footing response on sands using a direct method based on cone penetration tests. *Full Scale Testing and Foundation Design* (Proceedings GSP 227 honoring Bengt Fellenius), ASCE, Reston, Virginia: 664-679.

- Mesri, G. (1973). "Coefficient of Secondary Compression". *Journal of the Soil Mechanics and Foundations Division, Proc. ASCE*, Vol. 99, No. SM1, pp. 123-137.
- Meyerhof, G. G. (1957). "The Ultimate Bearing Capacity of Foundations on Slopes." In *Proc., 4th International Conference on Soil Mechanics and Foundation Engineering*, Vol. 1, London, UK: 384-386.
- Meyerhof, G.G. (1956). "Penetration tests and bearing capacity of cohesionless soils." *Journal of the Soil Mechanics and Foundations Division ASCE* Vol. 82 (SM1): 1-19.
- Munfakh, G., Arman, A., Gollin, J. G., Hung, J. C. J., and Brouillette, R. P. (2001). *Shallow Foundations Reference Manual, FHWA-NHI-01—023*. Federal Highway Administration, U.S. Department of Transportation, Washington, DC.
- Niazi, F.S. and Mayne, P.W. (2012). Field stiffness reduction evaluations from back-analysis of pile load tests. *Proceedings GeoCongress 2012* (GSP 225, Oakland), ASCE, Reston, Virginia: 155-160.
- Niazi, F.S., Mayne, P.W. and Woeller, D.J. (2014). Pile axial load-displacement response from geophysical component of seismic CPT. *Proceedings, 3rd Intl. Symposium on Cone Penetration Testing*, Las Vegas, Omnipress: 1103-1112. www.cpt14.com
- Paikowsky, S.G., Canniff, M.C., Lesny, K., Kisse, A., Amatya, S., and Muganga, R. (2010). *LRFD Design and Construction of Shallow Foundations for Highway Bridge Structures*. NCHRP Report 651, National Cooperative Highway Research Program, Transportation Research Board, Washington, DC: 149 pages. www.trb.org
- Perloff, W.H. and Baron, W. (1976). *Soil Mechanics: Principles and Applications*, John Wiley & Sons, New York, 745.
- Plewes, H.D., Pillai, V.S., Morgan, M.R. and Kilpatrick, B.L. (1994). "In-situ sampling, density measurements, and testing of foundation soils at Duncan Dam." *Canadian Geotechnical Journal* 31 (6): 927-938.
- Poulos, H.G. (1968). "The behaviour of a rigid circular plate resting on a finite elastic layer". *Civil Engineering Transactions* , Vol. CE 10, Institution of Engineers, Australia, 213-219.
- Poulos, H.G. and Davis, E.H. (1974). *Elastic Solutions for Soil and Rock Mechanics*. John Wiley & Sons, New York: 411 pages. Downloadable from: www.usucger.org
- Prandtl, L. (1921). Ueber die Eindringfestigkeit (Haerte) plastischer Baustoffe und die Festigkeit von Schneiden. *Zeitschrift für angewandte Mathematik und Mechanik* 1, Band 1, 15–20.
- Reissner, H. (1924). ""Zum Erddruckproblem."" *Proc., 1st International Congress of Applied Mechanics*, Delft, 295–311.
- Robertson, P.K. (2004). "Evaluating soil liquefaction and post-earthquake deformations using the CPT". *Geotechnical & Geophysical Site Characterization*, Vol. 1 (Proc. ISC-2, Porto), Millpress, Rotterdam: 233-249.

Robertson, P.K. (2009). "Interpretation of cone penetration tests: a unified approach". *Canadian Geotechnical Journal*, Vol. 46, No. 11, pp. 1337-1355.

Robertson, P.K. and Wride, C.E. (1998). "Evaluating cyclic liquefaction potential using the cone penetration test." *Canadian Geotechnical Journal*, Vol. 35, No. 3, pp. 442-459.

Robertson, P.K., Campanella, R.G., Gillespie, D. and Greig, J. (1986). "Use of piezometer cone data". *Use of In-Situ Tests in Geotechnical Engineering* (GSP 6), ASCE, Reston/VA: 1263-1280.

Sabatini, P.J., Bachus, R.C., Mayne, P.W., Schneider, J.A. and Zettler, T.E. (2002). *Manual on Evaluating Soil & Rock Properties, Geotechnical Engineering Circular No. 5*, Report No. FHWA-IF-02-034, Federal Highway Administration, Washington, D.C., 385 pages.

Salgado, R., Bandini, P., and Karim, A. (2000) "Shear strength and stiffness of silty sand." *Journal of Geotechnical and Geoenvironmental Engineering* 126, no. 5: 451-462.

Salgado, R., Mitchell, J. K., and Jamiolkowski, M. (1998). "Calibration chamber size effects on penetration resistance in sand." *Journal of Geotechnical and Geoenvironmental Engineering* 124, no. 9: 878-888.

Samtani, N.C., Nowatzki, E.A., and Mertz, D.R. (2010). *Selection of Spread Footings on Soils to Support Highway Bridge Structures* (No. FHWA-RC/TD-10-001). Federal Highway Administration, U.S. Department of Transportation, Washington, DC: 98 pages.

Sargand, S.M., Masada, T., and Abdalla, B. (2003). "Evaluation of cone penetration test based settlement prediction methods for shallow foundations on cohesionless soils at highway bridge construction sites. *Journal of Geotechnical & Geoenvironmental Engineering*, Vol. 129 (10): 900-908.

Sargand, S.M. and Masada, T. (2006). Further Use of Spread Footing Foundations for Highway Bridges. *Final Rept. FHWA-OH-2006/8*, Ohio University and Ohio Research Institute for Transportation and the Environment (ORITE), Athens, OH: 332 pages.

Schmertmann, J.H. (1970). "Static cone to compute static settlement over sand", *Journal of the Soil Mechanics and Foundations Division* (ASCE) 96 (SM3), 1011-1043.

Schmertmann, J.H. (1986). "Dilatometer to compute Foundation Settlement". *Use of In-Situ Tests in Geotechnical Engineering*, (Proc. In-Situ'86, Virginia Tech, Blacksburg, VA), GSP 6, ASCE, Reston, Virginia: 303-321.

Schmertmann, J.H., Hartman, J.P., and Brown, P.R. (1978). "Improved strain influence factor diagrams". *Journal of Geotechnical Engineering Division* (ASCE) Vol. 104, 1131-1135.

Schnaid, F. (2009). *In-Situ Testing in Geomechanics: the Main Tests*. CRC Press / Taylor & Francis Group, London: 352 p.

Skempton, A.W. (1986). "SPT procedures and the effects in sands of overburden pressure, relative density, particle size, aging, and overconsolidation." *Geotechnique*, Vol. 36, No. 3, 425-447.

- Skempton, A.W. and Bjerrum, L. (1957), "A contribution to the settlement analysis of foundations on clay", *Geotechnique*, Vol. 7 (4), 168-178.
- Small, J.C. (1995). "FLEA5 - finite layer elastic analysis: users manual for PC version for Windows". *Report FLEA5*, Geotechnical Research Centre, University of Sydney, Australia.
- Stamatopoulos, A.C. and Kotzias, P.C. (1978). "Soil compressibility as measured in the oedometer". *Geotechnique* 28 (4), 363-375.
- Sully, J.P. and Escheturia, H.J. (1988). In-situ density measurement with the nuclear cone penetrometer. *Penetration Testing 1988*, Vol. 2 (Proc. ISOPT, Orlando), Balkema, Rotterdam: 1001-1006.
- Széchy, K. and Varga, L. (1978). *Foundation Engineering: Soil Exploration and Spread Foundations*. Technical University of Budapest, Akadémiai Kiadó, Hungary, 351-353.
- Tatsuoka, F. and Shibuya, S. (1992). "Deformation characteristics of soils and rocks from field and laboratory tests". *Report of the Institute of Industrial Science*, Vol. 37, No. 1, Serial No. 235, The University of Tokyo, 138 p.
- Tatsuoka, F., Teachavorasinsku, S., Dong, J., Kohata, Y. and Sato, T. (1994). "Importance of measuring local strains in cyclic triaxial tests on granular materials". *Dynamic Geotechnical Testing II* (STP 1213), ASTM, Philadelphia, 288-302.
- Taylor, B.B., Lewis, J.F. and Ingersoll, R.W. (1993) "Comparison of interpreted seismic profiles to geotechnical borehole data at Hibernia." *Proceedings of the 4th Canadian Conference on Marine Geotechnical Engineering*, St. John's, Newfoundland: 685-708.
- Terzaghi, K., Peck, R. B., & Mesri, G. (1996). *Soil Mechanics in Engineering Practice*. John Wiley & Sons: 565p.
- Thompson, G.R. and Long, L.G. (1989) "Hibernia geotechnical investigation and site characterization." *Canadian Geotechnical Journal* 26 (4): 653-678.
- Ueshita, K. and Meyerhof, G.G. (1967). "Deflection of multilayer soil systems". *Journal of the Soil Mechanics and Foundations Division* (ASCE) 93 (SM5), 257-282.
- Ueshita, K. and Meyerhof, G.G. (1968). "Surface displacement of an elastic layer under uniformly-distributed loads". *Highway Research Record* 228, National Research Council, Washington, D.C., 1-10.
- Uzielli, M. and Mayne, P.W. (2012). Load-displacement uncertainty of vertically-loaded shallow footings on sands and effects on probabilistic settlement estimation. *Georisk: Assessment and Management of Risk for Engineered Systems and GeoHazards*. Vol. 6 (1): Taylor & Francis: 50-69.
- Vesić, A. (1975). "Bearing Capacity of Shallow Foundations." *Foundation Engineering Handbook*, H. F. Winterkorn and H. Y. Fang, eds., Van Nostrand Reinhold, New York: 121–147.

Viswanath, M. and Mayne, P.W. (2012). Direct SPT method for footing response in sands using a database approach. *Geotechnical and Geophysical Site Characterization 4*, Vol. 2 (Proc. ISC-4, Pernambuco), CRC Press, London: 1131-1137.

Weary, D.J. (2005). An Appalachian regional karst map and progress towards a new national karst map. *US Geological Survey Report 5160 part A*: 93-101: www.usgs.gov

Youd, T.L., et al., (2001) "Liquefaction Resistance of Soils: Summary Report from the 1996 NCEER and 1998 NCEER/NSF Workshops on Evaluation of Liquefaction Resistance of Soils". *Journal of Geotechnical and Geoenvironmental Engrg.* 127 (10): 817-833.

Yu, H.S. and Mitchell, J.K. (1998). "Analysis of cone resistance: review of methods" *Journal of Geotechnical and Geoenvironmental Engineering* 124, (2): 140-149.

Appendix A: Guidelines on how to use the Excel spreadsheets

Guidelines on Using the BC-Settlement Design Spreadsheet using SPT input data

1. Open the input data tab and enter the project relevant information in the data entry cells that include: GDOT project ID, project name, project location, boring number, and the testing date.
2. Under the input tab, fill the values of ground water table (feet), and the energy rating (%) of the conducted SPT.
3. Under the input tab, fill footing input parameters: embedment depth in (feet) which is the shallowest depth of footing embedment below final grade, typically taken as 1 ft to account for frost protection (in Georgia), footing thickness in (feet) which is taken as zero for MSE walls, layer thickness in (feet) leave as 999 feet unless depth to bedrock refusal is known to account for a thick homogeneous soil layer, modulus of elasticity of foundation material in (ksf) which can be taken as 4000 ksf for MSE walls and approximately 600,000 ksf for reinforced concrete.
4. Under the input tab, check the foundation shape and geometry, if the footing length (L) is known then fill it in the relevant cell in feet, otherwise determine if your footing is square (using L/B ratio of 1), rectangular (using $1 < L/B \text{ ratio} < 10$) or strip (using L/B ratio of 10 or more). If the footing width (B) is known or a specific value needs to be investigated then fill the relevant cell in feet where the specific L/B ratio for the case under study will be automatically evaluated.
5. Fill in the specific settlement values that need to be evaluated in inches.
6. If the bottom of wall footing/leveling pad/spread footing elevation is more than 5 feet below the ground elevation in your boring log, begin inputting boring log data from the elevation that corresponds to 5 feet above the bottom of wall footing/leveling pad/spread footing elevation.
7. In the input tab fill in the SPT raw readings: fill in the depth (feet) and the SPT readings, either: (a) individual blows for 6-inch increments #1, #2, and #3; or (b) the summed up N_{measured} value in blows per foot.
8. Fill in each of the soil type cells with depth following the USCS classification system. The following soil types are recognized in the spreadsheet: PT, OL, OH, ML, MH, CL, CH, SW, SP, GW, GP, GM, GC, SM, SC, CL-ML, SM-ML, ML-SM, SM-MH, MH-SM, GP-GC, GP-GM, GW-GC, GW-GM, SC-SM, GC-GM, SP-SC, SP-SM, SW-SC, SC-H, SM-H, SM-SC, GM-GC, and SW-SM.
9. After providing the soil type cell according to USCS, a number of unfavorable problematic soil types will be highlighted, flagged and colored: silts, clays, organics, and peat. Any mistake in typing the soil type or any non-USCS classified soils will be flagged as "UNKNOWN".
10. Next to the soil type column check if there are any messages of "CONTACT SENIOR GEOTECH ENGINEER" which will appear in the case of organics with

low plasticity (OL), or organics with high plasticity (OH), or peat (PT), indicating the insuitability of the studied location.

11. Also check if there are any messages of “CONTACT GEOTECH ENGINEER – CHECK OCR PROFILE” which will appear in case of soft normally consolidated to lightly over consolidated clays or silts with low overconsolidation ratio values < 3 . A guideline on acceptable and unacceptable OCRs is provided in Section 4.8 of this report.
12. Check the percentage of clay readings relative to the total number of readings which should be acceptable if the value is below 10% and provided that OCRs > 3 .
13. After filling the raw SPT and footing data, any additional notes can be added in the “additional notes” box provided, for the particular case under study.
14. After filling the data in the input tab, the averaged geoparameters (soil unit weight, angle of internal friction, and soil modulus of elasticity) will be automatically calculated and averaged in the SPT-CALCS tab using a geometric mean function. The averaged geoparameters exclude any data at depth smaller than the embedment depth.
15. Under the Geoparameter Plots tab there will be summary plots of N_{measured} , N_{60} , unit weight (γ), soil modulus of elasticity (E), angle of internal friction (ϕ), and overconsolidation ratio (OCR) with a cutoff OCR value of 3 versus depth in both metric and English units.
16. Under the summary tab, there will be plots of all LRFD solutions for shallow foundations bearing capacity and settlement design charts for square, rectangular, and strip footings on granular soils.
17. Based on the type of analyses required, choose the corresponding tab for more details. In the analyses tabs, a default value of 0.2 is assigned for the Poisson’s ratio of the soil (drained behavior) and of the foundation material. And since the spreadsheet is evaluating bearing capacity and settlement for granular soils then a default effective cohesion intercept (c') value of zero is assigned. All other values are automatically populated based on previously entered information.
18. For factored bearing resistance versus footing width for different settlement values use the tabs: Constant L, Square, Rectangle, or Strip. If the footing width (B) is known or a specific value is needed for investigation and filled in the input data tab, then this value will be calculated and highlighted in green in all the analyses tables.
19. The constant L tab will be used if the footing length (L) is known and filled in the input data tab. Use the square tab in case of square footings with L/B ratio = 1. For rectangular footings use the rectangle tab with the intermediate value of $1 < L/B$ ratio < 10 . For strip footings use the strip tab that uses L/B ratio of 10 or more.

20. For a different representation of the results, there are plots in terms of factored bearing resistance versus settlement for different footing width values. Using this representation there are two options; either a footing with a constant length L for which you will use the stress-settlement for constant L tab or a square footing with L / B ratio = 1 for which you will use the stress-settlement-square tab.

Guidelines on Using the BC-Settlement Design Spreadsheet using CPT input data

1. Open the input tab and enter the project relevant information in the data entry cells that include: GDOT project ID, project name, project location, boring number, and the testing date.
2. Under the input tab, fill footing input parameters: embedment depth in (feet) which is the shallowest depth of footing embedment below final grade, typically taken as 1 ft to account for frost protection (in Georgia), footing thickness in (feet) which is taken as zero for MSE walls, layer thickness in (feet) leave as 999 feet unless depth to bedrock refusal is known to account for a thick homogeneous soil layer, modulus of elasticity of foundation material in (ksf) which can be taken as 4000 ksf for MSE walls and approximately 600,000 ksf for reinforced concrete.
3. Under the input tab, fill the ground water table (feet).
4. Under the input tab, check the foundation shape and geometry, if the footing length is known then fill it in the relevant cell in feet, otherwise determine if your footing is square (using L/B ratio of 1), rectangular (using $1 < L/B$ ratio < 10) or strip (using L/B ratio of 10 or more). If the footing width (B) is known or a specific value needs to be investigated then fill the relevant cell in feet where the specific L/B ratio for the case under study will be automatically evaluated.
5. Fill in the specific settlement values that need to be evaluated in inches.
6. If the bottom of wall footing/leveling pad/spread footing elevation is more than 5 feet below the ground elevation in your boring log, begin inputting boring log data from the elevation that corresponds to 5 feet above the bottom of wall footing/leveling pad/spread footing elevation.
7. In the input tab, fill in the CPT readings: put the depth (feet) and the corresponding CPT readings: cone tip resistance (q_t in ksf), sleeve friction (f_s in ksf), and porewater pressure (u_2 in ksf). Hint: The input of CPT data is probably best accomplished by preparing the CPT data with depth, q_t , f_s , and u_2 in a matrix of four columns wide by many rows of the full length of the sounding and cutting & pasting the data over the input page at the proper columns.
8. The soil type cell with depth will be automatically evaluated indicating the type of the soil formation encountered. For the unfavorable problematic soil types (i.e., silts, clays, and organics) the cells will be highlighted, flagged and colored.
9. Check if there are any messages of "CONTACT GEOTECH ENGINEER – CHECK OCR PROFILE" which will appear in case of normally consolidated to lightly over consolidated clays or silts or sensitive clays with low overconsolidation ratio values < 3 . See Section 4.8 on a discussion of acceptable and unacceptable OCRs in clays.

10. Next to the soil type column check if there are any messages of “CONTACT SENIOR GEOTECHNICAL ENGINEER” which will appear in the case of organic clays indicating the insuitability of the studied location.
11. Check the percentage of clay readings relative to the total number of readings which should be acceptable if the value is below 10% provided that OCRs > 3.
12. After filling the raw CPT and footing data, any additional notes can be added in the “additional notes” box provided, for the particular case under study.
13. After completing the data input, the values of the geoparameters (soil unit weight, effective friction angle, and soil modulus of elasticity) will be automatically calculated and averaged in the CPT-CALCS tab using a geometric mean function. The averaged geoparameters exclude any data at depth smaller than the embedment depth..
14. Under the Geoparameter Plots tab there will be summary plots of cone tip resistance (q_t), sleeve friction (f_s), and porewater pressure (u_2), unit weight, soil modulus of elasticity, angle of internal friction, and overconsolidation ratio with a cutoff OCR value of 3 versus depth, reported in both metric and English units.
15. Under the summary tab, there will be plots of all LRFD solutions for shallow foundations bearing capacity and settlement design charts for square, rectangular, and strip footings on granual soils.
16. In the analyses tabs, a default value of 0.2 is assigned for the Poisson’s ratio of the soil (drained behavior) and of the foundation material. A default effective cohesion intercept (c') value of zero is assigned. All other values are automatically populated based on previously entered information.
17. For factored bearing resistance versus footing width for different settlement values use the tabs: Constant L, Square, Rectangle, or Strip. If the footing width (B) is known or a specific value is needed for investigation and filled in the input data tab, then this value will be calculated and highlighted in green in all the analyses tables.
18. The constant L tab will be used if the footing length (L) is known and filled in the input data tab. Use the square tab in case of square footings with L/B ratio = 1. For rectangular footings use the rectangle tab with the intermediate value of $1 < L/B$ ratio < 10. For strip footings use the strip tab that uses L/B ratio of 10 or more.
19. For a different representation of the results, there are plots in terms of factored bearing resistance versus settlement for different footing width values. Using this representation there are two options; either a footing with a constant length L for which you will use the stress-settlement for constant L tab or a square footing with L / B ratio = 1 for which you will use the stress-settlement-square tab.

Guidelines on Using the BC-Settlement Design Spreadsheet using DMT input data

1. Open the input tab and enter the project relevant information in the data entry cells that include: GDOT project ID, project name, project location, boring number, and the testing date.
2. Under the input tab, fill footing input parameters: embedment depth in (feet) which is the shallowest depth of footing embedment below final grade, typically taken as 1 ft to account for frost protection (in Georgia), footing thickness in (feet) which is taken as zero for MSE walls, layer thickness in (feet) leave as 999 feet unless depth to bedrock refusal is known to account for a thick homogeneous soil layer, modulus of elasticity of foundation material in (ksf) which can be taken as 4000 ksf for MSE walls and approximately 600,000 ksf for reinforced concrete.
3. Under the input tab, fill the calibration factor ΔA (in bars), calibration factor ΔB (in bars), and the ground water table (feet). Additional details on the calibration factors (ΔA and ΔB) are provided in Sections 6.3 and 6.4 of this report. In usual practice, values of these calibration factors are around 0.1 to 0.3 bars.
4. Under the input tab, check the foundation shape and geometry, if the footing length is known then fill it in the relevant cell in feet, otherwise determine if your footing is square (using L/B ratio of 1), rectangular (using $1 < L/B$ ratio < 10) or strip (using L/B ratio of 10 or more). If the footing width (B) is known or a specific value needs to be investigated then fill the relevant cell in feet where the specific L/B ratio for the case under study will be automatically evaluated.
5. Fill in the specific settlement values that need to be evaluated in inches.
6. If the bottom of wall footing/leveling pad/spread footing elevation is more than 5 feet below the ground elevation in your boring log, begin inputting boring log data from the elevation that corresponds to 5 feet above the bottom of wall footing/leveling pad/spread footing elevation.
7. In the input tab fill in the DMT raw readings: input the depth (feet) and the DMT readings: A and B in bars. Hint: it may prove easier to set up a three column data set with the readings: depth, A, B; and then cut & paste these into the Input Cells.
8. The soil type cell with depth will be automatically evaluated indicating the type of the soil formation encountered. For the unfavorable problematic soil types (silts or clays) the cells will be highlighted and colored.
9. Check if there are any messages of "CONTACT GEOTECH ENGINEER – CHECK OCR PROFILE" which will appear in case of normally-consolidated to lightly overconsolidated clays or silts with low overconsolidation ratio values < 3 . Guidance as to acceptable and unacceptable OCRs are discussed in Section 4.8 of this report.

10. Check the percentage of clay readings relative to the total number of readings which should be acceptable if the value is below 10%, provided that OCRs > 3.
11. After filling the raw DMT and footing data, any additional notes can be added in the “additional notes” box provided, for the particular case under study.
12. After completing the data in the input tab, the averaged geoparameters (soil unit weight, effective friction angle, and soil modulus of elasticity) will be automatically calculated and averaged in the DMT-CALCS tab using a geometric mean function. The averaged geoparameters exclude any data at depth smaller than the embedment depth..
13. Under the Geoparameter Plots tab there will be summary plots of the DMT p_0 and p_1 , unit weight, soil modulus of elasticity, angle of internal friction, and overconsolidation ratio with a cutoff OCR value of 3 versus depth in both metric and English units.
14. Under the summary tab, there will be plots of all LRFD solutions for shallow foundations bearing capacity and settlement design charts for square, rectangular, and strip footings on granular soils.
15. In the analyses tabs, a default value of 0.2 is assigned for the Poisson’s ratio of the soil and of the foundation material. A default effective cohesion intercept (c') value of zero is assigned. All other values are automatically populated based on previously entered information.
16. For factored bearing resistance versus footing width for different settlement values use the tabs: Constant L, Square, Rectangle, or Strip. If the footing width (B) is known or a specific value is needed for investigation and filled in the input data tab, then this value will be calculated and highlighted in green in all the analyses tables.
17. The constant L tab will be used if the footing length (L) is known and completed in the input data tab. Use the square tab in case of square footings with L/B ratio = 1. For rectangular footings use the rectangle tab with the intermediate value of $1 < L/B \text{ ratio} < 10$. For strip footings use the strip tab that uses L/B ratio of 10 or more.
18. For a different representation of the results, there are plots in terms of factored bearing resistance versus settlement for different footing width values. Using this representation there are two options; either a footing with a constant length L for which you will use the stress-settlement tab for constant L or a square footing with L / B ratio = 1 for which you will use the stress-settlement-square tab.

Appendix B: Illustrated Example using SPT data

Standard Penetration Test Data		
GDOT Project ID:	Test Data Number 2	← data entry
Project Name:	Georgia LRFD Site	← data entry
Location:	Newnan	← data entry
Boring Number:	SPT-X552	← data entry
Date:	18 March 2016	← data entry

SPT procedures per ASTM D 1586

Figure B.1 Raw SPT Input Data

FOOTING INPUT PARAMETERS

Embedment Depth, D_f (ft) = ← data entry

Footing Thickness, t (ft) = ← data entry

Layer Thickness, h (ft) = ← data entry

Modulus of Foundation, E_{FDTN} (ksf) = ← data entry

Ground Water Table feet ← data entry

Energy Rating % ← data entry

Figure B.2 Footing Input Parameters and Energy Rating

FOUNDATION SHAPES and GEOMETRY

Footing Length L (ft) = ← data entry if known

Footing Width B (ft) = ← data entry if known

Current Case - L/B = 13

Square - L/B = 1

Rectangular - L/B = 5

Strip - L/B = 10

Figure B.3 Foundation Shape and Geometry

Total Number of Readings	25
Number of Clay Readings	3
% Clay Readings	12.00

Figure B.4 Percentage of Clay Readings

SPECIFIC SETTLEMENT VALUE (in)

0.5	← data entry
1	← data entry
1.5	← data entry
2	← data entry
2.5	← data entry
3	← data entry
4	← data entry

Figure B.5 Specific Settlement Values Input

Depth (feet)	SPT Reading N-value (bpf)	USCS Soil Type	
0.00			
data entry → 1.50	12	SM	
data entry → 3.00	18	SC	
data entry → 4.50	22	PT	CONTACT SENIOR GEOTECH ENGINEER
data entry → 6.00	26	MH	
data entry → 7.50	28	ML	
data entry → 9.00	15	SM-SC	
data entry → 10.50	16	SW-SC	
data entry → 12.00	17	OL	CONTACT SENIOR GEOTECH ENGINEER
data entry → 13.50	19	SM	
data entry → 15.00	22	GW	

Figure B.6 Alternative (a): Raw SPT Input Data: Depth, Measured N (bpf), and Soil Type

Raw SPT Blows Per 6 inches			
#1	#2	#3	N-value (bpf)
data entry → 2	8	4	12
data entry → 3	9	9	18
data entry → 4	10	12	22
data entry → 5	14	12	26
data entry → 6	14	14	28
data entry → 6	8	7	15
data entry → 3	6	10	16
data entry → 4	10	7	17
data entry → 5	10	9	19
data entry → 6	12	10	22

Figure B.7 Alternative (b): Raw SPT Input Data: Row Field Blows per 6 inches

Additional Notes:

Figure B.8 Additional Notes Box

GEOPARAMETER		SI Units		English Units	
Average	Unit Weight	18.68	kN/m ³	0.1189	kcf
	Friction Angle ϕ	38.496	degrees	38.496	degrees
	Modulus of Elasticity	347.20	bar	725.15	ksf

Figure B.9 Average Unit Weight, Friction Angle, and Soil Modulus of Elasticity using SPT Input Data

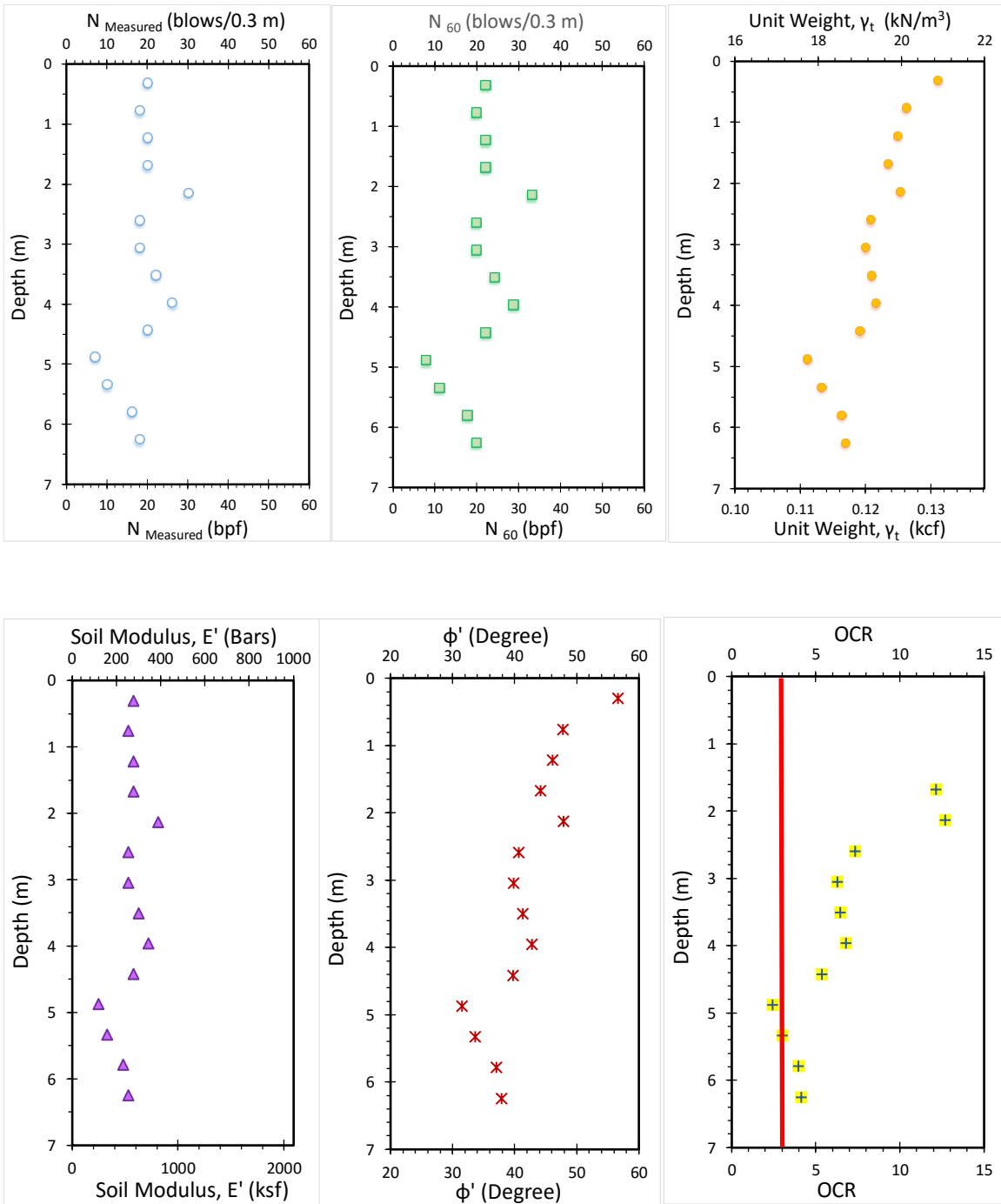


Figure B.10 Profiles of SPT Input and Output Data

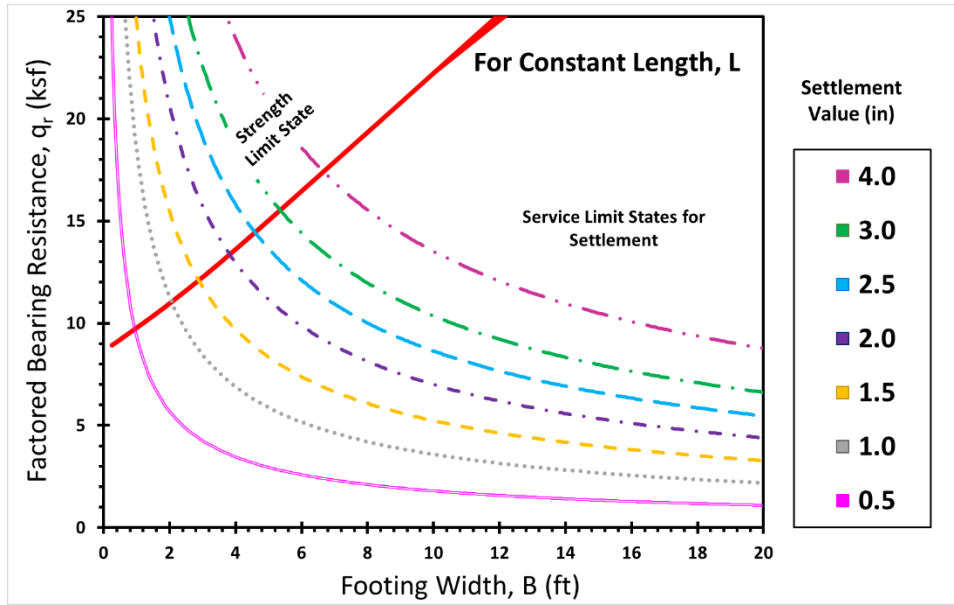


Figure B.11 Factored BC-Footing Width Design Chart with different settlement contours for Constant L value

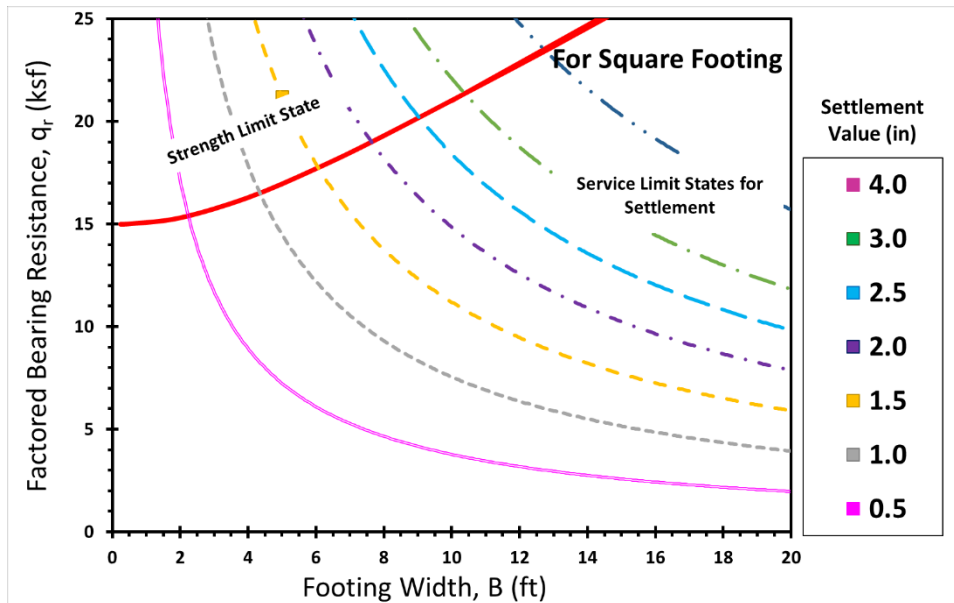


Figure B.12 Factored BC-Footing Width Design Chart with different settlement contours for Square Footing (Constant L/B ratio = 1)

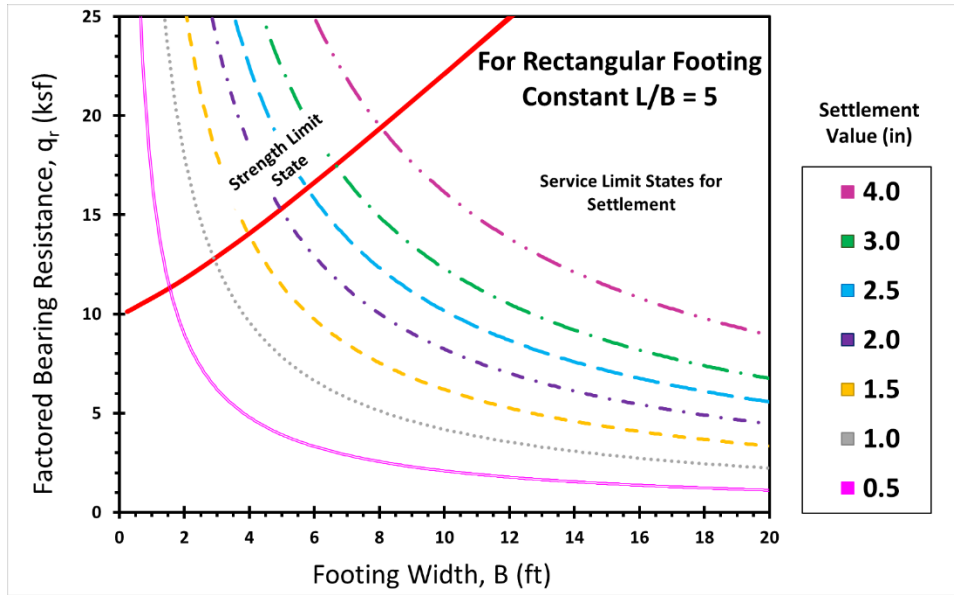


Figure B.13 Factored BC-Footing Width Design Chart with different settlement contours for Rectangular Footing ($L/B = 5$)

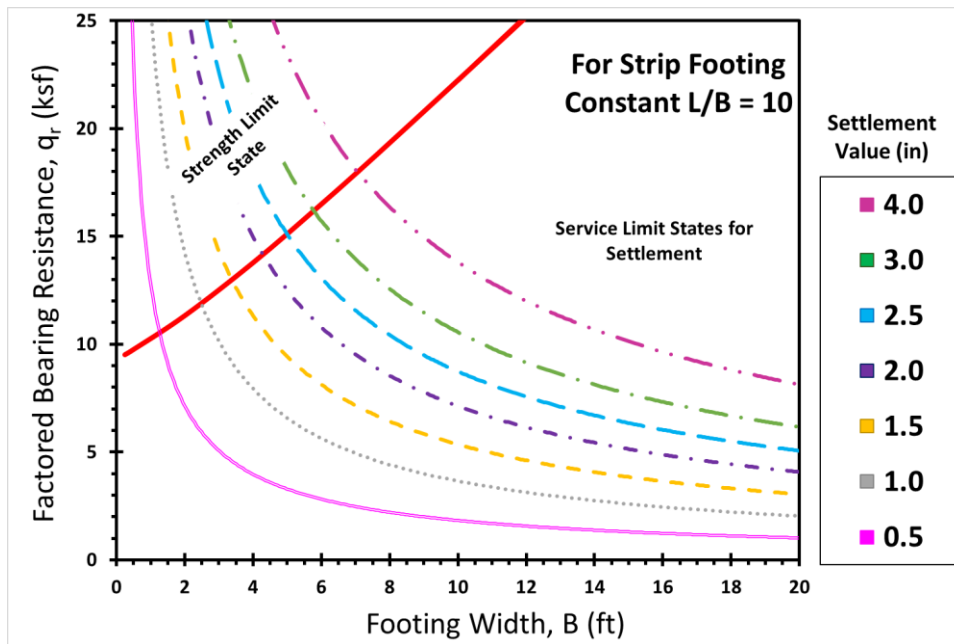


Figure B.14 Factored BC-Footing Width Design Chart with different settlement contours for Strip Footing ($L/B = 10$)

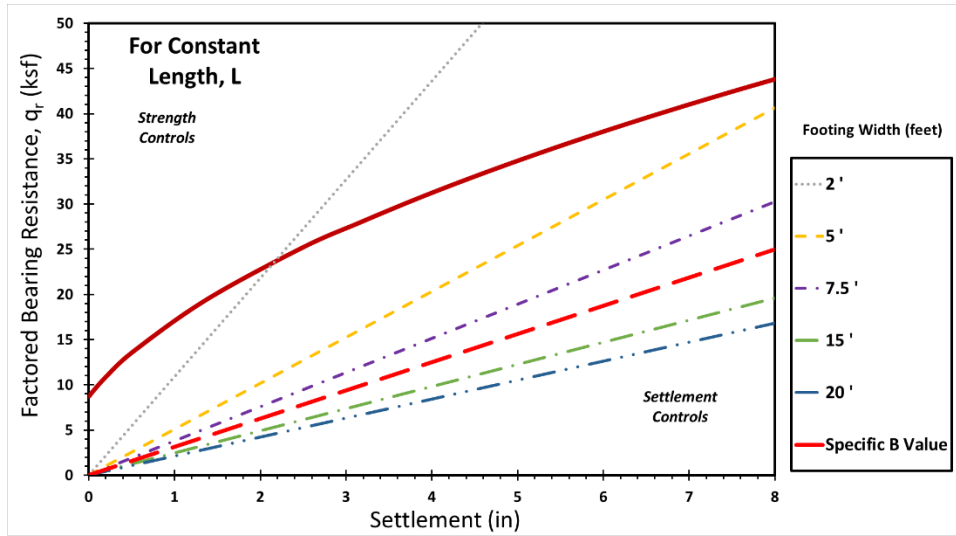


Figure B.15 Factored BC-Settlement Design Chart with different footing width contours for footings with Constant Length

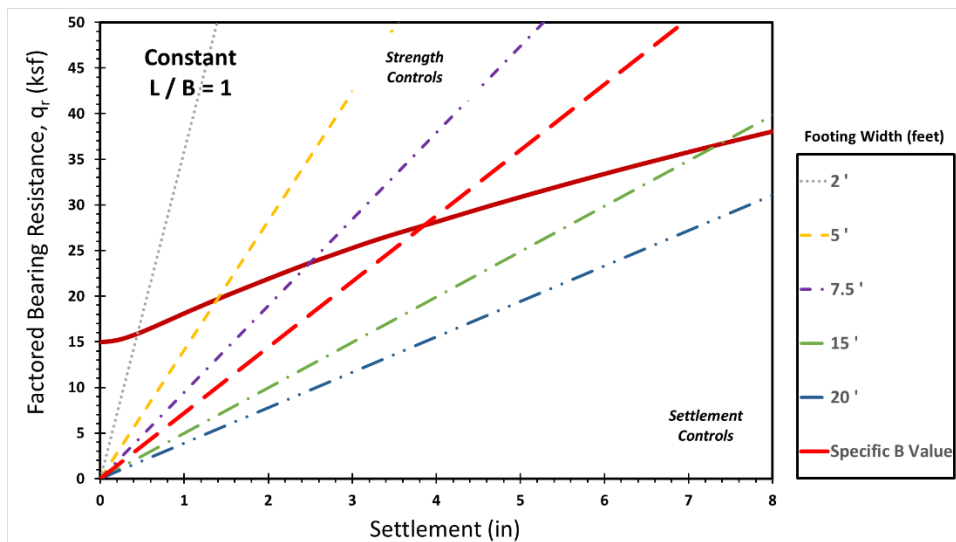


Figure B.16 Factored BC-Settlement Design Chart with different footing width contours for Square Footing ($L/B = 1$)

Appendix C: Illustrated Example using CPT data

Cone Penetration Test Data		
GDOT Project ID:	Test Data Number 1	← data entry
Project Name:	XXXXX	← data entry
Location:	XXXXX	← data entry
Boring Number:	CPT-01	← data entry
Date:	18 March 2016	← data entry

CPT procedures per ASTM D 5778

Figure C.1 Raw CPT Input Data

FOOTING INPUT PARAMETERS

Embedment Depth, D_f (ft) =	<input type="text"/>	← data entry
Footing Thickness, t (ft) =	<input type="text"/>	← data entry
Layer Thickness, h (ft) =	<input type="text"/>	← data entry
Modulus of Foundation, E_{FDTN} (ksf) =	<input type="text"/>	← data entry

Ground Water Table feet ← data entry

Figure C.2 Footing Input Parameters

FOUNDATION SHAPES and GEOMETRY

Footing Length L (ft) =	<input type="text" value="100"/>	← data entry if known
Footing Width B (ft) =	<input type="text" value="8"/>	← data entry if known
Current Case - L/B =	13	
Square - L/B =	1	
Rectangular - L/B =	5	
Strip - L/B =	10	

Figure C.3 Foundation Shape and Geometry

Total Number of Readings 755
Number of Clay Readings 5
% Clay Readings 0.662

Figure C.4 Percentage of Clay Readings

		CPT Readings		
Depth (ft)		q_t (ksf)	f_s (ksf)	u_2 (ksf)
0.00				
data entry →	0.46	12.90	0.01	0.00
data entry →	0.52	19.66	0.04	0.00
data entry →	0.59	27.24	0.05	0.00
data entry →	0.66	36.87	0.08	0.00
data entry →	0.72	45.88	0.14	0.00
data entry →	0.79	52.64	0.16	0.00
data entry →	0.85	55.71	0.20	0.00
data entry →	0.92	57.96	0.22	0.00
data entry →	0.98	60.83	0.28	0.00
data entry →	1.05	64.51	0.32	0.00
data entry →	1.12	67.38	0.38	0.00
data entry →	1.18	70.87	0.39	0.00
data entry →	1.25	74.35	0.42	0.00
data entry →	1.31	77.22	0.46	0.00
data entry →	1.38	77.21	0.49	0.00
data entry →	1.44	76.80	0.50	0.00

Figure C.5 Raw CPT Input Data

Depth (ft)	Soil Type
0.00	
0.46	gravelly SAND
0.52	gravelly SAND
0.59	gravelly SAND
0.66	gravelly SAND
0.72	gravelly SAND
0.79	gravelly SAND
0.85	gravelly SAND
0.92	gravelly SAND
0.98	gravelly SAND
1.05	gravelly SAND
1.12	gravelly SAND
1.18	gravelly SAND
1.25	gravelly SAND
1.31	gravelly SAND
1.38	SAND

Figure C.6 Soil Type based on CPTu Input Data

Additional Notes:

Figure C.7 Additional Notes Box

GEOPARAMETER		SI Units		English Units	
Average	Unit Weight	19.09	kN/m ³	0.1215	kcf
	Friction Angle ϕ	39.498	degrees	39.498	degrees
	Modulus of Elasticity	39925.55	kPa	833.86	ksf

Figure C.8 Average Unit Weight, Friction Angle, and Soil Modulus of Elasticity from CPT Input Data

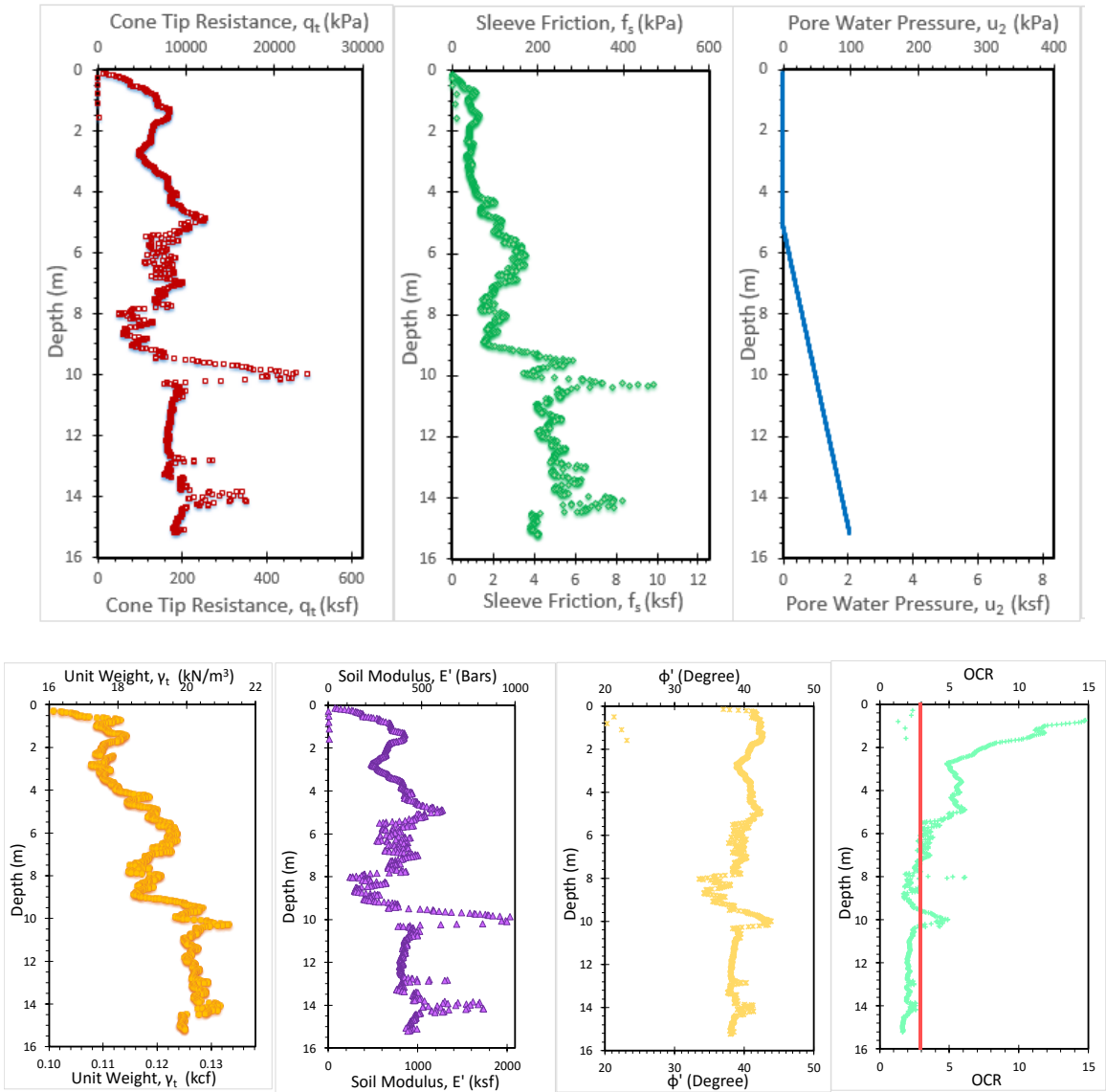


Figure C.9 CPT Profiles of Input and Output Data

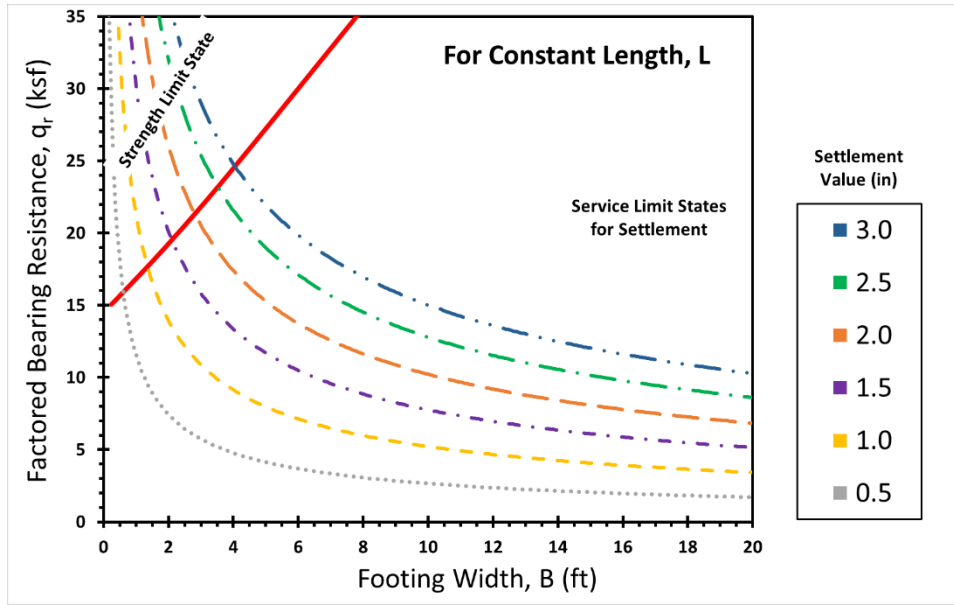


Figure C.10 Factored BC-Footing Width Design Chart with different settlement contours for Constant L value

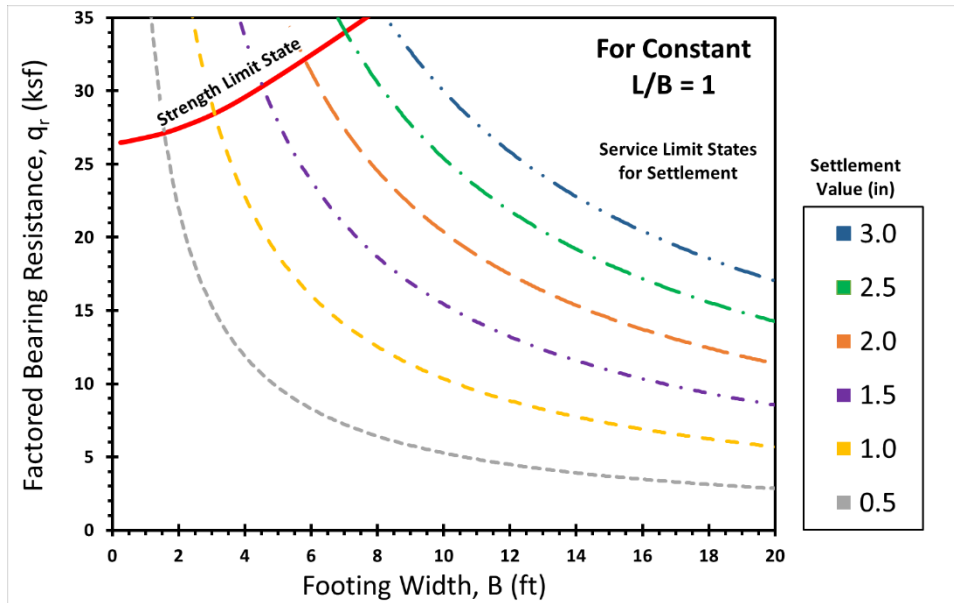


Figure C.11 Factored BC-Footing Width Design Chart with different settlement contours for Square Footing (Constant L/B ratio = 1)

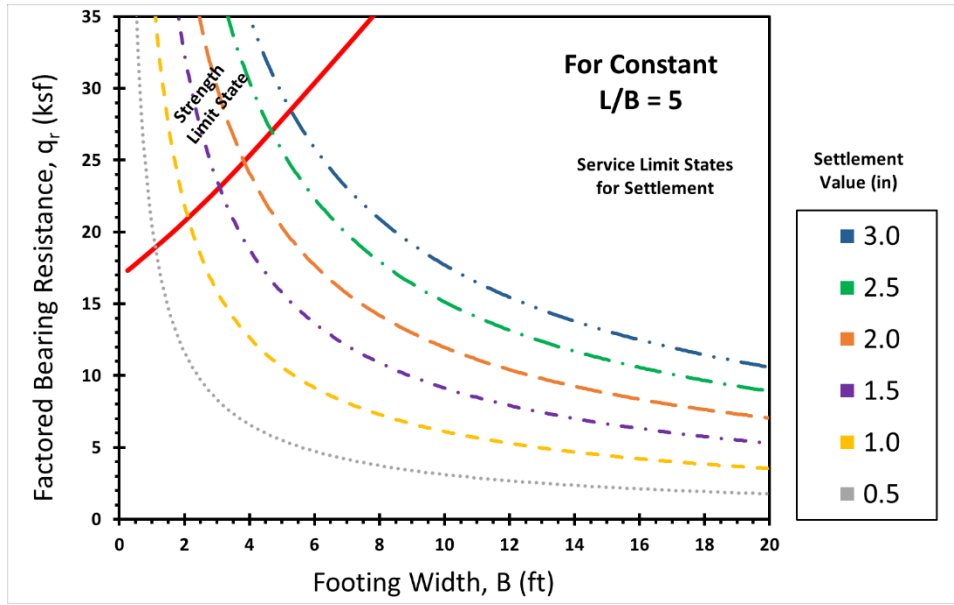


Figure C.12 Factored BC-Footing Width Design Chart with different settlement contours for Rectangular Footing ($L/B = 5$)

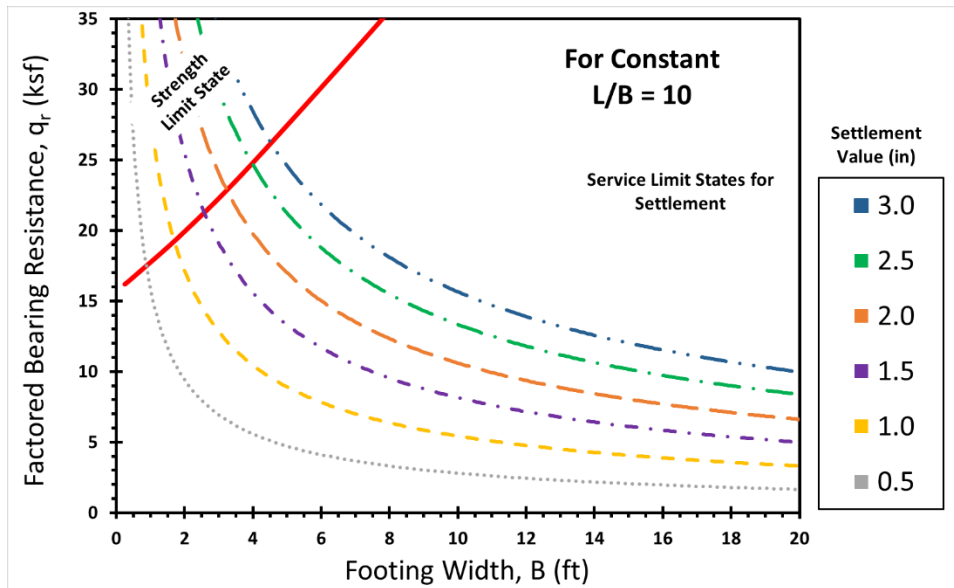


Figure C.13 Factored BC-Footing Width Design Chart with different settlement contours for Strip Footing ($L/B = 10$)

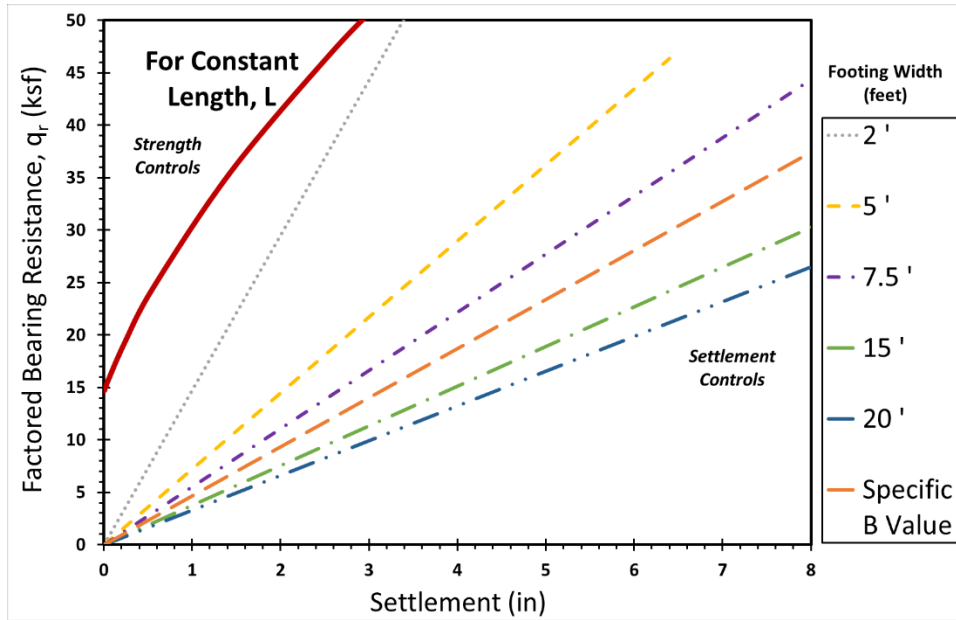


Figure C.14 Factored BC-Settlement Design Chart with different footing width contours for footings with Constant Length

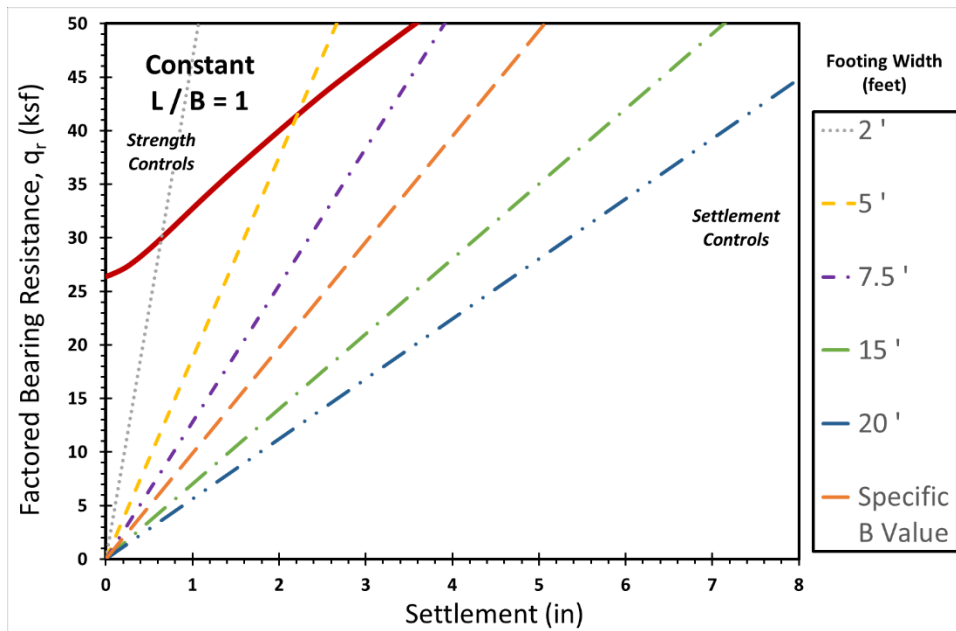


Figure C.15 Factored BC-Settlement Design Chart with different footing width contours for Square Footing ($L/B = 1$)

Appendix D: Illustrated Example using DMT data

Flat Plate Dilatometer Test Data		
GDOT Project ID:	Test Data Number 1	← data entry
Project Name:	xxxxx	← data entry
Location:	xxxxx	← data entry
Boring Number:	DMT-01	← data entry
Date:	18 March 2016	← data entry

DMT procedures per ASTM D 6635

Figure D.1 Raw Input DMT Data

FOOTING INPUT PARAMETERS

Embedment Depth, D_f (ft) =	<input type="text"/>	← data entry
Footing Thickness, t (ft) =	<input type="text"/>	← data entry
Layer Thickness, h (ft) =	<input type="text"/>	← data entry
Modulus of Foundation, E_{FDTN} (ksf) =	<input type="text"/>	← data entry

Calibration Factor ΔA	<input type="text" value="0"/>	bar	← data entry
Calibration Factor ΔB	<input type="text" value="0"/>	bar	← data entry
Ground Water Table	<input type="text" value="3.28"/>	feet	← data entry

Figure D.2 Footing Input Parameters and DMT Calibration Factors

FOUNDATION SHAPES and GEOMETRY

Footing Length L (ft) =	<input type="text" value="100"/>	← data entry if known
Footing Width B (ft) =	<input type="text" value="8"/>	← data entry if known
Current Case - L/B =	13	
Square - L/B =	1	
Rectangular - L/B =	5	
Strip - L/B =	10	

Figure D.3 Foundation Shape and Geometry

Total Number of Readings	51
Number of Clay Readings	1
% Clay Readings	1.96

Figure D.4 *Percentage of Clay Readings*

		DMT Readings	
		A (bar)	B (bar)
Depth (ft)			
	0.00		
data entry →	0.66	2.40	8.30
data entry →	1.31	2.10	6.90
data entry →	1.97	1.80	9.20
data entry →	2.62	1.30	7.80
data entry →	3.28	1.70	8.70
data entry →	3.94	3.00	12.20
data entry →	4.59	1.90	12.00
data entry →	5.25	2.60	12.70
data entry →	5.91	3.80	13.60
data entry →	6.56	1.50	9.00
data entry →	7.22	1.90	8.40
data entry →	7.87	1.40	7.70
data entry →	8.53	1.90	8.30
data entry →	9.19	2.00	10.00
data entry →	9.84	2.10	10.40
data entry →	10.50	2.00	10.50

Figure D.5 *Raw DMT Input Data*

Depth (ft)	Soil Type
0.00	
0.66	Silty Sand
1.31	Silty Sand
1.97	Sand
2.62	Sand
3.28	Sand
3.94	Sand
4.59	Sand
5.25	Sand
5.91	Silty Sand
6.56	Sand
7.22	Sand
7.87	Sand
8.53	Sand
9.19	Sand
9.84	Sand
10.50	Sand

Figure D.6 Soil Type based on DMT Input Data

Additional Notes:

Figure D.7 Additional Notes Box

GEOPARAMETER		SI Units		English Units	
Average	Unit Weight	18.53	kN/m ³	0.1179	kcf
	Friction Angle ϕ	39.412	degrees	39.412	degrees
	Modulus of Elasticity	43148.34	kPa	901.17	ksf

Figure D.8 Average Unit Weight, Friction Angle, and Soil Modulus of Elasticity using DMT Input Data

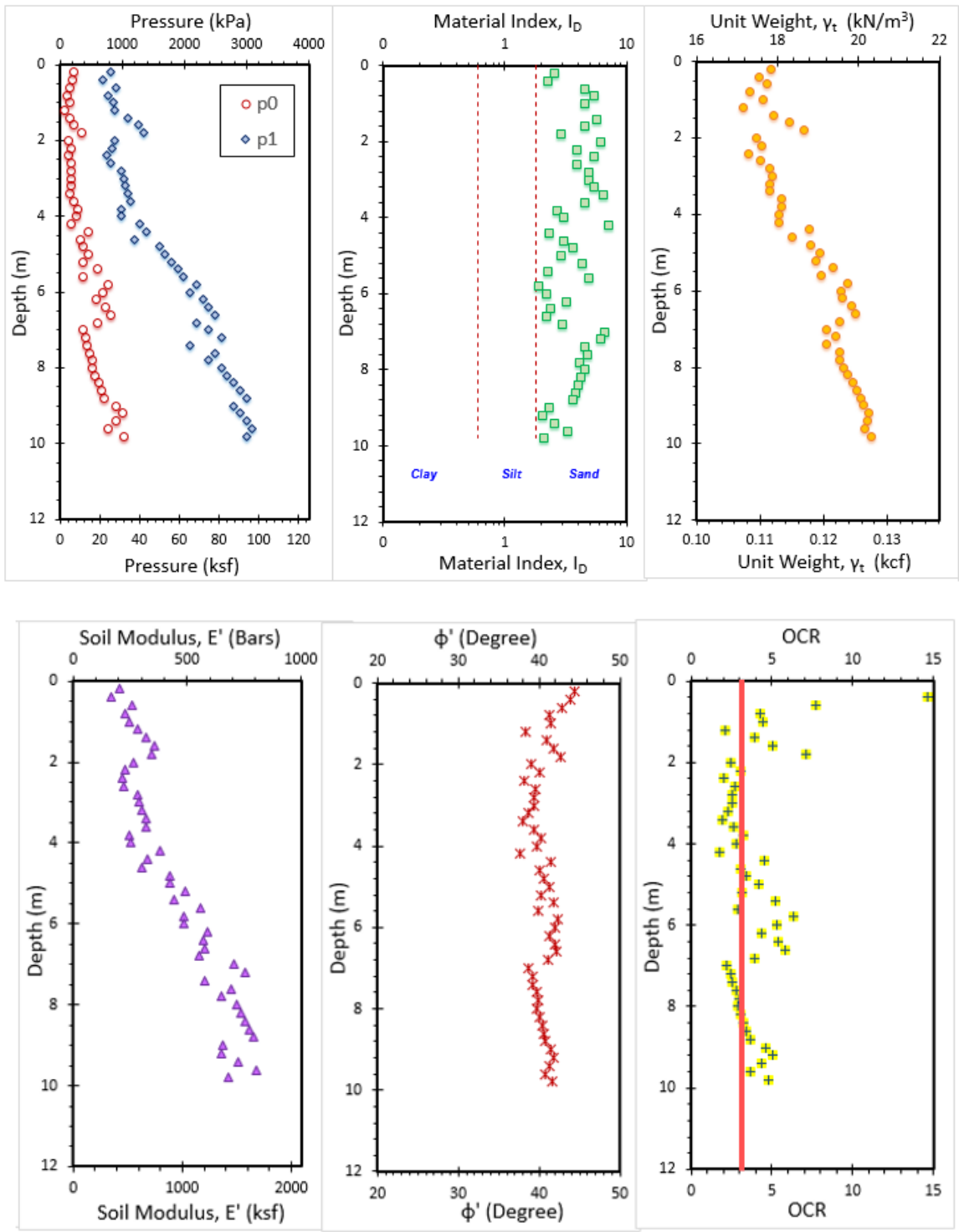


Figure D.9 Profiles of DMT Input and Output Data

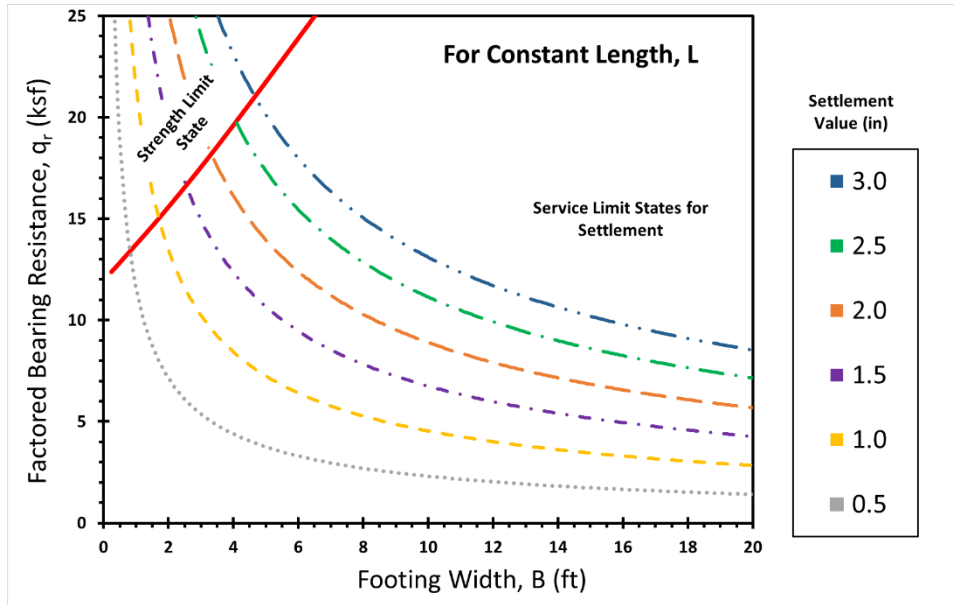


Figure D.10 Factored BC-Footing Width Design Chart with different settlement contours for Constant L value

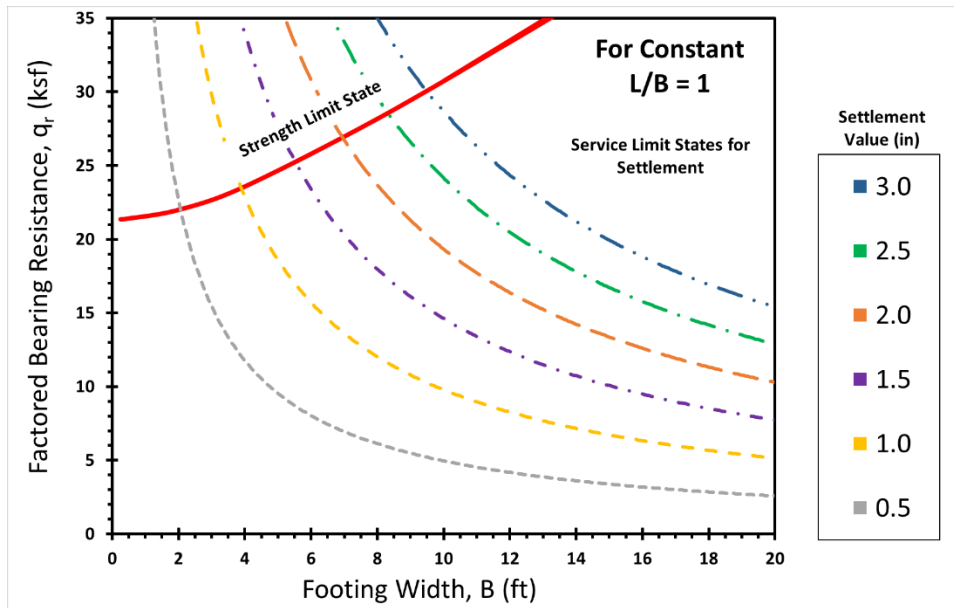


Figure D.11 Factored BC-Footing Width Design Chart with different settlement contours for Square Footing (Constant L/B ratio = 1)

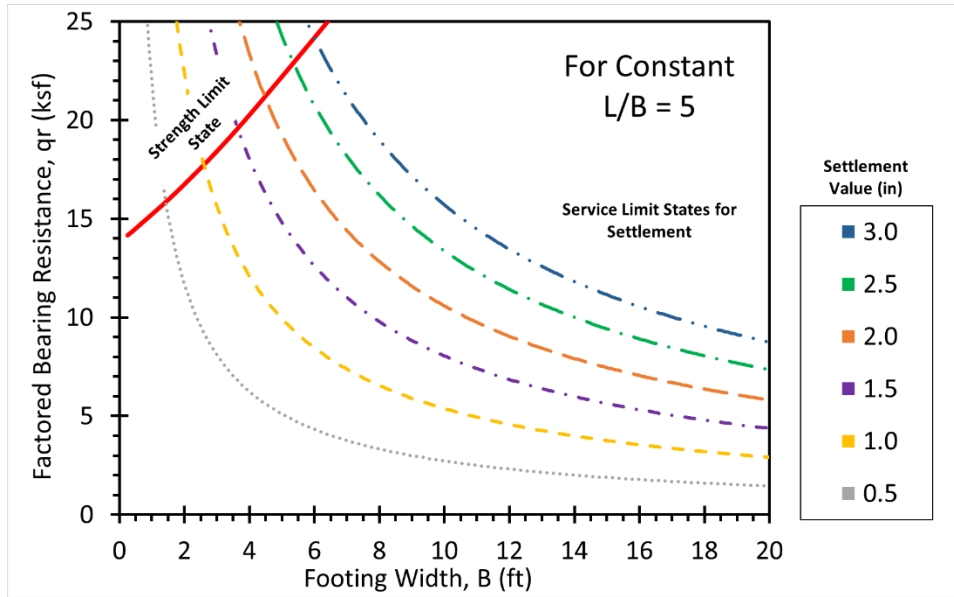


Figure D.12 Factored BC-Footing Width Design Chart with different settlement contours for Rectangular Footing ($L/B = 5$)

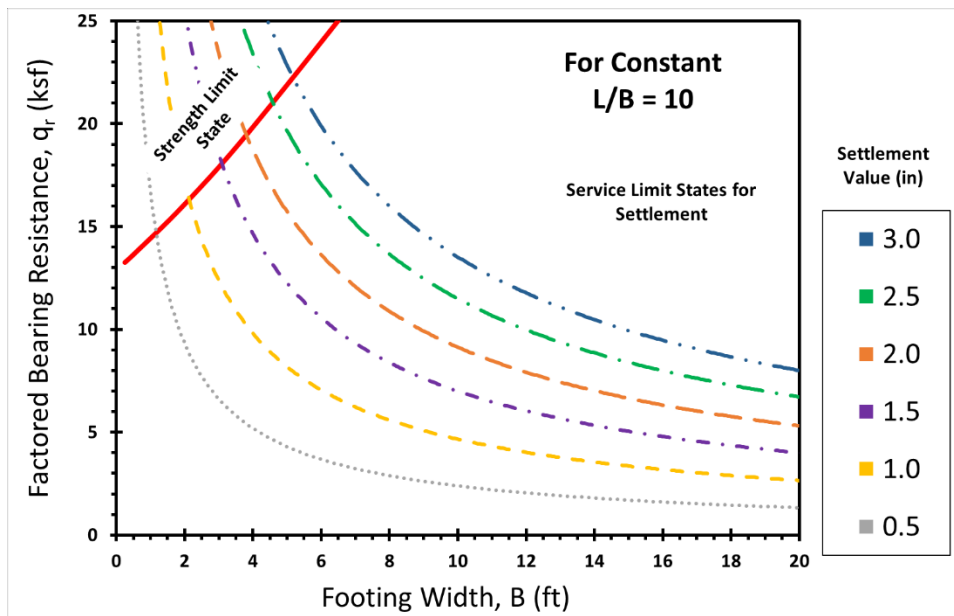


Figure D.13 Factored BC-Footing Width Design Chart with different settlement contours for Strip Footing ($L/B = 10$)

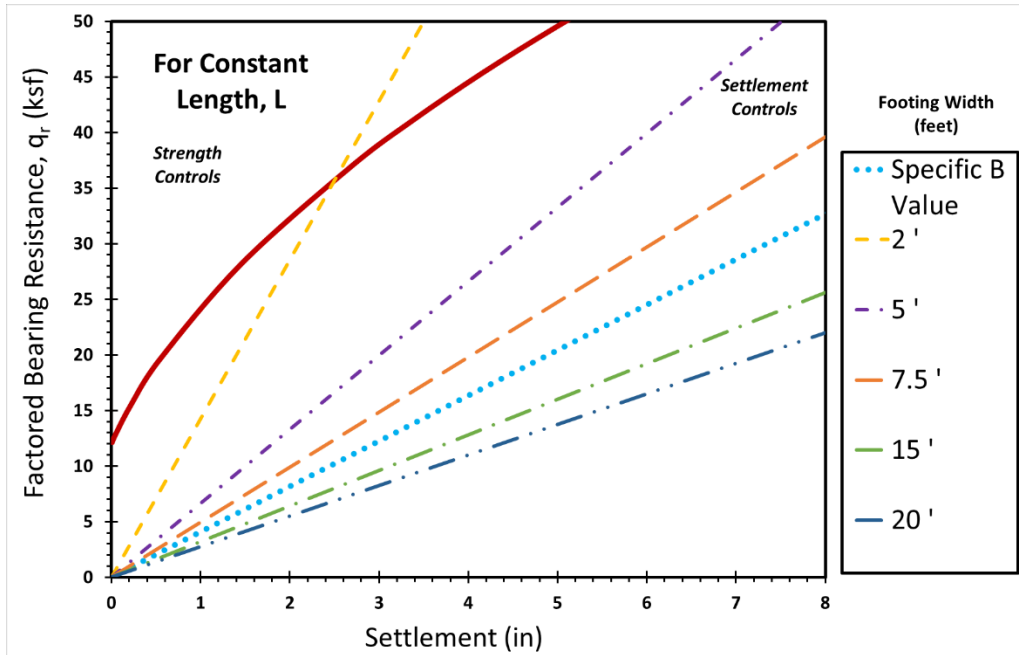


Figure D.14 Factored BC-Settlement Design Chart with different footing width contours for footings with Constant Length

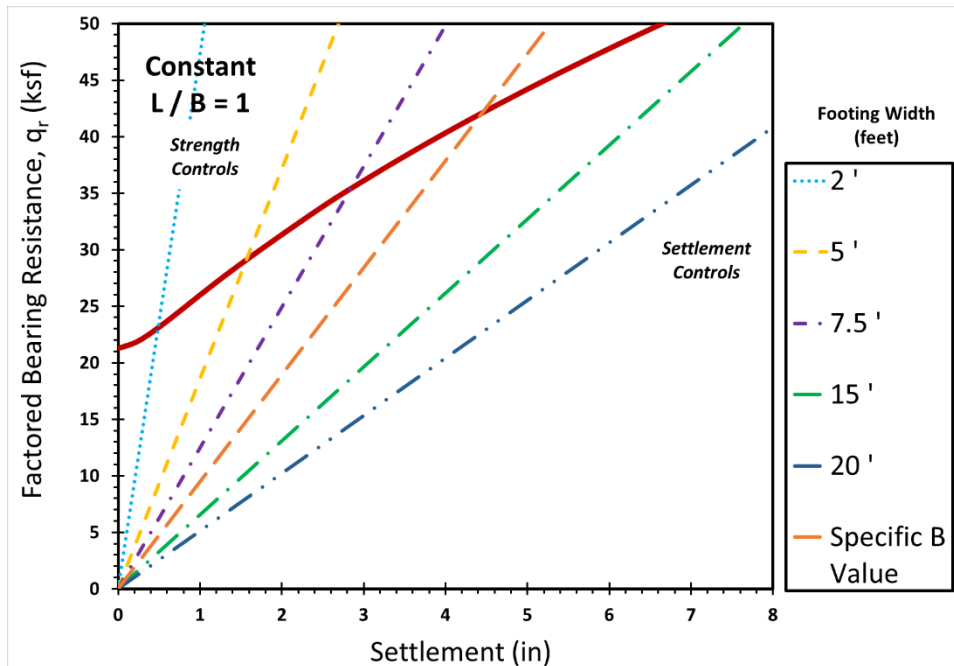


Figure D.15 Factored BC-Settlement Design Chart with different footing width contours for Square Footing ($L/B = 1$)